Hong Kong Journal of Radiology

Hong Kong Journal of Radiology

HKJR

香港放射科醫學雜誌

VOLUME 26 · NUMBER 3 · 2023

ISSN 2223-6619

Highlights of this issue:

- Magnetic Resonance Imaging–Guided Cryotherapy for Precision Tumour Ablation
- Effect of Elective Inguinal Irradiation in Low Rectal Cancer with Anal Canal Invasion
- Conventional and Advanced Post-treatment Magnetic Resonance Imaging of Primary and Metastatic Brain Tumours: A Pictorial Essay

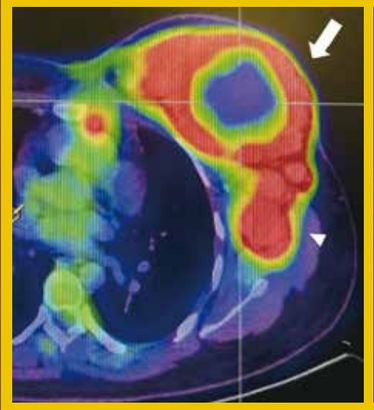

In the article “Molecular Classification and Respective Radiological Phenotypes of Breast Cancers: A Pictorial Essay”. Positron emission tomography/computed tomography of a young patient with triple-negative left breast cancer, showing hypermetabolic uptake in the necrotic tumour (arrow) and left axillary lymphadenopathy (arrowhead).

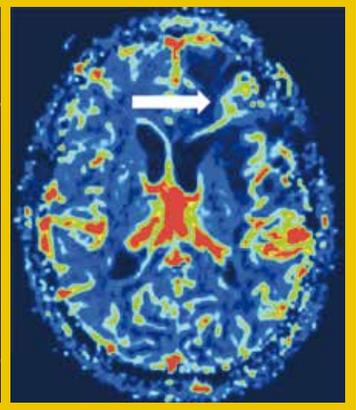

In the article “Conventional and Advanced Post-treatment Magnetic Resonance Imaging of Primary and Metastatic Brain Tumours: A Pictorial Essay”. In a relative cerebral blood volume (rCBV) map derived from magnetic resonance imaging performed in a patient with left frontal glioblastoma 3 months after excision, there is elevated rCBV in the left frontal region (arrow), suggestive of disease progression.

Official Publication of
Hong Kong College of Radiologists

HKAM PRESS

Vol. 26 No. 3, 2023 Pages 165-236

The Royal College of Radiologists

HONG KONG COLLEGE OF RADIOLOGISTS 香港放射科醫學院

RADIOLOGY HONG KONG 2023

10th Joint Scientific Meeting of RCR & HKCR
31st Annual Scientific Meeting of HKCR

18TH - 19TH NOVEMBER 2023
(SAT & SUN)

HONG KONG ACADEMY OF MEDICINE
JOCKEY CLUB BUILDING
HONG KONG SAR, CHINA

Multidisciplinary Symposium
Prostate Cancer

Subspecialty Focus
Urological Malignancies
Cardiovascular Radiology
Head & Neck Malignancies
Medico-legal Issues

君子莫急

If it be true the gentleman hadst known about modern diagnostic imaging and treatments of prostate cancer, the gent wouldst behold less worried

For details

HKJR

COVER IMAGES

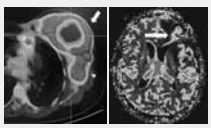

..... SEE PAGES 213 & 222

Hong Kong Journal of Radiology

Hong Kong Journal of Radiology is a continuation of the *Journal of the Hong Kong College of Radiologists*. This journal is dedicated to publish all aspects of clinical oncology, diagnostic radiology, and nuclear medicine.

VOLUME 26 • NUMBER 3 • SEPTEMBER 2023

Original Articles

Perspective

Case Reports

Pictorial Essays

ePub-only Articles

The following ePub-only articles can be found on the HKJR website <http://www.hkjr.org>.

When citing this journal, abbreviate as ***Hong Kong J Radiol***.

INFORMATION FOR SUBSCRIBERS

Hong Kong Journal of Radiology (香港放射科醫學雜誌) is the official peer-reviewed publication of the Hong Kong College of Radiologists and is published by the Hong Kong Academy of Medicine Press.

Frequency
Quarterly, 1 volume a year.

Correspondence concerning subscriptions should be addressed to:

Executive Assistant
Hong Kong Journal of Radiology
Room 909, 9/F, Hong Kong Academy of Medicine Jockey Club Building
99 Wong Chuk Hang Road, Aberdeen, Hong Kong
Tel: (852) 2871 8788; Fax: (852) 2554 0739
Email: hkjr@hkcr.org

Annual subscription rate

Hong Kong delivery:	HK$400 per volume.
Overseas delivery (by airmail):	US$100* per volume.
	* Bank charges shall be borne by the subscriber.

- Rates are the same for individuals and institutions.
- Renewals should be promptly received to avoid a break in journal delivery. The Hong Kong College of Radiologists does not guarantee to supply back issues on late renewals.

Change of address
The College must be notified 60 days in advance. Journals undeliverable because of an incorrect address will be destroyed. Send address changes to:

Hong Kong Journal of Radiology
Room 909, 9/F, Hong Kong Academy of Medicine Jockey Club Building
99 Wong Chuk Hang Road, Aberdeen, Hong Kong

Please return your Subscription Order Form to:

Hong Kong Journal of Radiology
Room 909, 9/F, Hong Kong Academy of Medicine Jockey Club Building
99 Wong Chuk Hang Road, Aberdeen, Hong Kong

I enclose payment (US$/HK$) _____
Please make bank draft, cheque, or cashier's order payable to **"Hong Kong College of Radiologists"**

Name (in English): _____

Address: _____

_____

Tel: _____ Fax: _____ Email: _____

Please (✓) accordingly
I would like to subscribe to the *Hong Kong Journal of Radiology*

❒ Hong Kong delivery: HK$400/volume
❒ Overseas delivery: US$100/volume*
(Postage charge included)
*Bank charges shall be borne by the subscriber.

❒ 3 volumes ❒ 2 volumes ❒ 1 volume

Subscription period: From Volume _____ to Volume _____

Hong Kong Journal of Radiology

Aims and Editorial Policy

Hong Kong Journal of Radiology **香港放射科醫學雜誌** is the official peer-reviewed academic journal of Hong Kong College of Radiologists, a founder College of the Hong Kong Academy of Medicine. The Journal is published quarterly and is indexed in EMBASE/*Excerpta Medica*, SCOPUS, Emerging Sources Citation Index, and Index Copernicus. Papers are published on all aspects of diagnostic imaging, clinical oncology, and nuclear medicine, including original research, editorials, review articles, and case reports. Papers on radiological protection, quality assurance, audit in radiology, and matters related to radiological training or education are included.

All papers submitted are subject to peer review, and the Editorial Board reserves the right to edit papers in preparation for publication in the Journal. Authors are asked to refer to the *Information for Authors* published in each issue of the Journal, regarding the style and presentation of their articles. Failure to do so may result in rejection of their papers by the Editorial Board.

Manuscripts should be submitted online via the HKAMedTrack <www.hkamedtrack.org/hkjr>. Correspondence should be sent to:

Managing Editor, HKJR Editorial Office
c/o Hong Kong Academy of Medicine Press
10/F, Hong Kong Academy of Medicine Jockey Club Building
99 Wong Chuk Hang Road, Aberdeen, Hong Kong
Tel: (852) 2871 8809; Fax: (852) 2515 9061
Email: hkjr@hkam.org.hk

Advertisements

Correspondence concerning advertisements should be addressed to:

Executive Assistant
Hong Kong College of Radiologists
Room 909, 9/F Hong Kong Academy of Medicine Jockey Club Building
99 Wong Chuk Hang Road, Aberdeen, Hong Kong.
Tel: (852) 2871 8788; Fax: (852) 2554 0739
Email: hkjr@hkcr.org

Reprints

Reprints of individual articles are available to authors only. Reprints in large quantities (non-authors), for commercial or academic use, may be purchased from the publisher. For information and prices, please send an email to: hkjr@hkam.org.hk.

Copyright

On acceptance of an article by the Journal, the corresponding author will be asked to transfer copyright of the article to the College. The Copyright Transfer Assignment Form will be sent to the author at the time of acceptance.

Disclaimer

Hong Kong Journal of Radiology and the publisher do not guarantee, directly or indirectly, the quality or efficacy of any product or service described in the advertisements or other material which is commercial in nature in this issue. All articles published, including editorials and letters, represent the opinions of the authors and do not reflect the official policy of the Journal, Hong Kong College of Radiologists, the publisher, or the institution with which the author is affiliated, unless this is clearly specified.

Hong Kong Journal of Radiology
ISSN 2223-6619 (Print)
ISSN 2307-4620 (Online)

Hong Kong J Radiol. 2023;26:168-73. Epub 2 Aug 2023 | https://doi.org/10.12809/hkjr2317243

ORIGINAL ARTICLE **CME**

Magnetic Resonance Imaging–Guided Cryotherapy for Precision Tumour Ablation

JB Chiang, WL Poon, PCH Kwok, HS Fung

Department of Radiology and Imaging, Queen Elizabeth Hospital, Hong Kong SAR, China

ABSTRACT

Introduction: *Percutaneous ablation has played an increasingly prominent role in both palliative and curative treatment of solid tumours, allowing minimally invasive tumour destruction and pain control. Percutaneous ablation is frequently performed under ultrasound or computed tomography guidance, both of which are imperfect in delineating the ablation zone. Magnetic resonance imaging (MRI) guidance provides superior soft tissue contrast, real-time radiation-free imaging, and accurate visualisation of the ablation zone. This study aimed to describe the technique, assess its safety and benefits.*

Methods: *We retrospectively reviewed the clinical management of patients who had undergone MRI-guided ablation from 1 May 2019 to 31 January 2020 and collected patient data including tumour characteristics, procedure details, and follow-up imaging results.*

Results: *A total of 14 cases were analysed (10 renal cell carcinomas, 1 hepatocellular carcinoma, 1 adrenal metastasis, 1 external iliac lymph node metastasis, and 1 chest wall fibromatosis). All cases were technically successful with ice ball coverage of the tumour in line with operative intent. Three minor adverse events (two cases of frostbite and one perinephric haematoma) occurred. One patient declined follow-up imaging. Eleven patients showed no residual or recurrence; the patient with chest wall fibromatosis showed shrinkage of the lesion.*

Conclusion: *MRI guidance is safe and allows accurate tumour visualisation, real-time needle puncture for cryoprobe and hydrodissection needle insertion, and precise delineation of the ablation zone in many procedures.*

Key Words: *Ablation techniques; Carcinoma, renal cell; Cryosurgery; Magnetic resonance imaging, cine; Magnetic resonance imaging, interventional*

Correspondence: *Dr JB Chiang, Department of Radiology and Imaging, Queen Elizabeth Hospital, Hong Kong SAR, China*
Email: jbchian@gmail.com

Submitted: 10 Jun 2020; Accepted: 26 Aug 2020.

Contributors: JBC designed the study, acquired the data, analysed the data, and drafted the manuscript. All authors critically revised the manuscript for important intellectual content. All authors had full access to the data, contributed to the study, approved the final version for publication, and take responsibility for its accuracy and integrity.

Conflicts of interest: All authors have disclosed no conflicts of interest.

Funding/support: This research received no specific grant from any funding agency in the public, commercial, or not-for-profit sectors.

Data Availability: All data generated or analysed during the present study are available from the corresponding author on reasonable request.

Ethics approval: This research was approved by the Kowloon Central/Kowloon East Cluster Research Ethics Committee of Hospital Authority, Hong Kong (Ref No.: KC/KE-20-0045/ER-4). Informed consent for treatment and procedures of this retrospective study was waived by the Committee.

中文摘要

磁共振引導精確腫瘤消融冷凍療法

蔣碧茜、潘偉麟、郭昶熹、馮漢盛

簡介：經皮消融可實現微創腫瘤消除和控制疼痛，在實體腫瘤的姑息性和根治性治療中正發揮愈趨重要的作用。經皮消融通常在超聲或電腦斷層引導下進行，兩者在劃定消融區方面都有局限性。磁共振引導具有明確優勢，它的軟組織對比度好，可實時無輻射成像，並可準確描繪消融區。本研究旨在描述該技術，評估其安全性和效益。

方法：我們對在2019年5月1日至2020年1月31日期間接受磁共振引導消融的患者臨床管理進行回顧性分析，並收集患者資料，包括腫瘤特徵、手術細節和隨訪影像檢查結果。

結果：本研究共分析了14例（腎細胞癌10例，肝細胞癌1例，腎上腺轉移1例，骼外淋巴結轉移1例及胸壁纖維瘤病1例）。所有病例均技術成功，冰球覆蓋腫瘤符合手術計劃。共發生3宗輕微副反應事件（2例凍傷及1例腎周血腫）。一名患者拒絕影像學隨訪。11例患者無殘留腫瘤或復發。胸壁纖維瘤病患者表現病灶縮小。

結論：磁共振引導安全，並且可以在許多手術中實現準確的腫瘤可視化、實時插入冷凍探針和水分離針，及精確描繪消融區域。

INTRODUCTION

Percutaneous tumour ablation is important in the treatment of both benign and malignant diseases, allowing minimally invasive treatment for tumour destruction and pain control. Percutaneous tumour ablation is frequently performed under ultrasound (US) or computed tomography (CT) guidance, both of which have significant limitations. For example, US provides limited visualisation of deep structures and is readily deflected by overlying gas and bone. CT, on the other hand, emits radiation, rendering real-time needle insertion unfavourable. Additionally, CT has limited soft tissue spatial resolution, making it difficult if not impossible to visualise the tumour and important surrounding structures. Most importantly, both techniques of imaging guidance do not allow accurate visualisation of ablation zones.[1] Magnetic resonance imaging (MRI) guidance has swiftly achieved global prominence as it provides superior soft tissue contrast, radiation-free real-time imaging during needle insertion, and, most importantly, clear visualisation of the ablation zone. Superior soft tissue spatial resolution is particularly important as it allows accurate visualisation of tumour and important adjacent structures,[1,2] which is otherwise difficult under other imaging techniques. With these qualities, MRI guidance allows safer, more precise, and radiation-free imaging guidance of tumour ablation. Recently, the technique has been available in Hong Kong. The aim of this retrospective single-institution study is to describe the technique and evaluate its safety while highlighting its use and benefits.

METHODS

Population

From 1 May 2019 to 31 January 2020, 14 patients (9 males, 5 females) underwent MRI-guided cryoablation in our institution. Thirteen procedures were performed on tumours with curative intent, and one as a staged procedure to treat chest wall fibromatosis. Patients were referred for local ablative treatment either because the patient was not a suitable candidate for surgery or because the lesions could not be treated by surgery (e.g., desmoid tumours, bone metastases or lymph node metastases). Patient and lesion characteristics are summarised in the Table.

Magnetic Resonance Imaging–Guided Cryoablation

All interventions were performed in an MRI suite dedicated to interventional procedures (Aera 1.5T; Siemens Medical Systems, Erlangen, Germany) under strict aseptic technique. Procedures were performed under local lidocaine anaesthesia (n = 13) or general anaesthesia (n = 1). Cryotherapy was performed with

Table. Patient details and tumour characteristics.

	Patient	Age, y	Sex	Tumour	Tumour size, cm	Technical success	Complications	Recurrence on follow-up imaging	Follow-up period, mo
Malignancy with curative intent	1	60	F	RCC	0.9	Y	Frost bite with wound infection requiring debridement and antibiotics	N	11
	2	75	F	RCC	1.1	Y	N	N	9
	3	61	M	RCC	1.6	Y	N	N	10
	4	60	M	RCC	1.9	Y	N	N	7
	5	83	M	RCC	3.2	Y	N	N	7
	6	72	F	RCC	0.8	Y	N	N	7
	7	64	M	RCC	2.1	Y	Perinephric haematoma	Declined	-
	8	53	M	RCC	1.1	Y	N	N	6
	9	73	M	RCC	1.9	Y	N	N	6
	10	70	M	RCC	2.0	Y	N	N	3
	11	73	M	Adrenal metastasis from hepatocellular carcinoma	1.4	Y	N	N	11
	12	75	F	Hepatocellular carcinoma (recurrent)	1.1	Y	Frostbite, recovery with debridement	N	8
	13	81	M	External iliac lymph node from rectal cancer	1.6	Y	N	Y	6
Benign disease	14	24	F	Chest wall fibromatosis	24	Y	N	Size reduction	3

Abbreviations: F = female; M = male; N = no; RCC = renal cell carcinoma; Y = yes.

a cryoablation system (BTG Visual-ICE; Boston Scientific, Marlborough [MA], United States) with one or more cryoprobes (IceRod MRI or IceSeed MRI; Galil Medical, Arden Hills [MN], United States) depending on lesion characteristics, with manipulation of cryoprobes to create different shapes and sizes of ablation zones, often using the synergistic effects of multiple probes. Cryoprobe insertion was performed under real-time magnetic resonance fluoroscopic guidance using a prototype interactive balanced steady-state free precession sequence implemented for interactive real-time tip tracking with interactive real-time tip tracking module (BEAT IRTTT; Siemens Medical Systems, Erlangen, Germany), which allows active adjustment of scan plane orientation depending on the needs of the operator. Occasionally, and particularly for ice ball monitoring, multiplanar T2-weighted periodically rotated overlapping parallel lines with enhanced reconstruction (PROPELLER [periodically rotated overlapping parallel lines with enhanced reconstruction]) or half-Fourier acquisition single-shot turbo spin-echo (HASTE) sequences were acquired.

Tumour treatment was performed by ensuring that the ablation zone included the entire tumour with an additional safety margin of 5 to 10 mm. Treatment of the chest wall fibromatosis was performed in this case as a staged procedure with partial coverage of the lesion for size reduction.

Data Collection

Patient information on the Clinical Management System of Hospital Authority from 1 May 2019 to 31 January 2020 was collected, which included patient age and sex; target tumour type, location, size, and proximity to important critical structures; procedure details including mode of anaesthesia and need for hydrodissection; complications; and duration of follow-up period. The size of the target lesion is defined as the maximum diameter on preprocedural MRI on the day of the procedure. Complications were graded using the National Cancer Institute's Common Terminology Criteria for Adverse Events (CTCAE) version 5.0. Patient outcome was evaluated by postoperative imaging, on clinic visits, and electronic medical records.

RESULTS

In total, 14 procedures were performed (10 renal cell carcinomas, 1 hepatocellular carcinoma, 1 adrenal metastasis, 1 external iliac lymph node metastasis, and 1 chest wall fibromatosis) from 1 May 2019 to 31 January 2020 (Table). Mean age ± standard deviation of the patients was 66 ± 14.3 years. Most procedures (n = 13) were performed with curative intent; for these

cases, mean tumour diameter was 1.6 ± 5.8 cm. One non-curative procedure performed was a staged cryoablation of chest wall fibromatosis measuring 24 cm, performed for lesion size control.

All procedures performed with curative intent were technically successful with adequate coverage of the tumour observed during intraoperative MRI. For the patient with cryoablation of chest wall fibromatosis performed as a staged procedure, technical success was achieved with coverage of the intended region of the tumour. MRI-guided hydrodissection was performed in two patients (14.3%) due to close proximity to the colon (n = 1) and external iliac vessels (n = 1). A total of 85.7% (12 out of 14) patients had two freeze/thaw cycles, whereas 14.3% (2 out of 14) required three freeze/thaw cycles.

Three minor complications occurred. Two (14.3%) developed CTCAE Grade 3 complications, both developing a small area of frostbite at the needle insertion site, one of which developed before activation of the freeze cycle. Both patients recovered after a minor debridement. One patient (7%) developed a minor perinephric haematoma (CTCAE Grade 1), which recovered without intervention. No major complications were observed.

The mean follow-up period was 7.2 ± 3.03 months. One patient was lost to follow-up and excluded from analysis. Of the patients with malignant disease (n = 12, mean follow-up period = 7.6 months), tumour coverage with no imaging evidence of residual or recurrence was seen in 91.7% (n = 11). One patient with ablation of an external iliac lymph node showed suspicious fluorodeoxyglucose avidity in the iliac fossa on follow-up positron emission tomography–CT, undetermined but possibly residual disease. In the case of chest wall fibromatosis, lesion size reduction was seen in the first month after cryoablation. In this case, the disease that was not cryoablated also showed interval shrinkage and is softer on palpation (Figure 1), attributed to abscopal effect. No other clinical

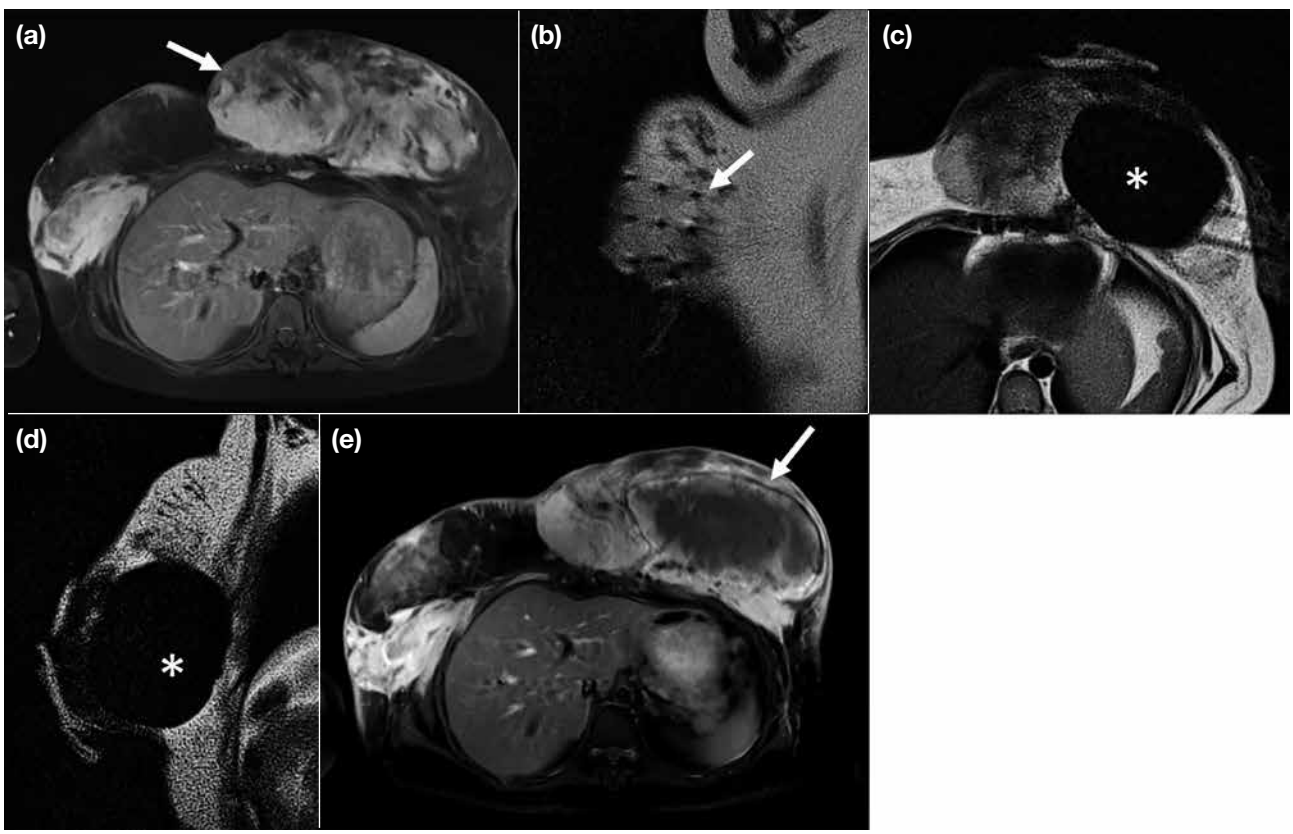

Figure 1. (a) Left chest wall fibromatosis (arrow) in a 24-year-old woman with a history of multiple prior resections with local recurrence. (b) Magnetic resonance imaging (MRI) showing the 10 cryoprobes that were inserted into the large mass (arrow). (c and d) The ice ball is clearly identified as a signal void (asterisk) allowing accurate visualisation of the ablation zone. As the lesion was too large for complete ablation, the procedure was performed with the goal of size reduction. (e) Post-ablation MRI 1 month after surgery showing a necrotic region (arrow) with the non-ablated regions reduced in size, attributed to immune reaction from cryoablation. Clinically, the mass is softer on palpation.

complications, such as pain, were observed in any of the patients.

DISCUSSION

Cryotherapy is a thermal ablative technique that causes tumour destruction by inducing cell damage by freezing and thawing. Current systems use argon and helium gases delivered via cryoprobes that induce freezing and thawing based on the Joule-Thomson effect (temperature change as an effect of rapid expansion of certain gases).[3] Cryoablation has advantages over other ablation modalities such as radiofrequency ablation due to its intrinsic analgesic effects and potential treatment of large tumours.[4] Additionally, cryotherapy allows visualisation of the ice ball, particularly under MRI, which improves predictability of tumour coverage and prevents non-target ablation.

MRI is particularly useful in conjunction with cryotherapy as it allows accurate visualisation of ice ball as a signal void[1] (Figure 2) as well as continuous radiation-free multiplanar ice ball monitoring,[4] allowing accurate assessment of ablation zone, which ensures tumour coverage while avoiding non-target ablation. Due to MRI's superior soft-tissue differentiation, MRI allows better tumour visualisation and hence improved accuracy with needle positioning. Many lesions may only be seen on MRI, such as non-exophytic renal masses or hepatic dome lesions,[5] where MRI greatly improves the accuracy of needle positioning.

MRI-guided intervention may be performed in an open- or closed-bore system.[1] Open-bore systems allow easier access to the patient and enhanced operator flexibility but are limited by lower magnetic field strength (0.2-1 T).[1] Closed-bore systems are more desirable as they provide higher magnetic field strength, which improves imaging rate and quality,[1-3] although at the expense on operator comfort and flexibility. Such systems have specific requirements to allow for

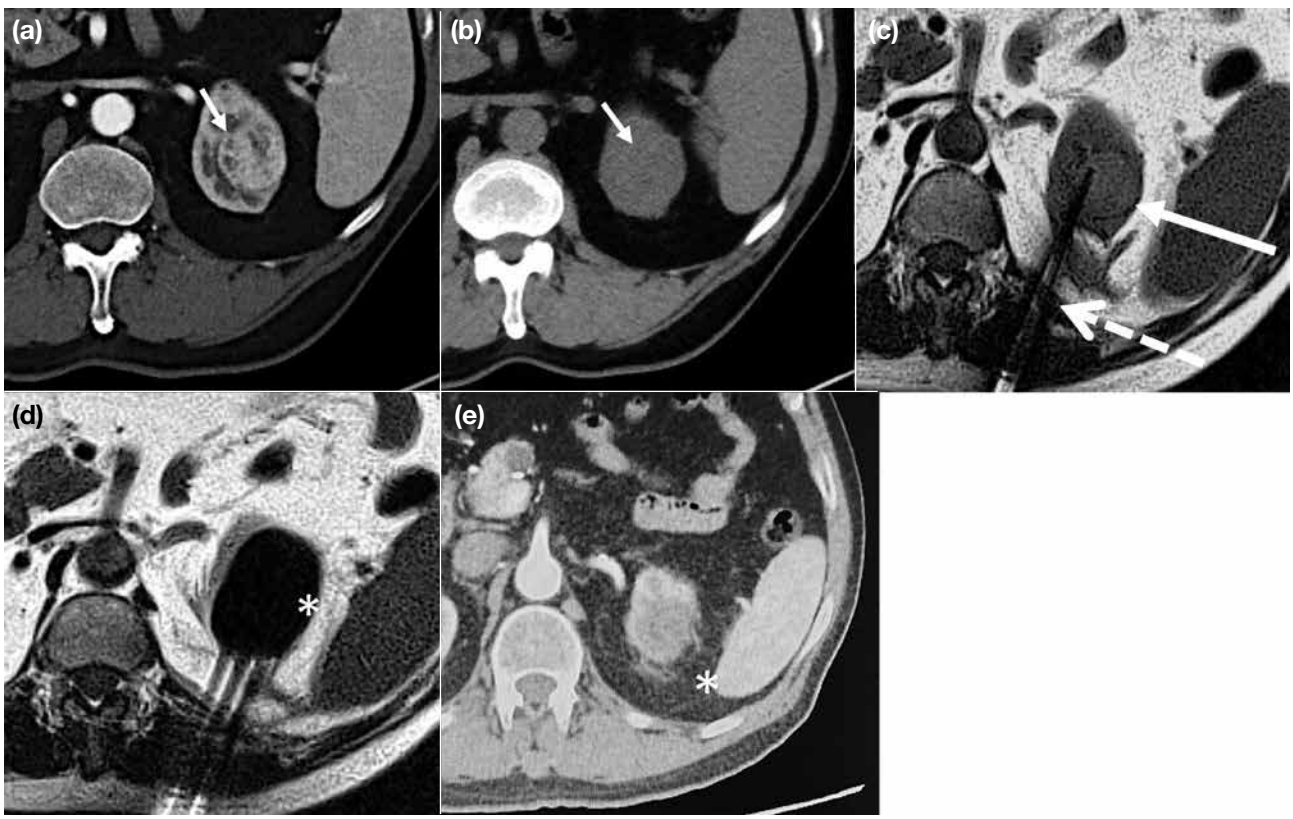

Figure 2. Clear cell renal cell carcinoma detected on (a) contrast-enhanced computed tomography (CT) [arrow] which cannot be delineated on (b) non-contrast CT (arrow), which is commonly used as guidance modality. (c) The lesion is apparent on magnetic resonance imaging due to the superior soft tissue differentiation (white arrow) allowing accurate real-time cryoprobe (dashed arrow) positioning within the tumour and avoiding critical structures. (d) The ice ball is seen as a signal void (asterisk), allowing accurate visualisation of the ablation zone, ensuring adequate tumour coverage and reduced risk of non-target ablation. (e) Post-ablation contrast-enhanced CT showing hypodensity with no evidence of enhancement (asterisk).

interventional use, such as a large bore width (70 cm) and short bore length (125-150 cm).[1] This is necessary to allow the interventional radiologist to stretch into the bore to work at the isocentre, allowing real-time freehand manipulation. Additional body and surface coils may be used to increase contrast resolution of images[6] but of all the procedures described, the spine or body coil within the magnet may suffice.

MRI-guided cryoablation has been described in the literature as a treatment option for a variety of tumours. Ahrar et al[2] described percutaneous cryotherapy of small renal tumours in 18 patients in a 1.5-T MRI. The mean follow-up period was 16.7 months, with rates of overall survival, disease-specific survival, and metastasis-free survival of 88.9%, 100%, and 100%, respectively. Similarly, MRI-guided liver cryotherapy was described to be safe and feasible. Mala et al[7] described percutaneous cryoablation of six patients with liver metastases from colorectal carcinoma using an open 0.5-T MRI, which they concluded allowed good visualisation of tumour for cryoprobe positioning in order to puncture the tumour. Shimizu et al[8] treated 16 tumours with MRI-guided cryoablation on a 0.3-T open-bore magnet with 1- and 3-year overall survival rates of 93.8% and 79.3%, respectively. The complete ablation rate was reported as 80.8% at 3 years.

As the indications for ablation have expanded in both malignant and benign tumours and with palliative and curative intent, MRI guidance may be the preferred imaging technique in certain lesions. MRI guidance has proven beneficial for established ablation targets including renal,[1,2,9] prostate,[1,10] and soft tissue[1] tumours such as desmoids. Although less established, we find MRI guidance highly useful in liver ablation, especially in recurrent tumours and lesions located in the hepatic dome, as described by Wang et al.[5]

Limitations

This paper describes our early experience of MRI-guided cryoablation with multiple shortcomings including a small sample size, short follow-up periods, and heterogeneity of treated lesions. Existing studies have mainly been retrospective analyses of cohorts of MRI or CT guidance in heterogeneous patient groups; controlled trials with larger sample sizes and comparison with other methods of imaging guidance will be useful.

CONCLUSION

MRI guidance is a safe imaging technique that allows accurate tumour and non-target organ visualisation, real-time needle puncture, and precise delineation of the ablation zone.

REFERENCES

1. Cazzato RL, Garnon J, Shaygi B, Tsoumakidou G, Caudrelier J, Koch G, et al. How to perform a routine cryoablation under MRI guidance. Top Magn Reson Imaging. 2018;27:33-8.
2. Ahrar K, Ahrar JU, Javadi S, Pan L, Milton DR, Wood CG, et al. Real-time magnetic resonance imaging–guided cryoablation of small renal tumors at 1.5 T. Invest Radiol. 2013;48:437-44.
3. Ahmed M, Brace CL, Lee FT Jr, Goldberg SN. Principles of and advances in percutaneous ablation. Radiology. 2011;258:351-69.
4. Cazzato RL, Garnon J, Ramamurthy N, Koch G, Tsoumakidou G, Caudrelier J, et al. Percutaneous image–guided cryoablation: current applications and results in the oncologic field. Med Oncol. 2016;33:140.
5. Wang L, Liu M, Liu L, Zheng Y, Xu Y, He X, et al. MR-guided percutaneous biopsy of focal hepatic dome lesions with free-hand combined with MR fluoroscopy using 1.0-T open high-field scanner. Anticancer Res. 2017;37:4635-41.
6. Ahrar JU, Stafford RJ, Alzubaidi S, Ahrar K. Magnetic resonance imaging–guided biopsy in the musculoskeletal system using a cylindrical 1.5-T magnetic resonance imaging unit. Top Magn Reson Imaging. 2011;22:189-96.
7. Mala T, Edwin B, Samset E, Gladhaug I, Hol PK, Fosse E. Magnetic-resonance–guided percutaneous cryoablation of hepatic tumours. Eur J Surg. 2001;167:610-7.
8. Shimizu T, Sakuhara Y, Abo D, Hasegawa Y, Kodama Y, Endo H. Outcome of MR-guided percutaneous cryoablation for hepatocellular carcinoma. J Hepatobiliary Pancreat Surg. 2009;16:816-23.
9. Mogami T, Harada J, Kishimoto K, Sumida S. Percutaneous MR-guided cryoablation for malignancies, with a focus on renal cell carcinoma. Int J Clin Oncol. 2007;12:79-84.
10. King AJ, Dudderidge T, Darekar A, Schimitz K, Heard R, Everitt C. Establishing MRI-guided prostate intervention at a UK centre. Br J Radiol. 2019;92:20180918.
11. Moynagh MR, Kurup AN, Callstrom MR. Thermal ablation of bone metastases. Semin Intervent Radiol. 2018;35:299-308.

Hong Kong J Radiol. 2023;26:174-84. Epub 7 Sep 2023 | https://doi.org/10.12809/hkjr2217659

ORIGINAL ARTICLE **CME**

Effect of Elective Inguinal Irradiation in Low Rectal Cancer with Anal Canal Invasion

HS Wong, WYL Choi, KT Yuen

Department of Oncology, Princess Margaret Hospital, Hong Kong SAR, China

ABSTRACT

Introduction: *We investigated whether omitting elective inguinal irradiation during neoadjuvant or adjuvant radiation/chemoradiation therapy is feasible for patients with low rectal cancer with anal canal invasion (ACI) and nonpalpable inguinal lymph nodes (ILNs) at presentation.*

Methods: *Ninety low rectal cancer patients with ACI who underwent neoadjuvant or adjuvant radiation/chemoradiation therapy with or without elective inguinal radiotherapy (RT) between 2011 and 2021 were recruited. None had palpable ILN. The failure pattern, ILN recurrence rate, survival data, and prognostic factors were analysed.*

Results: *Among 81 patients omitting elective inguinal RT, the 3-year ILN failure rate was 4.9%. Meanwhile, there was no inguinal failure with elective RT. One case of isolated ILN failure was successfully salvaged by surgery. In multivariate Cox regression analysis, positive pathological lymph node(s) after neoadjuvant treatment predicted a worse locoregional recurrence-free survival (odds ratio [OR] = 9.066; $p \leq 0.001$), distant metastasis recurrence-free survival (OR = 6.426; $p = 0.002$), and overall survival (OR = 11.750; $p \leq 0.001$). Chemotherapy concurrent with RT was associated with better locoregional recurrence-free survival (OR = 33.338; $p = 0.001$) and overall survival (OR = 13.917; $p = 0.006$). Grade ≥3 acute and chronic toxicities occurred in 33.3% and 19.8%, respectively, of patients with elective inguinal irradiation, compared with 11.1% and 7.4%, respectively, in patients who did not receive it.*

Conclusion: *Omission of elective inguinal irradiation resulted in a low inguinal failure rate and similar survival outcomes for low rectal cancer patients with ACI. Additionally, it might spare patients from unnecessary acute and chronic RT toxicities.*

Key Words: *Chemoradiotherapy; Chemoradiotherapy, adjuvant; Neoadjuvant therapy; Rectal neoplasms*

Correspondence: *Dr HS Wong, Department of Oncology, Princess Margaret Hospital, Hong Kong SAR, China*
Email: whs871@ha.org.hk

Submitted: 26 Oct 2022; Accepted: 12 Dec 2022.

Contributors: HSW designed the study, acquired and analysed the data, and drafted the manuscript. WYLC and KTY critically revised the manuscript for important intellectual content. All authors had full access to the data, contributed to the study, approved the final version for publication, and take responsibility for its accuracy and integrity.

Conflicts of Interest: The authors have disclosed no conflicts of interest.

Funding/Support: This research received no specific grant from any funding agency in the public, commercial, or not-for-profit sectors.

Data Availability: All data generated or analysed during the present study are available from the corresponding author on reasonable request.

Ethics Approval: This research was approved by the Kowloon West Cluster Research Ethics Committee of Hospital Authority, Hong Kong [Ref No.: KW/EX-22-035 (171-04)]. A waiver of patient consent was obtained from the Committee due to the retrospective nature of the study.

Declaration: This manuscript was posted on Research Square as a registered online preprint (https://doi.org/10.21203/rs.3.rs-1914914/v1).

中文摘要

伴肛門侵犯的低位直腸癌患者進行預防性腹股溝照射的影響

王曉生、蔡源霖、袁錦堂

引言：我們探討為臨床上出現肛門侵犯及觸摸不到腹股溝淋巴結的低位直腸癌患者進行前輔助放療或輔助放療／放化療時不接受預防性腹股溝照射是否可行。

方法：本研究招募了90名出現肛門侵犯的低位直腸癌患者，他們在2011至2021年間曾進行前輔助放療或輔助放療／放化療，部分有接受預防性腹股溝放療，部分則沒有。全部患者均沒有觸摸到的腹股溝淋巴結。本研究分析了失敗模式、腹股溝淋巴結復發率、存活數據及預後因素。

結果：在81名沒有接受預防性腹股溝放療的患者中，三年腹股溝淋巴結失敗率為4.9%。同時，預防性放療並沒有腹股溝失敗的情況。一例個別的腹股溝淋巴結失敗成功通過手術挽救。多變量Cox迴歸分析顯示，前輔助放療後的陽性病理性淋巴結預測較差的局部無復發存活（勝算比 = 9.066；$p \leq 0.001$）、無遠端轉移復發存活（勝算比 = 6.426；$p = 0.002$）及整體存活（勝算比 = 11.750；$p \leq 0.001$）。放療期間同時進行化療與較佳的局部無復發存活（勝算比 = 33.338；$p = 0.001$）及整體存活（勝算比 = 13.917；$p = 0.006$）相關。在接受預防性腹股溝照射的患者中，分別有33.3%及19.8%出現≥3級急性及慢性毒性；沒有接受該照射的患者出現上述兩種毒性的比例則分別為11.1%及7.4%。

結論：沒有接受預防性腹股溝照射的伴肛門侵犯的低位直腸癌患者，其腹股溝失敗率低，與有接受該照射的患者相比，存活結果相近，而且可能避免出現不必要的急性及慢性放療毒性。

INTRODUCTION

Neoadjuvant chemoradiotherapy (CRT) reduces the risk of a positive circumferential margin and local recurrence in patients with low rectal cancer.[1] Prospective randomised trials have demonstrated significantly lower locoregional recurrence rates with adjuvant CRT when compared with observation or either modality alone in stage II/III rectal cancer.[2]

The clinical target volume (CTV) during radiation/chemoradiation therapy must cover areas with potential metastatic risk while avoiding organs at risk to avoid radiation-related complications. In low rectal cancer with anal canal invasion (ACI), tumour can spread to inguinal lymph nodes (ILNs) through the perirectal and pudendal lymphatics, as well as the lymphatics draining the infradentate and perianal skin. An advanced rectal primary tumour can cause proximal lymphatic obstruction and retrograde lymph node metastasis.[3] The European Society for Medical Oncology Clinical Practice Guidelines proposed in 2010 recommends prophylactic irradiation of medial ILNs if the rectal tumour extends below the dentate line.[4] Radiation of ILNs in cases where tumour extends into the anal sphincter has been advocated by the 2016 international consensus guidelines on CTV delineation.[5] According to the 2020 American Society for Radiation Oncology Clinical Practice Guidelines, ILNs and external iliac nodes should be conditionally included in the CTV for patients with rectal malignancies with ACI.[6] However, the contouring atlas of the Radiation Therapy Oncology Group has no consensus on the subject.[7]

In three retrospective trials,[8-10] the ILN failure rates in rectal cancer patients with ACI who received neoadjuvant or adjuvant radiation/chemoradiation therapy without elective inguinal irradiation were not high enough (3-year failure rate: 3.7%[8]; 5-year actuarial rate: 3.5%-4%[9,10]) to justify inguinal irradiation as a standard procedure.

The treatment policy at our institution for low rectal cancer with ACI and clinically negative ILN at presentation has been based on the practice of the attending oncologists. We looked at the feasibility of omitting elective inguinal irradiation for patients with low rectal cancer with ACI and clinically negative ILN.

METHODS

Data Collection

From 2011 to 2021, the clinical data of 110 patients with

low rectal cancer with ACI who received neoadjuvant or adjuvant radiation/chemoradiation therapy in our tertiary oncology centre were collected from the institutional database and retrospectively reviewed. The inclusion criteria were: (1) histologically confirmed locally advanced rectal adenocarcinoma without distant metastasis (based on the Eighth Edition of the American Joint Committee on Cancer Staging Manual); (2) tumours with ACI, defined as the tumour's lower edge being within 3 cm of the anal verge (or being located at or below the dentate line) on digital rectal examination, colonoscopy or magnetic resonance imaging; and (3) an Eastern Cooperative Oncology Group performance status score of 0 to 2.

The exclusion criteria were: (1) inguinal metastasis on presentation by clinical and imaging studies; (2) occurrence of distant failure before surgery; (3) ineligibility for radical surgery as determined by clinical and imaging studies; (4) local excision; (5) incomplete radiation/chemoradiation therapy; (6) in the setting of recurrence indicated for radiation/chemoradiation therapy; and (7) second malignancies within 5 years.

Missing data were dealt with by listwise deletion. Patients lost to follow-up were censored and their life expectancy was counted till the last follow-up date.

Pretreatment Workup

Pretreatment workup for clinical staging included digital rectal examination, complete blood count, liver and renal function tests, serum carcinoembryonic antigen, colonoscopy, chest radiography, computed tomography (CT) of the thorax, abdomen and pelvis with or without transrectal ultrasonography, and pelvic magnetic resonance imaging. Fluorine-18 fluorodeoxyglucose positron emission tomography/CT (PET/CT) was performed at the physician's discretion and patient accessibility.

Chemoradiotherapy Treatment

The patients received either long-course or short-course radiotherapy (RT). Long-course RT was administered to the entire pelvis at a dose of 45 Gy in 25 daily fractions, followed by a 5.4-Gy boost in three daily fractions over 5.5 weeks. Short-course RT was delivered to the whole pelvis at a dose of 25 Gy in 5 daily fractions over 1 week. All patients underwent CT simulation for three-dimensional conformal planning, with a comfortably full bladder and an empty rectum. In patients declining elective inguinal irradiation, a three-field treatment plan was adopted using a posterior-anterior field and lateral opposing beams. With patients electing inguinal irradiation, a pair of anterior-posterior opposing fields was used. The prescription dose was set at the 100% isodose line. The initial radiation field encompassed the gross tumour volume (GTV) (preoperative radiation/chemoradiation therapy) or tumour bed (postoperative CRT), and the regional lymphatics including the mesorectal, internal iliac, presacral, and distal common iliac lymphatics plus or minus ILN. The superior boundary was the L5-S1 junction; the inferior border was set 3 cm caudal to the GTV or tumour bed and the anterior border was placed 3 cm anterior to the sacral promontory, while the posterior border was placed 1 cm posterior to the sacrum. The GTV or tumour bed was included in the boost field, with 3-cm margins in all directions.

Chemotherapy was administered concurrently with long-course RT using bolus 5-fluorouracil (FU) [500 mg/m^2 intravenous bolus; Days 1-3 and Days 29-31].[11] As there has been evidence for better treatment outcomes with continuous oral capecitabine,[12,13] continuous oral capecitabine (825 mg/m^2 twice per day) was used as a concomitant chemotherapeutic agent since April 2021. If patients were deemed unsuitable for chemotherapy, long-course RT alone was an alternative. Either abdominal-perineal resection or low anterior resection with complete mesorectal excision was performed. Typically, the interval between preoperative CRT and surgery was 8 weeks, and that between surgery and postoperative CRT was 10 weeks. Four months of adjuvant chemotherapy was administered using six cycles of capecitabine and oxaliplatin, eight cycles of modified leucovorin/fluorouracil/oxaliplatin, or six cycles of capecitabine depending on patients' tolerance.

Study Endpoints

The 3-year inguinal failure rate, locoregional recurrence-free survival (LRFS), distant metastasis recurrence-free survival (DMRFS), overall survival (OS), and failure pattern were analysed. LRFS, DMRFS, and OS risk factors were also investigated. LRFS was measured from the start of treatment to locoregional relapse, death from any causes, or last follow-up. DMRFS was measured from the start of treatment to distant relapse, death from any causes, or last follow-up. OS was calculated from the date of the first treatment to the date of death or the last follow-up.

Follow-up
The patients were evaluated for symptoms, physical examination findings, and blood tests including carcinoembryonic antigen in outpatient clinics on a regular basis. A thorax, abdomen, and pelvic CT or PET/CT would be arranged if there was clinical suspicion of disease recurrence. Colonoscopies were performed 1 year after surgery and every 3 years thereafter.

Statistical Analysis
The 3-year LRFS, DMRFS, and OS rates were presented using the Kaplan-Meier method. Fisher's exact tests were used to explore the difference between categorical variables, while Mann–Whitney *U* tests were used to explore the difference between continuous variables. Clinicopathologic variables were entered into a Cox proportional hazard regression multivariable regression model and analysed for effects on LRFS, DMRFS and OS. All analyses were performed using SPSS (Windows version 21.0; IBM Corp, Armonk [NY], United States). A p value of <0.05 was considered statistically significant.

Research Reporting Guidelines
The STROBE (Strengthening the Reporting of Observational Studies in Epidemiology) checklist for observational cohort studies was implemented in the preparation of the manuscript.

RESULTS
Patient Characteristics
This study enrolled 90 eligible individuals from a larger primary cohort of 110 patients. The full course of radiation/chemoradiation therapy was completed by all patients. The study excluded five patients who refused or were ineligible for surgery, six patients who had local excision only, one patient with upfront distant metastasis, four patients who developed distant metastasis after neoadjuvant radiation/chemoradiation, two patients with upfront inguinal metastasis, and two patients with recurrent rectal cancer.

The median duration of follow-up was 45 months (range, 2-118). Tables 1 and 2 list the clinical data, pathological data, and treatment characteristics of the patients.

Failure Rates and Patterns
Patients who did not receive elective inguinal radiation (n = 81) had a 3-year ILN failure rate of 4.9% (n = 4). Patients who received elective inguinal radiation (n = 9) did not experience any inguinal failure. Of the four patients with ILN failure, only one of them had isolated ILN failure, while the other three had synchronous locoregional recurrence and/or distant failure. In other words, omitting inguinal irradiation resulted in only one case (1.2%) of isolated inguinal nodal failure. Salvage surgery was successfully performed for this patient, who achieved disease remission and survived. Palliative chemotherapy was administered to patients with synchronous locoregional recurrence and/or distant failure, two of whom died due to disease progression. Failure patterns and characteristics of patients with ILN recurrence are listed in Table 3.

Survival Outcomes and Prognostic Factors
The Figure illustrates the Kaplan-Meier curves, depicting 3-year LRFS, DMRFS, and OS of 81.1%, 77.0%, and 86.8%, respectively.

In multivariable Cox regression analysis, positive pathological lymph node after neoadjuvant treatment predicted worse LRFS (odds ratio [OR] = 9.066, 95% confidence interval [CI] = 3.291-24.972; $p < 0.001$), DMRFS (OR = 6.426, 95% CI = 1.944-21.244; $p = 0.002$) and OS (OR = 11.750, 95% CI = 3.583-38.526; $p < 0.001$). Positive tumour resection margin correlated with worse LRFS (OR = 27.296, 95% CI = 5.592-133.241; $p < 0.001$) and OS (OR = 49.982, 95% CI = 4.561-547.759; $p = 0.001$). Chemotherapy concurrent with RT was associated with better LRFS (OR = 33.338, 95% CI = 4.525-245.633; $p = 0.001$) and OS (OR = 13.917, 95% CI = 2.095-92.437; $p = 0.006$). Meanwhile, elective inguinal RT was not associated with statistical differences in LRFS, DMRFS or OS. Details of simple and multivariable analyses are shown in Table 4.

Treatment Toxicities
Grade ≥3 acute toxicity occurred in 16 out of 81 of patients (19.8%) who did not receive inguinal radiation and 3 out of 9 patients (33.3%) who underwent inguinal RT. Inguinal irradiation caused 3 out of 9 patients (33.3%) to develop grade ≥3 perineal dermatitis, compared to 12 out of 81 patients (14.8%) who did not have inguinal irradiation. The above difference, however, did not reach statistical significance. Table 5 shows the acute toxicities profile (Common Terminology Criteria for Adverse Events Grade ≥3).

In terms of chronic toxicity, 1 out of 9 patients (11.1%) who had elective inguinal irradiation developed a protracted gap wound after excision of a perineal recurrence, while there were no recorded chronic perineal skin toxicities in patients who did not receive inguinal

Table 1. Baseline clinical and pathological characteristics of patients with and without elective inguinal irradiation.*

	Without elective inguinal irradiation (n = 81)	With elective inguinal irradiation (n = 9)	p Value
Sex			1.000
Male	56 (69.1%)	6 (66.7%)	
Female	25 (30.9%)	3 (33.3%)	
Age, y	67 (34-84)	69 (60-83)	0.282
ECOG performance status score	0.862		
0	35 (43.2%)	5 (55.6%)	
1	39 (48.1%)	4 (44.4%)	
2	6 (7.4%)	0	
Missing	1 (1.2%)	0	
Distance of lower edge of tumour from anal verge, cm			0.337
0	6 (7.4%)	2 (22.2%)	
1	10 (12.3%)	1 (11.1%)	
2	21 (25.9%)	1 (11.1%)	
3	42 (51.9%)	4 (44.4%)	
NA (located at or below dentate line)	2 (2.5%)	1 (11.1%)	
Baseline serum CEA level, ng/mL	4.80 (1-162)	2.5 (2-162)	0.066
≤4.7	35 (43.2%)	8 (88.9%)	0.013
>4.7	45 (55.6%)	1 (11.1%)	
Missing	1 (1.2%)	0	
cT stage			0.045
1	0	1 (11.1%)	
2	11 (13.6%)	2 (22.2%)	
3	57 (70.4%)	4 (44.4%)	
4	9 (11.1%)	2 (22.2%)	
Unknown	4 (4.9%)	0	
cN stage			0.624
0	18 (22.2%)	4 (44.4%)	
1	35 (43.2%)	4 (44.4%)	
2	12 (14.8%)	1 (11.1%)	
Equivocal/unknown	16 (19.8%)	0	
Tumour histological grade			0.105
Well differentiated adenocarcinoma	4 (4.9%)	0	
Moderate differentiated adenocarcinoma	59 (72.8%)	8 (88.9%)	
Poorly differentiated adenocarcinoma	11 (13.6%)	0	
Mucinous adenocarcinoma	1 (1.2%)	1 (11.1%)	
Unknown differentiated adenocarcinoma	6 (7.4%)	0	
Lymphovascular invasion			1.000
Positive	23 (28.4%)	2 (22.2%)	
Negative	53 (65.4%)	7 (77.8%)	
Missing	5 (6.2%)	0	
Perineural invasion			0.578
Positive	9 (11.1%)	6 (66.7%)	
Negative	45 (55.6%)	0	
Missing	27 (33.3%)	3 (33.3%)	
Circumferential resection margins			0.119
Positive (<1 mm)	3 (3.7%)	1 (11.1%)	
Close	6 (7.4%)	2 (22.2%)	
Negative	72 (88.9%)	6 (66.7%)	
Proximal and distal resection margin			1.000
Positive	2 (2.5%)	0	
Close	2 (2.5%)	0	
Negative	77 (95.1%)	9 (100%)	
ypT stage	n = 68	n = 6	0.206
0	7 (10.3%)	1 (16.7%)	
1	7 (10.3%)	1 (16.7%)	
2	17 (25%)	0	
3	34 (50%)	3 (50.0%)	
4	3 (4.4%)	1 (16.7%)	
ypN stage	n = 68	n = 6	0.733
0	48 (70.6%)	4 (66.7%)	
1	17 (25.0%)	2 (33.3%)	
2	3 (4.4%)	0	

Abbreviations: CEA = carcinoembryonic antigen; cN = clinical nodal; cT = clinical tumour; ECOG = Eastern Cooperative Oncology Group; NA= not available; ypN = posttreatment pathological nodal; ypT = posttreatment pathological tumour.

* Data are shown as No. (%) or median (range), unless otherwise specified.

Table 2. Treatment details.*

	Without elective inguinal irradiation (n = 81)	With elective inguinal irradiation (n = 9)	p Value
Type of (chemo)RT			0.049
Neoadjuvant	68 (84.0%)	6 (66.7%)	
Adjuvant	13 (16.0%)	3 (33.3%)	
RT schedule			0.100
Long-course	81 (100%)	8 (88.9%)	
Short-course	0	1 (11.1%)	
Concurrent chemotherapy			1.000
Bolus 5-FU/capecitabine	76 (93.8%)	9 (100%)	
No	5 (6.2%)	0	
Time interval between neoadjuvant (chemo)RT and surgery, wk	8 (3-35)	11 (6-17)	0.251
Time interval between surgery and adjuvant CRT, wk	9 (7-13)	7 (7-14)	0.412
Adjuvant chemotherapy			0.554
No	24 (29.6%)	1 (11.1%)	
Capecitabine	32 (39.5%)	5 (55.6%)	
CAPOX or mFOLFOX6	25 (30.9%)	3 (33.3%)	

Abbreviations: CAPOX = capecitabine and oxaliplatin; CRT = chemoradiotherapy; mFOLFOX6 = modified leucovorin/fluorouracil/oxaliplatin; FU = fluorouracil; RT = radiotherapy.
* Data are shown as No. (%) or median (range), unless otherwise specified.

Table 3. Failure patterns and characteristics of patients with inguinal lymph node recurrence.

Patient No.	Age, y	Sex	Clinical stage	Distance of lower edge of tumour from anal verge, cm	Tumour differentiation	yp stage or p stage	Lympho-vascular invasion	Failure pattern	Time to inguinal recurrence, mo*	Subsequent treatment	Survival after inguinal recurrence, mo†	Status
1	70	Male	cT3N0	0	Poorly differentiated	ypT3N2	No	Isolated	26.3	Salvage groin dissection	82.9	In remission
2	54	Male	cT3N1	2-3	Moderately differentiated	ypT3N2	Yes	Synchronous locoregional	43.0	Palliative chemotherapy	23.0	Stable disease Survived
3	81	Male	cT2N0	1-2	Unknown	pT3N0	No	Synchronous locoregional and distant	19.8	Palliative chemotherapy	32.7	Dead
4	82	Female	cT3N1	0-1	Moderately differentiated	ypT2N0	No	Synchronous locoregional	4.1	Palliative chemotherapy	12.2	Dead

Abbreviations: cT = clinical tumour; N = nodal; p = pathological; T = tumour; yp = posttreatment pathological.
* From start of treatment.
† Up to last follow-up date from start of treatment.

irradiation. Among the 81 patients who did not receive elective inguinal irradiation, five (6.2%) experienced intestinal obstruction and one (1.2%) developed rectovaginal fistula. No chronic gastrointestinal toxicities have been reported in patients with elective inguinal irradiation, though the abovementioned differences were not statistically significant. Table 6 shows the chronic toxicities profile (the Radiation Therapy Oncology Group and the European Organisation for Research and Treatment of Cancer Grade ≥3).

DISCUSSION

For rectal cancer, determining optimal radiation targets based on their location and mode of spread is a challenge. Despite the theoretical risk that tumour cells in low rectal cancer with ACI could spread to the ILN region, there has been no consensus on whether to include the inguinal nodal region in CTV for this patient subgroup. More clinical evidence is needed to optimise the CTV for these patients in order to reduce irradiation of normal tissue.

The low ILN failure rate (4.9%) in our study, which mirrored the findings of other retrospective studies,[8-10] showed that most patients with low rectal cancer with ACI would not benefit from elective inguinal

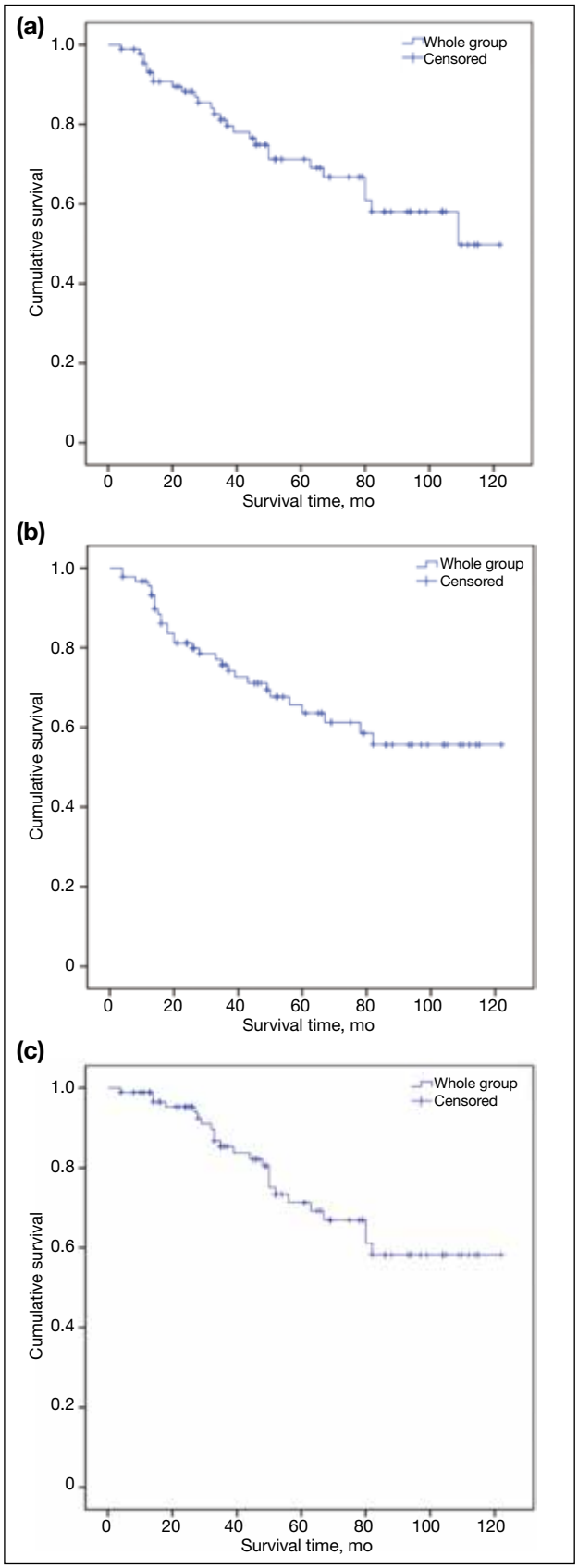

Figure. Kaplan-Meier survival curves for (a) locoregional recurrence-free survival, (b) distant metastasis recurrence-free survival, and (c) overall survival.

irradiation during neoadjuvant or adjuvant (chemo)RT. Some experts, however, still recommend elective ILN irradiation based on acceptable morbidities.[14] In our study, the acute toxicity associated with inguinal irradiation cannot be neglected. There were more acute grade 3 perineal dermatitis among patients who received elective inguinal irradiation (33.3% vs. 14.8%), though none required a treatment break. Meanwhile, the reported chronic complications of elective inguinal irradiation appeared relatively minor in our study. Only 1 out of 9 patients (11.1%) who had elective inguinal irradiation developed a protracted gap wound after perineal recurrence.

Measures were developed to identify patients who were at a higher risk of developing inguinal nodal metastasis. Firstly, Song et al[8] created a nomogram to predict the probability of ILN failures according to tumour location, histological grade, and presence of perineural invasion. It can be used as a guide to select patients for elective inguinal irradiation at high risk of ILN failure, but the presence of perineural invasion may not be known until postoperatively. Shiratori et al[15] have also noted that dentate line involvement and ILNs >8 mm may predict the development of inguinal nodal metastasis. PET/CT has been suggested to detect abnormal inguinal uptake for inguinal nodal region irradiation. Although up to 17% of patients with distal rectal cancer, especially those ultra-low tumours, had inguinal nodes showing fluorodeoxyglucose uptake on PET/CT, the false positivity rate was high, as nearly half of these nodes no longer demonstrated uptake after CRT despite the fact that the inguinal region is not included in the radiation field. Moreover, none of these patients in that study developed inguinal recurrence after 22 months of follow-up.[16] A review of sentinel nodes in anal cancer revealed that 44% of all node metastases located in lymph nodes measured <5 mm in diameter.[17] The spatial resolution of PET/CT is limited to a few millimetres, suggesting it may not have sufficient sensitivity and specificity to select outpatients for inguinal irradiation.[18] The sentinel node technique was also studied in rectal cancer with ACI. A small prospective study of 15 patients showed no recurrence in the groin for patients whose sentinel lymph nodes were determined to be negative for metastatic adenocarcinoma.[19] However, a systematic review indicated that the sentinel lymph node procedure showed only a fair sensitivity rate of 82% (95% CI = 60%-93%), regardless of tumour stage, localisation or pathological technique.[20] Due to the relatively low sensitivity, technically demanding procedures, risk of surgical

Table 4. Simple and multivariable Cox regression models for locoregional recurrence-free survival (LRFS), distant metastasis recurrence-free survival (DMRFS), and overall survival (OS).

Variable	LRFS				DMRFS				OS			
	Simple OR (95% CI)	p Value	Multivariable OR (95% CI)	p Value	Simple OR (95% CI)	p Value	Multivariable OR (95% CI)	p Value	Simple OR (95% CI)	p Value	Multivariable OR (95% CI)	p Value
Age	1.031 (0.991-1.072)	0.136			1.018 (0.982-1.055)	0.339			1.028 (0.986-1.072)	0.191		
Sex (male vs. female)	1.291 (0.758-2.199)	0.346			1.820 (0.743-4.454)	0.190			1.675 (0.625-4.490)	0.305		
ECOG performance status score												
0-1	1				1				1			
2	3.138 (1.081-9.113)	0.035	1.762 (0.314-9.878)	0.520	2.500 (0.869-7.188)	0.089	1.065 (0.175-6.470)	0.946	3.917 (1.328-11.551)	0.013	1.744 (0.278-10.957)	0.553
Baseline serum CEA level, ng/mL (≥4.7 vs. <4.7)	1.319 (0.605-2.876)	0.486			1.886 (0.876-4.059)	0.105			1.530 (0.661-3.538)	0.320		
cT stage												
1-2	1				1				1			
3	0.999 (0.335-2.984)	0.999			1.023 (0.348-3.012)	0.967			0.832 (0.273-2.531)	0.746		
4	1.291 (0.321-5.185)	0.719			1.375 (0.343-5.502)	0.653			1.374 (0.343-5.506)	0.654		
cN (positive vs. negative)	1.389 (0.547-3.528)	0.490			1.472 (0.588-3.690)	0.409			1.195 (0.463-3.082)	0.713		
Distance of lower edge of tumour from anal verge, cm												
3	1				1				1			
0	1.535 (0.428-5.507)	0.511			1.257 (0.363-4.349)	0.718			1.090 (0.238-4.982)	0.912		
1	1.924 (0.611-6.053)	0.263			1.028 (0.297-3.559)	0.965			1.678 (0.461-6.106)	0.432		
2	1.552 (0.623-3.870)	0.346			1.070 (0.453-2.527)	0.877			1.683 (0.663-4.275)	0.274		
RT alone vs. CRT	12.185 (4.387-33.849)	<0.001	33.338 (4.525-245.633)	0.001	5.772 (2.145-15.527)	0.001	3.748 (0.557-25.199)	0.174	12.180 (4.146-35.786)	<0.001	13.917 (2.095-92.437)	0.006
SCRT vs. LCRT	20.460 (1.08×10^{11}–3.89×10^{13})	0.834			20.465 (8.1×10^{10}–5.18×10^{11})	0.805			20.451 (1.08×10^{19}–3.87×10^{21})	0.899		
CRT (adjuvant vs. neoadjuvant)	1.836 (0.732-4.606)	0.195			2.005 (0.852-4.715)	0.111			2.269 (0.886-5.815	0.088		
Without elective groin RT vs. with elective groin RT	1.802 (0.244-13.315)	0.564			2.097 (0.285-15.428)	0.467			1.537 (0.207-11.411)	0.675		
Tumour histological grade												
Low	1				1				1			
High	1.020 (0.349-2.976)	0.972			1.117 (0.387-3.226)	0.838			1.212 (0.358-4.106)	0.757		
LVI (positive vs. negative)	1.106 (0.567-2.156)	0.768			3.864 (1.827-8.171)	<0.001	1.203 (0.302-4.787)	0.793	3.741 (1.601-8.744)	0.002	2.144 (0.344-13.363)	0.414
PNI (positive vs. negative)	2.029 (0.660-6.243)	0.217			2.820 (1.020-7.795)	0.046	2.822 (0.699-11.389)	0.145	1.585 (0.446-5.633)	0.477		
Resection margin (R1 vs. R0)	6.130 (2.081-18.061)	0.001	27.296 (5.592-133.241)	<0.001	2.914 (0.873-9.727)	0.082			5.004 (1.466-17.079)	0.010	49.982 (4.561-547.759)	0.001
pT stage												
1-2	1				1				1			
3-4	39.396 (0.044-35181)	0.289			39.783 (0.075-21206)	0.250			40.216 (0.48-34015)	0.283		

Abbreviations: CEA = carcinoembryonic antigen; CI = confidence interval; cN = clinical nodal; CRT = chemoradiotherapy; cT = clinical tumour; ECOG = Eastern Cooperative Oncology Group; LCRT = long-course radiotherapy; LVI = lymphovascular invasion; OR = odds ratio; pCR = pathological complete remission; pN = pathological nodal; PNI = perineural invasion; pT = pathological tumour; RT = radiotherapy; SCRT = short-course radiotherapy; ypN = posttreatment pathological nodal; ypT = posttreatment pathological tumour.

Table 4. (cont'd)

Variable	LRFS				DMRFS				OS			
	Simple OR (95% CI)	p Value	Multivariable OR (95% CI)	p Value	Simple OR (95% CI)	p Value	Multivariable OR (95% CI)	p Value	Simple OR (95% CI)	p Value	Multivariable OR (95% CI)	p Value
pN status (positive vs. negative)	1.474 (0.284-7.661)	0.645			1.368 (0.270-6.940)	0.705			1.259 (0.243-6.521)	0.784		
ypT stage												
0	1				1				1			
1	1.004 (0.063-16.1104)	0.998			2.236 (0.202-24.728)	0.512			1.057 (0.066-16.950)	0.969		
2	2.441 (0.283-21.053)	0.417			2.336 (0.272-20.070)	0.439			1.999 (0.222-18.041)	0.537		
3	3.149 (0.402-24.683)	0.275			3.148 (0.407-24.363)	0.272			2.488 (0.312-19.861)	0.390		
4	4.547 (0.411-50.261)	0.217			7.290 (0.657-80.841)	0.106			4.649 (0.420-51.418)	0.210		
ypN stage												
0	1				1				1			
1-2	7.072 (2.828-17.682)	<0.001	9.066 (3.291-24.972)	<0.001	5.557 (2.368-13.044)	<0.001	6.426 (1.944-21.244)	0.002	5.617 (2.124-14.857)	<0.001	11.750 (3.583-38.526)	<0.001
pCR (no vs. yes)	2.687 (0.357-20.195)	0.337			2.851 (0.382-21.284)	0.307			2.214 (0.291-16.814)	0.442		
Adjuvant chemotherapy (no vs. yes)	1.389 (0.547-3.528)	0.490			1.444 (0.686-3.038)	0.333			1.950 (0.866-4.392)	0.107		

Table 5. Comparison of grade 3 or above acute radiotherapy (RT) toxicities with and without elective inguinal RT.*

	Without elective inguinal RT (n = 81)	With elective inguinal RT (n = 9)	p Value
General adverse events			
Radiation dermatitis	12 (14.8%)	3 (33.3%)	0.347
Weight loss	0	0	
Fatigue/lethargy	0	0	
Hand-foot syndrome	0	0	
Haematologic	0	0	
Cardiac disorder	0	0	
Infection	0	0	
Gastrointestinal toxicity			
Mucositis	0	0	
Nausea and vomiting	0	0	
Diarrhoea	3 (3.7%)	0	
Abdominal pain	0	0	
Obstruction/constipation	1 (1.2%)	0	
Proctitis and rectal bleeding	0	0	
Total	4 (4.9%)	0	1.000

* Data are shown as No. (%), unless otherwise specified.

Table 6. Comparison of grade 3 or above chronic radiotherapy (RT) toxicities with and without elective inguinal RT.*

	Without elective inguinal RT (n = 81)	With elective inguinal RT (n = 9)	p Value
Perineal skin reaction	0	1 (11.1%)	0.100
Chronic gastrointestinal toxicities	6 (7.4%)	0	0.521

* Data are shown as No. (%), unless otherwise specified.

morbidity, and doubtful impact on subsequent clinical management, this is not currently a standard practice for low rectal cancer with ACI.

Only one patient (25%) developed isolated ILN metastases among all the four patients with inguinal recurrence. Salvage treatment for isolated ILN recurrence can provide long-term ILN control in our study. As a result, prophylactic treatment of the inguinal region may not be necessary. The other three patients (75%) who experienced inguinal recurrence had synchronous locoregional and/or distant recurrences. One may question whether early detection and treatment of occult inguinal nodal metastases can help prevent subsequent distant metastases. Damin et al[18] observed that despite inguinal dissection, 75% of sentinel ILN–positive cases developed hepatic or pulmonary metastases within 6 months of the surgery. Thus, localised treatment of the inguinal region may not affect the final clinical outcome, which is determined mainly by the occurrence of metastasis to distant organs.[19] In this context, a sentinel lymph node metastasis could represent a potential marker for systemic dissemination of the disease.[19]

From our results, patients who had positive pathological lymph node(s) following neoadjuvant therapy and/or a positive resection margin had an inferior rate of 3-year LRFS and OS, implying that more aggressive neoadjuvant treatment is needed to shrink the tumour before surgery, such as the addition of an induction or consolidation chemotherapy regimen. Several recently published large-scale randomised controlled trials consistently showed that total neoadjuvant treatment can improve disease-free survival, pathological complete remission rate, and the risk of disease-related treatment failure in patients with high-risk rectal cancer.[20-23] Among them, the phase 3 STELLAR trial was the first trial to demonstrate OS benefit, which found that short-course RT followed by perioperative chemotherapy resulted in better 3-year OS rates than CRT followed by postoperative chemotherapy, with 86.5% vs. 75.1% (OR = 0.67, 95% CI = 0.46-0.97; p = 0.033).[23] Furthermore, in our study, as compared to radiation alone, concomitant chemotherapy was linked with a superior LRFS and OS. A Cochrane review found that preoperative CRT improved local control (OR = 0.56, 95% CI = 0.42-0.75; p < 0.0001) in resectable stage III rectal cancer but did not increase OS (OR = 1.01, 95% CI = 0.85-1.20; p = 0.88).[24] The STELLAR OS benefit may be attributable to different patient selection criteria as our included patient population was restricted to low rectal cancer with ACI. This high-risk group may derive more benefit from concurrent chemotherapy. Additional studies are encouraged to validate the OS benefit of preoperative CRT against RT alone in resectable low rectal cancer with ACI.

Song et al[8] also investigated the impact of excluding irradiation of ILNs during neoadjuvant (chemo)RT in low rectal cancer with ACI. Their 3-year ILN failure rate was 3.7%. Our 3-year RFS rate (76.6% vs. 77.7%) is comparable to their disease-free survival rate, but our 3-year OS rate (86.8% vs. 91.9%) outcome appeared slightly inferior. Reasons for our relatively inferior OS may be multifactorial. Our research population had an older median age (67 years vs. 57 years). Our study also covered a small number of patients with worse Eastern Cooperative Oncology Group performance status (a score of 2) [6.7%], whereas their study only included individuals with a score of 0 to 1. Almost all of our patients (93.3%) received bolus 5-FU as concurrent chemotherapy, with the exception of one patient who received oral capecitabine, compared to 78.1% of capecitabine patients in their study.[8] Patients receiving prolonged 5-FU infusion had a significantly longer time to relapse and improved survival compared with bolus 5-FU.[11] Two randomised controlled trials have shown that patients with rectal cancer who received neoadjuvant or adjuvant capecitabine CRT had non-inferior disease-free and OS when compared to continuous 5-FU.[12,13] Therefore, concurrent chemotherapy with oral capecitabine should produce better outcomes compared with bolus 5-FU. In addition, induction (7.0%) and consolidation chemotherapy (30.8%) were used in their research, which might further improve treatment outcomes.[8]

Limitations

Our study had several limitations. First, it was a retrospective study based on data from a single centre, and this may add selection and information bias. Second, our small sample size reduced the power of the study. Despite a trend towards lower acute and chronic skin toxicity rates without inguinal RT, it did not reach statistical significance. In light of the small number of patients with inguinal RT and the retrospective nature of the study, these results should be interpreted with caution. Moreover, the elective inguinal RT group's small sample size may make it difficult to statistically compare survival rates with those who did not receive inguinal RT. Third, some baseline characteristics (i.e., baseline carcinoembryonic antigen level, clinical tumour staging, and proportion of patients receiving neoadjuvant vs. adjuvant radiation/chemoradiation therapy between

patients with or without elective inguinal irradiation) were imbalanced, and this might create bias to the interpretation of results. Lastly, as there was no uniform follow-up imaging in our study population, survival outcomes may have been overstated.

CONCLUSION

Omission of elective inguinal irradiation resulted in a low inguinal failure rate and similar survival outcomes for low rectal cancer patients with ACI. This study demonstrated that the majority of inguinal recurrences also had synchronous locoregional recurrence and/or distant failure, while isolated inguinal recurrences were uncommon and could be salvaged by inguinal dissection. These findings added to the body of evidence supporting the omission of elective ILN irradiation for this patient subgroup. Better-designed randomised studies are warranted to define the role of elective inguinal irradiation and to elucidate the best strategy for treatment escalation.

REFERENCES

1. Li Y, Wang J, Ma X, Tan L, Yan Y, Xue C, et al. A review of neoadjuvant chemoradiotherapy for locally advanced rectal cancer. Int J Biol Sci. 2016;12:1022-31.
2. Kachnic LA. Adjuvant chemoradiation for localized rectal cancer: current trends and future directions. Gastrointest Cancer Res. 2007;1(4 Suppl 2):S64-72.
3. Lee IK. The Lymphatic Spread of the Rectal Cancer. In: Kim NK, Sugihara K, Liang JT, editors. Surgical Treatment of Colorectal Cancer: Asian Perspectives on Optimization and Standardization. Singapore: Springer; 2018. p 47-53.
4. Glynne-Jones R, Wyrwicz L, Tiret E, Brown G, Rödel C, Cervantes A, et al. Rectal cancer: ESMO Clinical Practice Guidelines for diagnosis, treatment and follow-up. Ann Oncol. 2017;28(suppl_4):iv22-40.
5. Valentini V, Gambacorta MA, Barbaro B, Chiloiro G, Coco C, Das P, et al. International consensus guidelines on clinical target volume delineation in rectal cancer. Radiother Oncol. 2016;120:195-201.
6. Wo JY, Anker CJ, Ashman JB, Bhadkamkar NA, Bradfield L, Chang DT, et al. Radiation therapy for rectal cancer: executive summary of an ASTRO Clinical Practice Guideline. Pract Radiat Oncol. 2021;11:13-25.
7. Myerson RJ, Garofalo MC, El Naqa I, Abrams RA, Apte A, Bosch WR, et al. Elective clinical target volumes for conformal therapy in anorectal cancer: a Radiation Therapy Oncology Group consensus panel contouring atlas. Int J Radiat Oncol Biol Phys. 2009;74:824-30.
8. Song M, Li S, Zhang Y, Geng J, Wang H, Zhu X, et al. Is elective inguinal or external iliac irradiation during neoadjuvant (chemo) radiotherapy necessary for locally advanced lower rectal cancer with anal sphincter invasion? Pract Radiat Oncol. 2022;12:125-34.
9. Taylor N, Crane C, Skibber J, Feig B, Ellis L, Vauthey JN, et al. Elective groin irradiation is not indicated for patients with adenocarcinoma of the rectum extending to the anal canal. Int J Radiat Oncol Biol Phys. 2001;51:741-7.
10. Yeo SG, Lim HW, Kim DY, Kim TH, Kim SY, Baek JY, et al. Is elective inguinal radiotherapy necessary for locally advanced rectal adenocarcinoma invading anal canal? Radiat Oncol. 2014;9:296.
11. O'Connell MJ, Martenson JA, Wieand HS, Krook JE, Macdonald JS, Haller DG, et al. Improving adjuvant therapy for rectal cancer by combining protracted-infusion fluorouracil with radiation therapy after curative surgery. N Engl J Med. 1994;331:502-7.
12. Allegra CJ, Yothers G, O'Connell MJ, Beart RW, Wozniak TF, Pitot HC, et al. Neoadjuvant 5-FU or capecitabine plus radiation with or without oxaliplatin in rectal cancer patients: a phase III randomized clinical trial. J Natl Cancer Inst. 2015;107:djv248.
13. Hofheinz RD, Wenz F, Post S, Matzdorff A, Laechelt S, Hartmann JT, et al. Chemoradiotherapy with capecitabine versus fluorouracil for locally advanced rectal cancer: a randomised, multicentre, non-inferiority, phase 3 trial. Lancet Oncol. 2012;13:579-88.
14. Lee WR, McCollough WM, Mendenhall WM, Marcus RB Jr, Parsons JT, Million RR. Elective inguinal lymph node irradiation for pelvic carcinomas. The University of Florida experience. Cancer. 1993;72:2058-65.
15. Shiratori H, Nozawa H, Kawai K, Hata K, Tanaka T, Kaneko M, et al. Risk factors and therapeutic significance of inguinal lymph node metastasis in advanced lower rectal cancer. Int J Colorectal Dis. 2020;35:655-64.
16. Perez RO, Habr-Gama A, São Julião GP, Proscurshim I, Ono CR, Lynn P, et al. Clinical relevance of positron emission tomography/computed tomography–positive inguinal nodes in rectal cancer after neoadjuvant chemoradiation. Colorectal Dis. 2013;15:674-82.
17. Damin DC, Rosito MA, Schwartsmann G. Sentinel lymph node in carcinoma of the anal canal: a review. Eur J Surg Oncol. 2006;32:247-52.
18. Damin DC, Tolfo GC, Rosito MA, Spiro BL, Kliemann LM. Sentinel lymph node in patients with rectal cancer invading the anal canal. Tech Coloproctol. 2010;14:133-9.
19. van der Pas MH, Meijer S, Hoekstra OS, Riphagen II, de Vet HC, Knol DL, et al. Sentinel-lymph-node procedure in colon and rectal cancer: a systematic review and meta-analysis. Lancet Oncol. 2011;12:540-50.
20. Bahadoer RR, Dijkstra EA, van Etten B, Marijnen CA, Putter H, Kranenbarg EM, et al. Short-course radiotherapy followed by chemotherapy before total mesorectal excision (TME) versus preoperative chemoradiotherapy, TME, and optional adjuvant chemotherapy in locally advanced rectal cancer (RAPIDO): a randomised, open-label, phase 3 trial. Lancet Oncol. 2021;22:29-42.
21. Bujko K, Wyrwicz L, Rutkowski A, Malinowska M, Pietrzak L, Kryński J, et al. Long-course oxaliplatin-based preoperative chemoradiation versus 5 × 5 Gy and consolidation chemotherapy for cT4 or fixed cT3 rectal cancer: results of a randomized phase III study. Ann Oncol. 2016;27:834-42.
22. Conroy T, Bosset JF, Etienne PL, Rio E, François É, Mesgouez-Nebout N, et al. Neoadjuvant chemotherapy with FOLFIRINOX and preoperative chemoradiotherapy for patients with locally advanced rectal cancer (UNICANCER-PRODIGE 23): a multicentre, randomised, open-label, phase 3 trial. Lancet Oncol. 2021;22:702-15.
23. Jin J, Tang Y, Hu C, Jiang LM, Jiang J, Li N, et al. Multicenter, randomized, phase III trial of short-term radiotherapy plus chemotherapy versus long-term chemoradiotherapy in locally advanced rectal cancer (STELLAR). J Clin Oncol. 2022;40:1681-92.
24. McCarthy K, Pearson K, Fulton R, Hewitt J. Pre-operative chemoradiation for non-metastatic locally advanced rectal cancer. Cochrane Database Syst Rev. 2012;12:CD008368.

Hong Kong J Radiol. 2023;26:185-93. Epub 18 Sep 2023 | https://doi.org/10.12809/hkjr2217532

PERSPECTIVE

Four-Dimensional Computed Tomography for Localisation of Parathyroid Adenomas

HS Leung[1], SYW Liu[2], KT Wong[1], SM Yu[1], AD King[1]

[1]Department of Imaging and Interventional Radiology, Prince of Wales Hospital, Hong Kong SAR, China
[2]Department of Surgery, Prince of Wales Hospital, Hong Kong SAR, China

ABSTRACT

Primary hyperparathyroidism is a relatively common disorder with a myriad of end-organ manifestations, and surgical treatment remains the only curative option. Minimally invasive parathyroidectomy has replaced bilateral neck exploration as the standard technique for the majority of patients with solitary adenomas. Preoperative imaging is essential for accurate localisation of parathyroid adenomas. Four-dimensional computed tomography of the parathyroids has emerged as a useful problem-solving tool in the initial workup. This article reviews the underlying imaging principles, techniques, and practical tips on image interpretation and reporting, all of which are essential in successful preoperative localisation of parathyroid adenomas.

Key Words: *Hyperparathyroidism; Hyperparathyroidism, primary; Parathyroid neoplasms; Parathyroidectomy*

中文摘要

用於副甲狀腺腺瘤定位的四維電腦斷層掃描

梁皓生、廖玉華、黃嘉德、于雪梅、金雅桃

原發性副甲狀腺功能亢進症是一種相對常見的疾病，並會影響多重器官功能，手術治療仍然是唯一的治癒選擇。微創副甲狀腺切除術已取代雙側頸部探查而成為用於大多數單一副甲狀腺腺瘤患者的標準技術。術前影像學檢查對於準確定位副甲狀腺腺瘤至關重要。副甲狀腺四維電腦斷層掃描已成為術前檢查中解決問題的有用工具。本文回顧基本成像原理、技術及圖像解釋和報告的實用技巧，以上均對術前定位至關重要。

Correspondence: *Dr HS Leung, Department of Imaging and Interventional Radiology, Prince of Wales Hospital, Hong Kong SAR, China*
Email: lhs655@ha.org.hk

Submitted: 5 Feb 2022; Accepted: 17 May 2022.

Contributors: HSL and KTW designed the study. HSL, KTW and SMY acquired the data. HSL and SMY analysed the data. HSL and ADK drafted the manuscript. SYWL, KTW, SMY and ADK critically revised the manuscript for important intellectual content. All authors had full access to the data, contributed to the study, approved the final version for publication, and take responsibility for its accuracy and integrity.

Conflicts of Interest: All authors have disclosed no conflicts of interest.

Funding/Support: This study received no specific grant from any funding agency in the public, commercial, or not-for-profit sectors.

Data Availability: All data generated or analysed during the present study are available from the corresponding author on reasonable request.

Ethics Approval: The study was approved by the Joint Chinese University of Hong Kong–New Territories East Cluster Clinical Research Ethics Committee (Ref No.: 2022.069). A waiver for obtaining patient consent was granted by the Committee due to the retrospective nature of the study.

INTRODUCTION

Primary hyperparathyroidism is a relatively common disorder with an average population prevalence of 0.3%.[1,2] Long-term primary hyperparathyroidism with the accompanying hypercalcaemia may cause skeletal (pathological fractures), renal (nephrolithiasis, polyuria, and polydipsia), and gastrointestinal (peptic ulceration and pancreatitis) abnormalities. With more widespread use of biochemical screening in developed countries, the paradigm has shifted to an asymptomatic presentation, with or without elevated calcium levels.[3-7]

Surgical treatment remains the only curative option, with a shift in approach for the majority of patients with a solitary adenoma from bilateral neck exploration to minimally invasive parathyroidectomy (MIP),[8] offering similar outcomes with reduction in complications and shorter postoperative recovery.[8,9] Preoperative imaging localisation of the parathyroid glands is essential to a successful MIP. Traditionally achieved by ultrasound and/or technetium-99m (^{99m}Tc) sestamibi scintigraphy, in recent years four-dimensional computed tomography (4DCT) has emerged as a robust alternative modality, offering more accurate localisation.[10,11] This article on 4DCT reviews the technique, practical guidelines, and tips on what to look for; diagnostic performance; and advantages/disadvantages compared with other imaging modalities.

INDICATIONS FOR PARATHYROID IMAGING

International guidelines[12-14] have suggested that preoperative imaging for parathyroid localisation followed by parathyroidectomy is indicated when there is primary hyperparathyroidism together with any of the following conditions: (1) symptomatic hyperparathyroidism; (2) significantly elevated calcium levels (>1 mg/dL or 0.25 mmol/L above upper reference limit); (3) evidence of end-organ involvement, including renal (nephrocalcinosis, hypercalciuria, and impaired renal function) or skeletal (osteoporosis, fragility fractures as a manifestation of osteoporosis or vertebral insufficiency fractures); and (4) recurrent or persistent hyperparathyroidism after initial surgery.[15]

In addition, preoperative imaging followed by parathyroidectomy may also be considered when there is biochemical hyperparathyroidism in any of the following circumstances: (1) presence of neurocognitive or neuropsychiatric symptoms attributable to hyperparathyroidism[16]; (2) aged <50 years old, in the absence of symptoms or evidence of end-organ involvement; and (3) inability or unwillingness to comply with follow-up protocols after the initial diagnosis of primary hyperparathyroidism.

IMAGING TECHNIQUE

4DCT refers to evaluation of the lesions acquired in three dimensions[17] and their enhancement characteristics over time.[18] Various protocols with different timed phases have been established in the literature,[18] although it most commonly consists of an arterial phase at 25 to 30 seconds after contrast injection, together with venous phase at 45 to 60 seconds and/or a delayed phase at 80 to 90 seconds. A very delayed phase at approximately 120 seconds has also been adopted in some centres.[19] The addition of a non-contrast phase is also controversial; a previous study has demonstrated that 22% of parathyroid lesions might have been missed if a pre-contrast scan had been excluded,[20] although another retrospective study[21] showed that a two-phase protocol has only slightly reduced accuracy which has to be balanced with the radiation exposure of an additional phase. The use of dual energy acquisition to generate virtual non-contrast images for parathyroid adenomas have also been reported,[22,23] although in our experience the virtual non-contrast images based on subtraction of iodine signal also diminished the hyperattenuation of the normal thyroid parenchyma, rendering more difficult visualisation of the parathyroid glands in the perithyroidal region.

Optimisation of the imaging protocol is of foremost importance in achieving accurate parathyroid localisation. The range of scanning has to cover all potential sites of ectopic parathyroid glands, from angle of the mandible to the upper mediastinum at the level of the aortic arch, although the pre-contrast scan can be limited to the thyroid bed (from hyoid bone to the inferior margin of clavicular head).[17] Prior to scanning, a technique to move the shoulders down is also applied by asking the patient to pull tightly onto a traction bedsheet across his/her soles (Figure 1) so as to reduce the beam hardening artefacts over the lower pole of the thyroid, the level where inferior parathyroid adenomas are most commonly located (Figure 2).[17] A rapid rate of contrast injection (at least 4 mL/s) is also important to better demonstrate the differences in enhancement characteristics. Contrast injection should be performed via a right arm vein to minimise streak artefacts over the midline upper mediastinum and lower neck. In our centre, we perform a non-contrast scan through the thyroid bed, followed by an arterial phase at 25 seconds

Figure 1. Technique to lower the shoulders prior to scanning using a traction bedsheet strapped around the patient's soles.

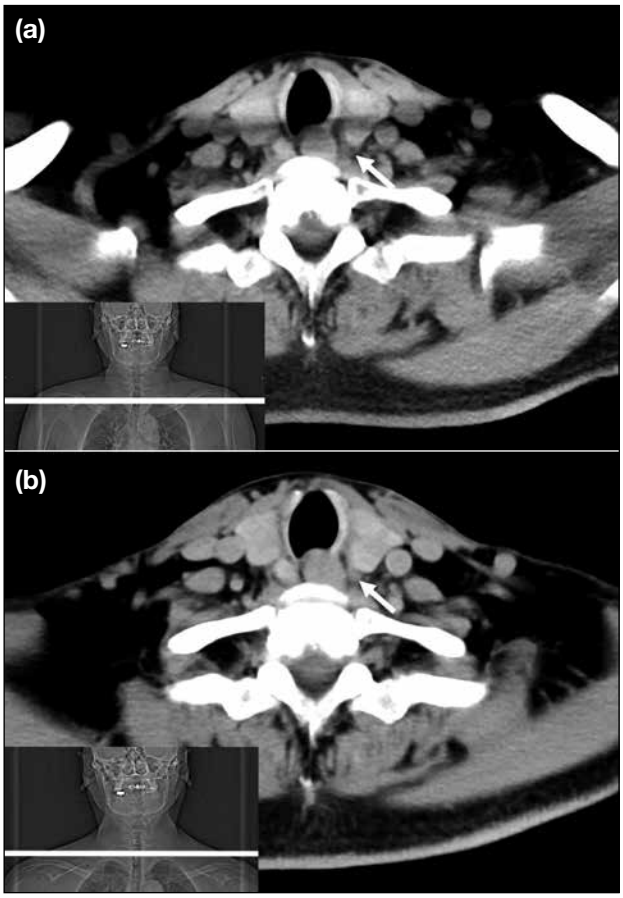

Figure 2. Pre-contrast images acquired without (a) and with (b) the use of the shoulder-lowering technique. With the technique, the shoulders are moved inferiorly to the level of the lower pole of the thyroid (scan plane is indicated by white line on the scanograms in the lower left-hand corner of [a] and [b]), with better demonstration of a small left-sided parathyroid adenoma (arrows) at this level.

and a delayed phase at 80 seconds in a caudocranial direction from the aortic arch through the mandibular angle. Scanning parameters using SOMATOM Drive system (Siemens Healthineers, Munich, Germany) are as follows: 100kV, 300 mA (pre-contrast) and 400 mA (arterial and delayed), pitch 0.8, and 0.6-mm section thickness with multiplanar reconstruction.

IMAGE INTERPRETATION AND REPORTING

A structured template for reporting is useful to ensure that all important areas for management are included.

How Many Lesions Are There?

Most cases of primary hyperparathyroidism (85%-90%) are the result of a solitary hyperfunctioning adenoma, with multiglandular disease (6%), double adenoma (4%), and carcinoma (1%) being less common. Conversely, most if not all second hyperparathyroidism from renal failure is due to multiglandular hyperplasia.

Practical tip

The number of enlarged, hyperfunctioning parathyroid glands is an important factor for surgical planning. Patients with solitary lesions are eligible for MIP while patients with >1 lesion may require a unilateral or bilateral neck exploration.

Position of Parathyroid Glands

Approximately 80% of patients have four normal glands in two symmetrical pairs. The superior glands originate from the fourth pharyngeal pouch and descend caudally, orthotopically located posterior to the upper two-thirds of the thyroid lobe (most at the equator of the gland) and posterior to the recurrent laryngeal nerve. The inferior parathyroid glands originate from the third pharyngeal pouch, joining the thymus with a longer route of descent and are usually found more ventrally around the inferior thyroid poles and anterior to the recurrent laryngeal nerve.[24,25] Supernumerary glands have been reported in approximately 15% of patients, while in 3% of cases only three glands can be found.[26]

Ectopic parathyroid glands have a prevalence of 14% to 16% in patients with hyperparathyroidism and up to 43% in anatomical studies.[27] Superior ectopic glands are most commonly found in the retro-oesophageal region and trachea-oesophageal groove.[28,29] These may result from over-descent in 10% to 20% of cases, mimicking, or

even more caudal to, an orthotopic inferior parathyroid.[30] Inferior ectopic parathyroid glands have a more variable location due to the longer descent, most commonly found in the thymic region and upper mediastinum with less common sites including undescended glands above the superior thyroid pole or within the carotid sheath.[28,29] Intrathyroid parathyroid glands have also been reported in 1% to 3% of patients[31,32] and are often difficult to detect by preoperative imaging or intra-operatively.

Practical tips

Firstly, a detailed description of location in relation to level and adjacent structures is required, such as hyoid, larynx, trachea, oesophagus, thyroid gland, carotid sheath, suprasternal notch, and mediastinal vessels. The relationship of an enlarged parathyroid gland to the trachea-oesophageal groove (expected location of recurrent laryngeal nerve) is also important, as superior parathyroid glands are posterior and inferior parathyroid glands are anterior to the groove (Figure 3). Secondly, check all areas from the angle of the mandible down to and including to the superior mediastinum. Lastly, the presence of an intervening fat plane is useful in distinguishing a parathyroid adenoma from a thyroid nodule, although this can be absent in small parathyroid adenomas within or abutting the thyroid capsule. It is therefore important to check all scanned phases, particularly the pre-contrast phase where parathyroid adenomas are relatively hypodense to the thyroid parenchyma.

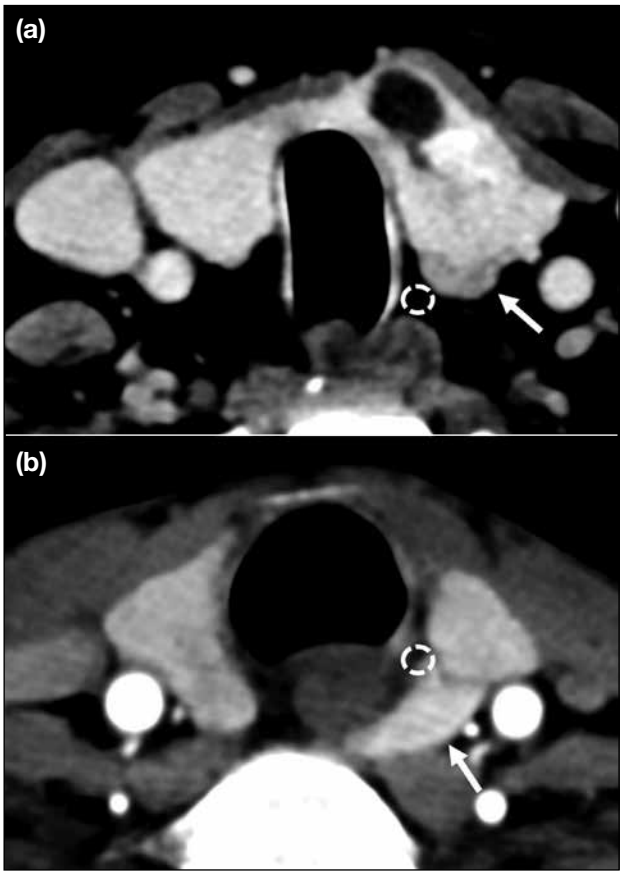

Figure 3. The trachea-oesophageal groove (dotted circles) is a useful landmark for the position of the recurrent laryngeal nerve. (a) Inferior parathyroid adenomas (arrow) lie anterior to the nerve and (b) superior parathyroid adenomas (arrow) lie posterior to it.

How to Call a Lesion as an Abnormal Parathyroid Gland?

Size and shape

The normal parathyroid gland is up to 2 mm in thickness and 5 to 10 mm in length[33]; hence, a gland is usually only visualised when enlarged and abnormal. Enlarged glands may be oval, round, pyramidal or lobulated and tend to be larger in parathyroid adenomas than multiple gland hyperplasia.

Enhancement pattern

The typical adenoma enhancement pattern would be hypodense to the thyroid on pre-contrast, hyperenhancing relative to the thyroid on arterial phase, and hypoenhancing on delayed phase. However, these imaging features are not consistently present in all parathyroid adenomas, as a recent study using dynamic CT[18] has demonstrated that hyperfunctioning parathyroid tissue only shows a short period of hyperenhancement relative to the thyroid, with vast heterogeneity in the presence and timing of hyperenhancement amongst different adenomas. Three types of variations in enhancement have been previously described (Figures 4 to 6).[20]

Ancillary features

The presence of a fat plane between the nodule and thyroid is used to discriminate a parathyroid adenoma from a thyroid nodule.

The presence of a polar vessel[34] entering the superior or inferior pole of the parathyroid is a useful ancillary feature to support the diagnosis of parathyroid adenoma (Figure 7a). Rim or central calcification (Figure 7b), internal cystic changes, or necrosis have been described as variant appearances of parathyroid adenomas, which can be present in up to 10% of cases.[35,36] Acute necrosis in a parathyroid adenoma has been associated with spontaneous reduction in hormone levels.[37] Accurate differentiation of parathyroid carcinoma from adenoma is difficult,[38] although the presence of a large (>3 cm)

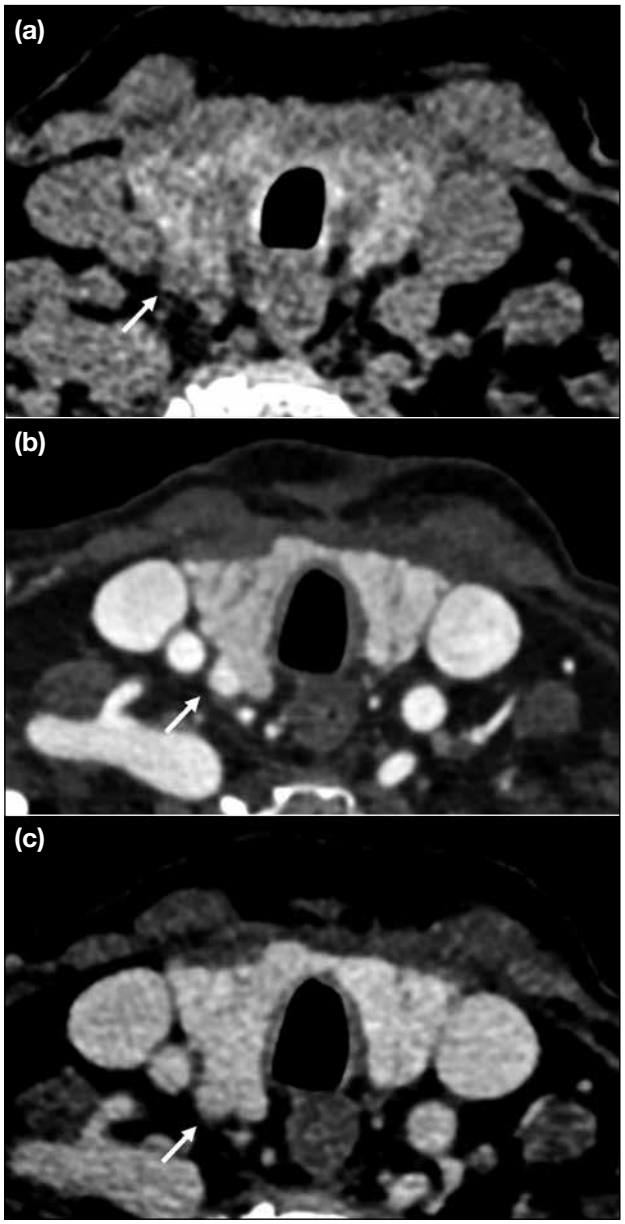

Figure 4. Parathyroid adenoma (arrows) with type A enhancement. It is hypodense to the adjacent thyroid parenchyma on pre-contrast imaging (a), hyperdense compared to the thyroid during the arterial phase (b), and isodense compared to the thyroid with contrast washout (c).

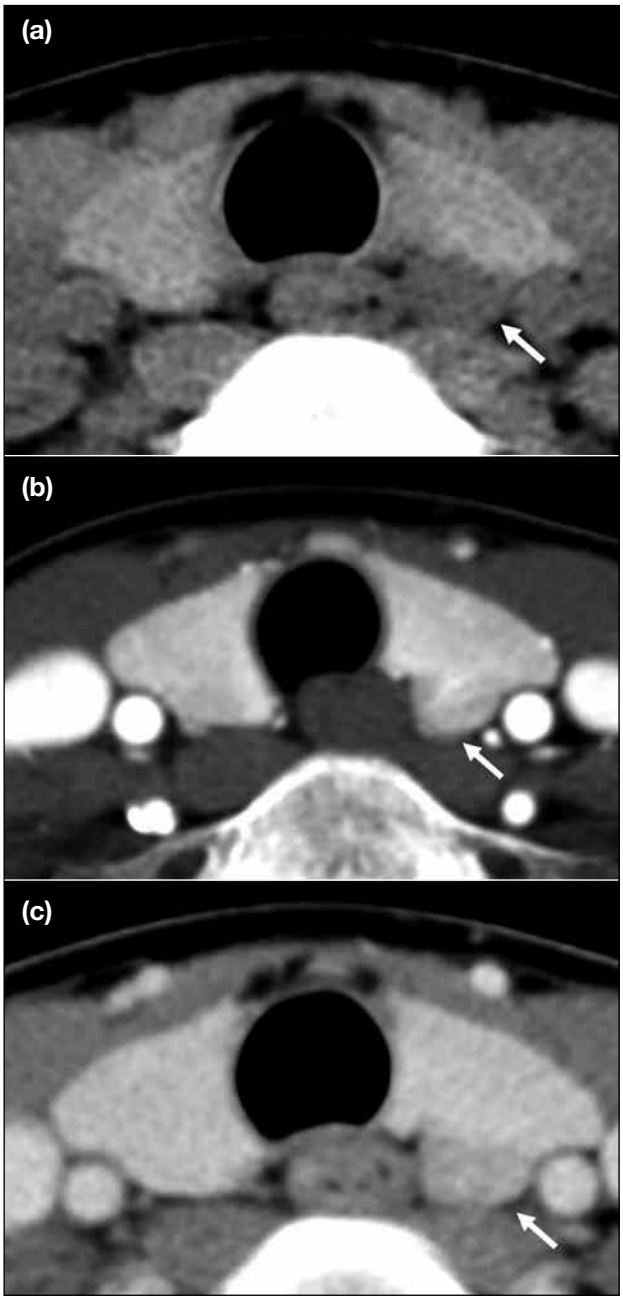

Figure 5. Parathyroid adenoma (arrows) with type B enhancement, defined by the absence of arterial hyperenhancement but presence of delayed phase hypoenhancement relative to the thyroid. It is hypodense to the adjacent thyroid parenchyma on the pre-contrast phase (a), showing hypodensity compared to the thyroid on the arterial phase (b) but with delayed phase hypoenhancement (c).

parathyroid gland, irregular borders and peritumoural infiltration into adjacent structures aids in distinguishing carcinoma from adenoma.[39,40]

Practical tips

Firstly, small lymph nodes may be mistaken for parathyroid adenomas, although the presence of progressive enhancement on delayed phase and the presence of a fatty hilum are useful distinguishing features. Secondly, for indeterminate lesions it is important to review previous ultrasound and scintigraphy, as lesions concordant with previous imaging findings afford much more diagnostic confidence. Repeating the ultrasound, especially in

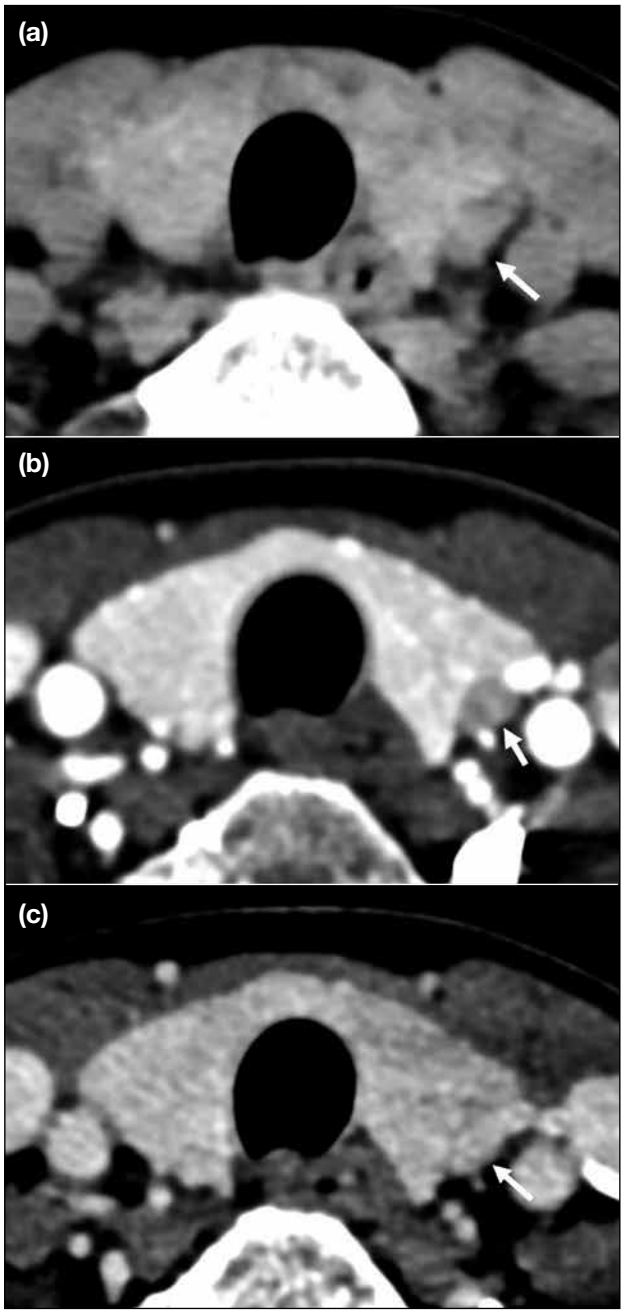

Figure 6. Parathyroid adenoma (arrows) with type C enhancement, defined by absence of arterial phase hyperenhancement and delayed phase hypoenhancement relative to the thyroid. It is hypodense on the pre-contrast phase (a) and shows hypoenhancement on the arterial phase (b) and isoenhancement on the delayed phase (c). Contrast enhancement is still demonstrated in the venous and delayed phases, with slight washout on the delayed phase (Hounsfield unit on pre-contrast +33, arterial phase +148, and delayed phase +122).

cases where a previous study was negative or discordant from 4DCT, is an important problem-solving tool and increases diagnostic confidence without incurring additional radiation exposure (Figure 8).

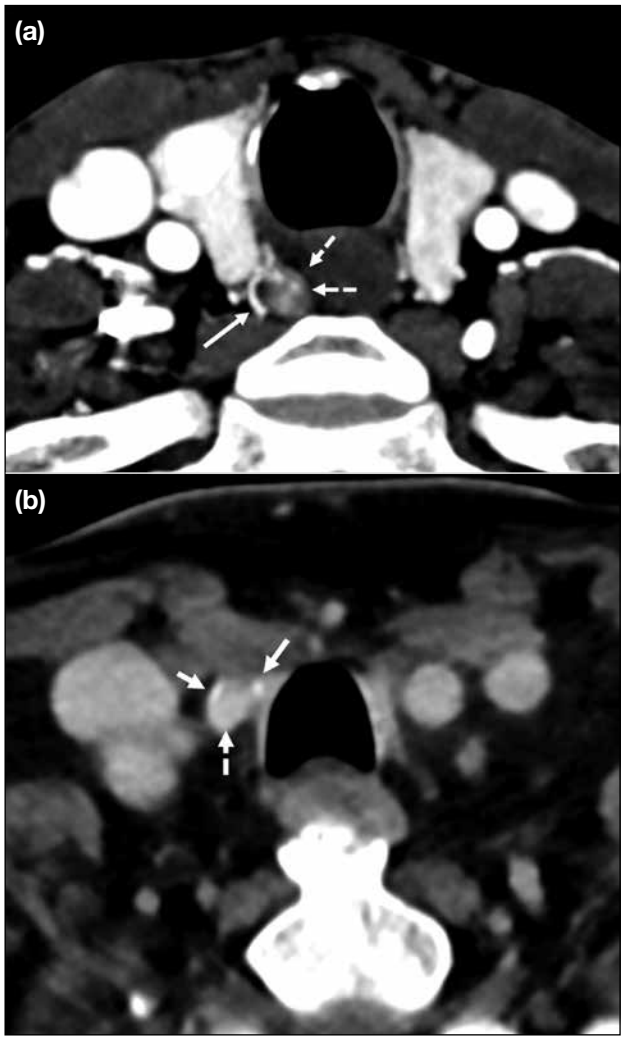

Figure 7. Ancillary features suggestive of parathyroid adenoma (dashed arrows) include presence of a polar vessel (solid arrow in [a]) and peripheral rim calcification (solid arrows in [b]).

Other Important Findings which may Affect Surgical Planning

The presence of concomitant thyroid nodules should be reported, which requires further evaluation with ultrasound and/or fine-needle aspiration cytology, as any suspicious thyroid nodule would necessitate a hemi- or total thyroidectomy in the same operation. This is also useful in investigating the possibility of a rare intrathyroid parathyroid adenoma, especially in patients where no other candidate lesion is identified. In addition, the presence of anomalies of the major arteries, such as an aberrant right subclavian artery, which can be associated with a non-recurrent laryngeal nerve,[41] should be highlighted as this constitutes potential

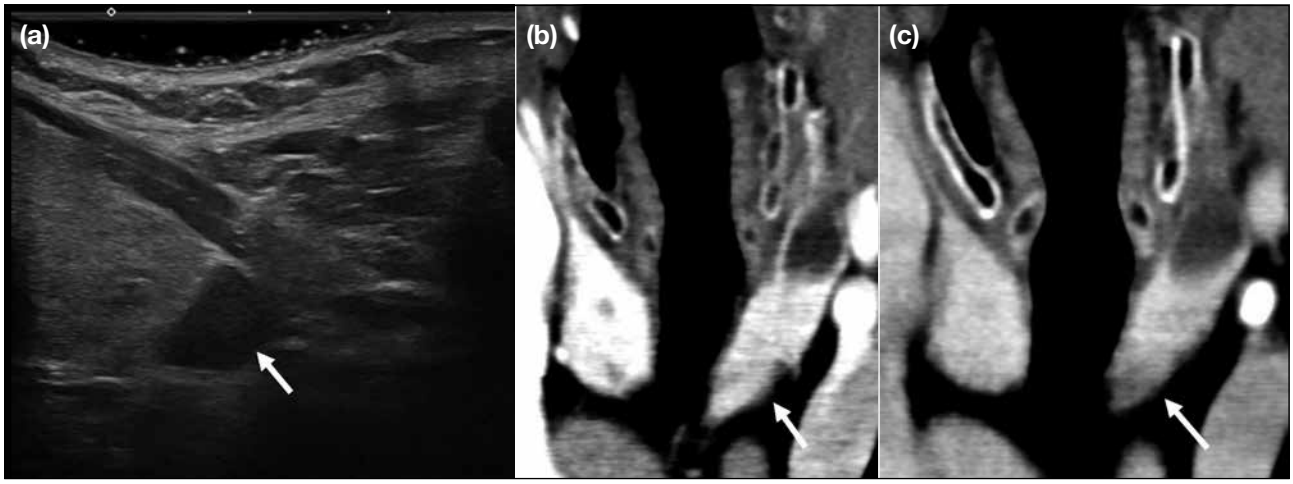

Figure 8. Ultrasound as a useful adjunct to four-dimensional computed tomography (4DCT) in problem solving. The parathyroid adenoma (arrows) is more conspicuous on this longitudinal ultrasound image showing the left lower pole of the thyroid (a), while it is only barely conspicuous on the arterial phase (b) and delayed phase (c) of 4DCT.

surgical hazard. Evidence of any previous head and neck surgery and altered anatomy should also be identified for accurate operative planning.

Performance of Four-Dimensional Computed Tomography and Comparison with Other Imaging Modalities

Ultrasound, nuclear scintigraphy, and 4DCT are widely accepted modalities for parathyroid localisation.[42] While 4DCT has been adopted in some centres as first-line imaging,[43] the choice and sequence of imaging investigations remain variable across centres depending on availability and expertise.[44,45] One of the main advantages of 4DCT is the ability to clearly demonstrate to the surgeon the location of a parathyroid adenoma and its relationship to adjacent structures. Multiple studies have proven 4DCT as a robust technique in parathyroid localisation,[10,19,44,46] with the latest meta-analysis showing a sensitivity of 81% and positive predictive value of 91%.[47] The 4DCT has been shown to be superior to ^{99m}Tc sestamibi and ultrasound for localisation in several studies,[10,11,48] although some other studies showed no significant difference in diagnostic accuracy.[49,50] In our centre, a combination of parathyroid ultrasound and ^{99m}Tc sestamibi scintigraphy, which are more readily available, still serves as a first-line diagnostic approach while 4DCT is reserved for patients with negative or discordant localisation. Repeated parathyroid ultrasound in the same session as 4DCT can often enhance diagnostic confidence.

The 4DCT technique has also been proven useful in hyperparathyroid patients with previously negative ultrasound and/or scintigraphy.[51] Limited studies have also explored its application in patients with secondary hyperparathyroidism,[52] in whom bilateral neck exploration remains mandatory but which can identify ectopic or supernumerary glands to improve the rate of surgical success.[44]

The issue of radiation exposure is also of concern. A previous study by Mahajan et al[53] has shown that the effective dose of 4DCT (10.4 mSv) is higher than ^{99m}Tc sestamibi scintigraphy (7.8 mSv). Although more recent studies have demonstrated a lower effective dose of 4DCT (4.5-8.9 mSv),[43] the organ dose to the thyroid bed from 4DCT remains significantly higher. The risk of attributed malignancy to radiation exposure from 4DCT should be balanced with the benefit of reducing surgical morbidity, by converting to a less complex MIP and lower chance of reoperation. This is especially helpful in younger patients where radiation exposure bears a more significant long-term cumulative effect. Despite a younger age of presentation of hyperparathyroidism in the Chinese population,[54] the majority of patients are still >50 years of age and the benefits of proceeding with 4DCT examination is mostly justified. In our institution, a combination of ultrasound and ^{99m}Tc sestamibi scintigraphy remains the initial investigation, with patients referred for 4DCT if the initial workup is inconclusive.

Finally, it is important to emphasise that all modalities have their advantages and disadvantages. Therefore, a multimodality approach and careful review of all previous parathyroid imaging studies are the keys to increase diagnostic confidence.

SUMMARY

4DCT of the parathyroids offers a promising alternative for preoperative localisation of parathyroid adenoma, not only as a problem-solving tool but with potential for becoming the modality of choice in the initial workup. A good understanding of underlying anatomy and imaging principles, optimisation of CT protocol, correlation with other imaging modalities, and structured reporting tailored to answer specific question by surgeons are all important in delivering accurate preoperative localisation for better surgical outcomes.

REFERENCES

1. Adami S, Marcocci C, Gatti D. Epidemiology of primary hyperparathyroidism in Europe. J Bone Miner Res. 2002;17 Suppl 2:N18-23.
2. Christensson T, Hellström K, Wengle B, Alveryd A, Wikland B. Prevalence of hypercalcaemia in a health screening in Stockholm. Acta Med Scand. 1976;200:131-7.
3. Pradeep PV, Jayashree B, Mishra A, Mishra SK. Systematic review of primary hyperparathyroidism in India: the past, present, and the future trends. Int J Endocrinol. 2011;2011:921814.
4. Liu JM, Cusano NE, Silva BC, Zhao L, He XY, Tao B, et al. Primary hyperparathyroidism: a tale of two cities revisited—New York and Shanghai. Bone Res. 2013;1:162-9.
5. Insogna KL. Primary hyperparathyroidism. N Engl J Med. 2018;379:1050-9.
6. Dawood NB, Yan KL, Shieh A, Livhits MJ, Yeh MW, Leung AM. Normocalcaemic primary hyperparathyroidism: an update on diagnostic and management challenges. Clin Endocrinol (Oxf). 2020;93:519-27.
7. Walker MD, Silverberg SJ. Primary hyperparathyroidism. Nat Rev Endocrinol. 2018;14:115-25.
8. Laird AM, Libutti SK. Minimally invasive parathyroidectomy versus bilateral neck exploration for primary hyperparathyroidism. Surg Oncol Clin N Am. 2016;25:103-18.
9. Udelsman R, Lin Z, Donovan P. The superiority of minimally invasive parathyroidectomy based on 1650 consecutive patients with primary hyperparathyroidism. Ann Surg. 2011;253:585-91.
10. Yeh R, Tay YD, Tabacco G, Dercle L, Kuo JH, Bandeira L, et al. Diagnostic performance of 4D CT and sestamibi SPECT/CT in localizing parathyroid adenomas in primary hyperparathyroidism. Radiology. 2019;291:469-76.
11. Cheung K, Wang TS, Farrokhyar F, Roman SA, Sosa JA. A meta-analysis of preoperative localization techniques for patients with primary hyperparathyroidism. Ann Surg Oncol. 2012;19:577-83.
12. National Institute for Health and Care Excellence. Hyperparathyroidism (primary): diagnosis, assessment and initial treatment. London: National Institute for Health and Care Excellence; 2019.
13. Wilhelm SM, Wang TS, Ruan DT, Lee JA, Asa SL, Duh QY, et al. The American Association of Endocrine Surgeons Guidelines for Definitive Management of Primary Hyperparathyroidism. JAMA Surg. 2016;151:959-68.
14. Bilezikian JP, Brandi ML, Eastell R, Silverberg SJ, Udelsman R, Marcocci C, et al. Guidelines for the management of asymptomatic primary hyperparathyroidism: summary statement from the Fourth International Workshop. J Clin Endocrinol Metab. 2014;99:3561-9.
15. Stack BC Jr, Tolley NS, Bartel TB, Bilezikian JP, Bodenner D, Camacho P, et al. AHNS Series: Do you know your guidelines? Optimizing outcomes in reoperative parathyroid surgery: definitive multidisciplinary joint consensus guidelines of the American Head and Neck Society and the British Association of Endocrine and Thyroid Surgeons. Head Neck. 2018;40:1617-29.
16. Walker MD, McMahon DJ, Inabnet WB, Lazar RM, Brown I, Vardy S, et al. Neuropsychological features in primary hyperparathyroidism: a prospective study. J Clin Endocrinol Metab. 2009;94:1951-8.
17. Hoang JK, Sung WK, Bahl M, Phillips CD. How to perform parathyroid 4D CT: tips and traps for technique and interpretation. Radiology. 2014;270:15-24.
18. Raeymaeckers S, De Brucker Y, Vanderhasselt T, Buls N, De Mey J. Detection of parathyroid adenomas with multiphase 4DCT: towards a true four-dimensional technique. BMC Med Imaging. 2021;21:64.
19. Starker LF, Mahajan A, Björklund P, Sze G, Udelsman R, Carling T. 4D parathyroid CT as the initial localization study for patients with de novo primary hyperparathyroidism. Ann Surg Oncol. 2011;18:1723-8.
20. Bahl M, Sepahdari AR, Sosa JA, Hoang JK. Parathyroid adenomas and hyperplasia on four-dimensional CT scans: three patterns of enhancement relative to the thyroid gland justify a three-phase protocol. Radiology. 2015;277:454-62.
21. Griffith B, Chaudhary H, Mahmood G, Carlin AM, Peterson E, Singer M, et al. Accuracy of 2-phase parathyroid CT for the preoperative localization of parathyroid adenomas in primary hyperparathyroidism. AJNR Am J Neuroradiol. 2015;36:2373-9.
22. Leiva-Salinas C, Flors L, Durst CR, Hou Q, Patrie JT, Wintermark M, et al. Detection of parathyroid adenomas using a monophasic dual-energy computed tomography acquisition: diagnostic performance and potential radiation dose reduction. Neuroradiology. 2016;58:1135-41.
23. Roskies M, Liu X, Hier MP, Payne RJ, Mlynarek A, Forest V, et al. 3-phase dual-energy CT scan as a feasible salvage imaging modality for the identification of non-localizing parathyroid adenomas: a prospective study. J Otolaryngol Head Neck Surg. 2015;44:44.
24. Mohebati A, Shaha AR. Anatomy of thyroid and parathyroid glands and neurovascular relations. Clin Anat. 2012;25:19-31.
25. Kunstman JW, Kirsch JD, Mahajan A, Udelsman R. Clinical review: parathyroid localization and implications for clinical management. J Clin Endocrinol Metab. 2013;98:902-12.
26. Akerström G, Malmaeus J, Bergström R. Surgical anatomy of human parathyroid glands. Surgery. 1984;95:14-21.
27. Noussios G, Anagnostis P, Natsis K. Ectopic parathyroid glands and their anatomical, clinical and surgical implications. Exp Clin Endocrinol Diabetes. 2012;120:604-10.
28. Phitayakorn R, McHenry CR. Incidence and location of ectopic abnormal parathyroid glands. Am J Surg. 2006;191:418-23.
29. Roy M, Mazeh H, Chen H, Sippel RS. Incidence and localization of ectopic parathyroid adenomas in previously unexplored patients. World J Surg. 2013;37:102-6.
30. Duke WS, Vernon HM, Terris DJ. Reoperative parathyroidectomy: overly descended superior adenoma. Otolaryngol Head Neck Surg. 2016;154:268-71.

31. Goodman A, Politz D, Lopez J, Norman J. Intrathyroid parathyroid adenoma: incidence and location—the case against thyroid lobectomy. Otolaryngol Head Neck Surg. 2011;144:867-71.
32. McIntyre RC Jr, Eisenach JH, Pearlman NW, Ridgeway CE, Liechty RD. Intrathyroidal parathyroid glands can be a cause of failed cervical exploration for hyperparathyroidism. Am J Surg. 1997;174:750-3; discussion 753-4.
33. Grimelius L, Bondeson L. Histopathological diagnosis of parathyroid diseases. Pathol Res Pract. 1995;191s:353-65.
34. Bahl M, Muzaffar M, Vij G, Sosa JA, Choudhury KR, Hoang JK. Prevalence of the polar vessel sign in parathyroid adenomas on the arterial phase of 4D CT. AJNR Am J Neuroradiol. 2014;35:578-81.
35. Chandramohan A, Sathyakumar K, John RA, Manipadam MT, Abraham D, Paul TV, et al. Atypical ultrasound features of parathyroid tumours may bear a relationship to their clinical and biochemical presentation. Insights Imaging. 2014;5:103-11.
36. Ahuja AT, Wong KT, Ching AS, Fung MK, Lau JY, Yuen EH, et al. Imaging for primary hyperparathyroidism—what beginners should know. Clin Radiol. 2004;59:967-76.
37. Chan WB, Chow CC, King AD, Yeung VT, Li JK, So WY, et al. Spontaneous necrosis of parathyroid adenoma: biochemical and imaging follow-up for two years. Postgrad Med J. 2000;76:96-8.
38. Al-Kurd A, Mekel M, Mazeh H. Parathyroid carcinoma. Surg Oncol. 2014;23:107-14.
39. Ferraro V, Sgaramella LI, Di Meo G, Prete FP, Logoluso F, Minerva F, et al. Current concepts in parathyroid carcinoma: a single centre experience. BMC Endocr Disord. 2019;19(Suppl 1):46.
40. Takumi K, Fukukura Y, Hakamada H, Nagano H, Kumagae Y, Arima H, et al. CT features of parathyroid carcinomas: comparison with benign parathyroid lesions. Jpn J Radiol. 2019;37:380-9.
41. Henry BM, Sanna S, Graves MJ, Vikse J, Sanna B, Tomaszewska IM, et al. The non-recurrent laryngeal nerve: a meta-analysis and clinical considerations. PeerJ. 2017;5:e3012.
42. Bunch PM, Randolph GW, Brooks JA, George V, Cannon J, Kelly HR. Parathyroid 4D CT: what the surgeon wants to know. Radiographics. 2020;40:1383-94.
43. Leong D, Ng K, Boeddinghaus R, Lisewski D. Three-phase four-dimensional computed tomography as a first-line investigation in primary hyperparathyroidism. ANZ J Surg. 2021;91:1798-803.
44. Expert Panel on Neurological Imaging; Zander D, Bunch PM, Policeni B, Juliano AF, Carneiro-Pla D, et al. ACR Appropriateness Criteria® Parathyroid Adenoma. J Am Coll Radiol. 2021; 18(11S):S406-22.
45. Bunch PM, Kelly HR. Preoperative imaging techniques in primary hyperparathyroidism: a review. JAMA Otolaryngol Head Neck Surg. 2018;144:929-37.
46. Brown SJ, Lee JC, Christie J, Maher R, Sidhu SB, Sywak MS, et al. Four-dimensional computed tomography for parathyroid localization: a new imaging modality. ANZ J Surg. 2015;85:483-7.
47. Sun L, Yao J, Hao P, Yang Y, Liu Z, Peng R. Diagnostic role of four-dimensional computed tomography for preoperative parathyroid localization in patients with primary hyperparathyroidism: a systematic review and meta-analysis. Diagnostics (Basel). 2021;11:664.
48. Suh YJ, Choi JY, Kim SJ, Chun IK, Yun TJ, Lee KE, et al. Comparison of 4D CT, ultrasonography, and ^{99m}Tc sestamibi SPECT/CT in localizing single-gland primary hyperparathyroidism. Otolaryngol Head Neck Surg. 2015;152:438-43.
49. Wan QC, Li JF, Tang LL, Lv J, Xie LJ, Li JP, et al. Comparing the diagnostic accuracy of 4D CT and ^{99m}Tc-MIBI SPECT/CT for localizing hyperfunctioning parathyroid glands: a systematic review and meta-analysis. Nucl Med Commun. 2021;42:225-33.
50. Krakauer M, Wieslander B, Myschetzky PS, Lundstrøm A, Bacher T, Sørensen CH, et al. A prospective comparative study of parathyroid dual-phase scintigraphy, dual-isotope subtraction scintigraphy, 4D-CT, and ultrasonography in primary hyperparathyroidism. Clin Nucl Med. 2016;41:93-100.
51. Beland MD, Mayo-Smith WW, Grand DJ, Machan JT, Monchik JM. Dynamic MDCT for localization of occult parathyroid adenomas in 26 patients with primary hyperparathyroidism. AJR Am J Roentgenol. 2011;196:61-5.
52. Hiramitsu T, Tomosugi T, Okada M, Futamura K, Tsujita M, Goto N, et al. Pre-operative localisation of the parathyroid glands in secondary hyperparathyroidism: a retrospective cohort study. Sci Rep. 2019;9:14634.
53. Mahajan A, Starker LF, Ghita M, Udelsman R, Brink JA, Carling T. Parathyroid four-dimensional computed tomography: evaluation of radiation dose exposure during preoperative localization of parathyroid tumors in primary hyperparathyroidism. World J Surg. 2012;36:1335-9.
54. Zhao L, Liu JM, He XY, Zhao HY, Sun LH, Tao B, et al. The changing clinical patterns of primary hyperparathyroidism in Chinese patients: data from 2000 to 2010 in a single clinical center. J Clin Endocrinol Metab. 2013;98:721-8.

Hong Kong J Radiol. 2023;26:194-7. Epub 4 Sep 2023 | https://doi.org/10.12809/hkjr2117505

CASE REPORT

Rupture of Renal Pelvis Secondary to Obstructing Calculus in Menkes Disease: A Case Report

TM Chiu, KKF Fung, EYL Kan

Department of Radiology, Hong Kong Children's Hospital, Hong Kong SAR, China

INTRODUCTION

Menkes disease is a rare X-linked hereditary multisystem disorder due to a defect in copper metabolism caused by a mutation in the *ATP7A* gene.[1] Patients can present with neurodegenerative manifestations and multiple connective tissue abnormalities.[1] We report the case of a 4-year-old boy, known to have Menkes disease, who presented with an obstructive ureteric stone complicated by rupture of the renal pelvis.

CASE REPORT

Our patient was diagnosed with Menkes disease at 6 months of age. Since then, he has developed recurrent urinary tract infections, attributed to the presence of multiple urinary bladder diverticula. He has received copper histidine injections since around 8 months of age and clean intermittent catheterisation since 19 months of age.

The patient presented with an episode of abdominal distension and septicaemia at the age of 4. There was no history of recent surgery or trauma. Ultrasound of the abdomen and pelvis revealed right-sided hydronephrosis and fluid collections around the right perinephric and right subphrenic regions (Figure 1). Further contrast-enhanced computed tomography (CT) scan of the abdomen and pelvis showed an obstructing stone at the right proximal ureter with gross upstream hydroureteronephrosis. Delayed phase images were subsequently obtained at 60 minutes post injection and confirmed the presence of a mural defect at the posterior aspect of the right renal pelvis with contrast extravasation from the corresponding area and contrast pooling around the right perinephric region (Figure 2). A ruptured right renal pelvis was diagnosed.

Following diagnosis, insertion of a double-J stent was attempted for urinary diversion but was unsuccessful due to difficulty in identifying the ureteric orifice in the presence of multiple urinary diverticula. Percutaneous nephrostomy was performed instead the following day. Ultrasound-guided drainage of a retroperitoneal collection was also performed subsequently for control of sepsis.

Correspondence: *Dr TM Chiu, Department of Radiology, Hong Kong Children's Hospital, Hong Kong SAR, China*
Email: ctm537@ha.org.hk

Submitted: 20 Nov 2021; Accepted: 7 Apr 2022.

Contributors: All authors designed the study, acquired and analysed the data. TMC drafted the manuscript. KKFF and EYLK critically revised the manuscript for important intellectual content. All authors had full access to the data, contributed to the study, approved the final version for publication, and take responsibility for its accuracy and integrity.

Conflicts of Interest: As an editor of the journal, KKFF was not involved in the peer review process. Other authors have disclosed no conflicts of interest.

Funding/Support: This study received no specific grant from any funding agency in the public, commercial, or not-for-profit sectors.

Data Availability: All data generated or analysed during the present study are available from the corresponding author on reasonable request.

Ethics Approval: The study was approved by the Hong Kong Children's Hospital Research Ethics Committee (Ref No.: HKCH-REC-2021-017). The patient was treated in accordance with the Declaration of Helsinki. Consent for publication was obtained from the patient's parent.

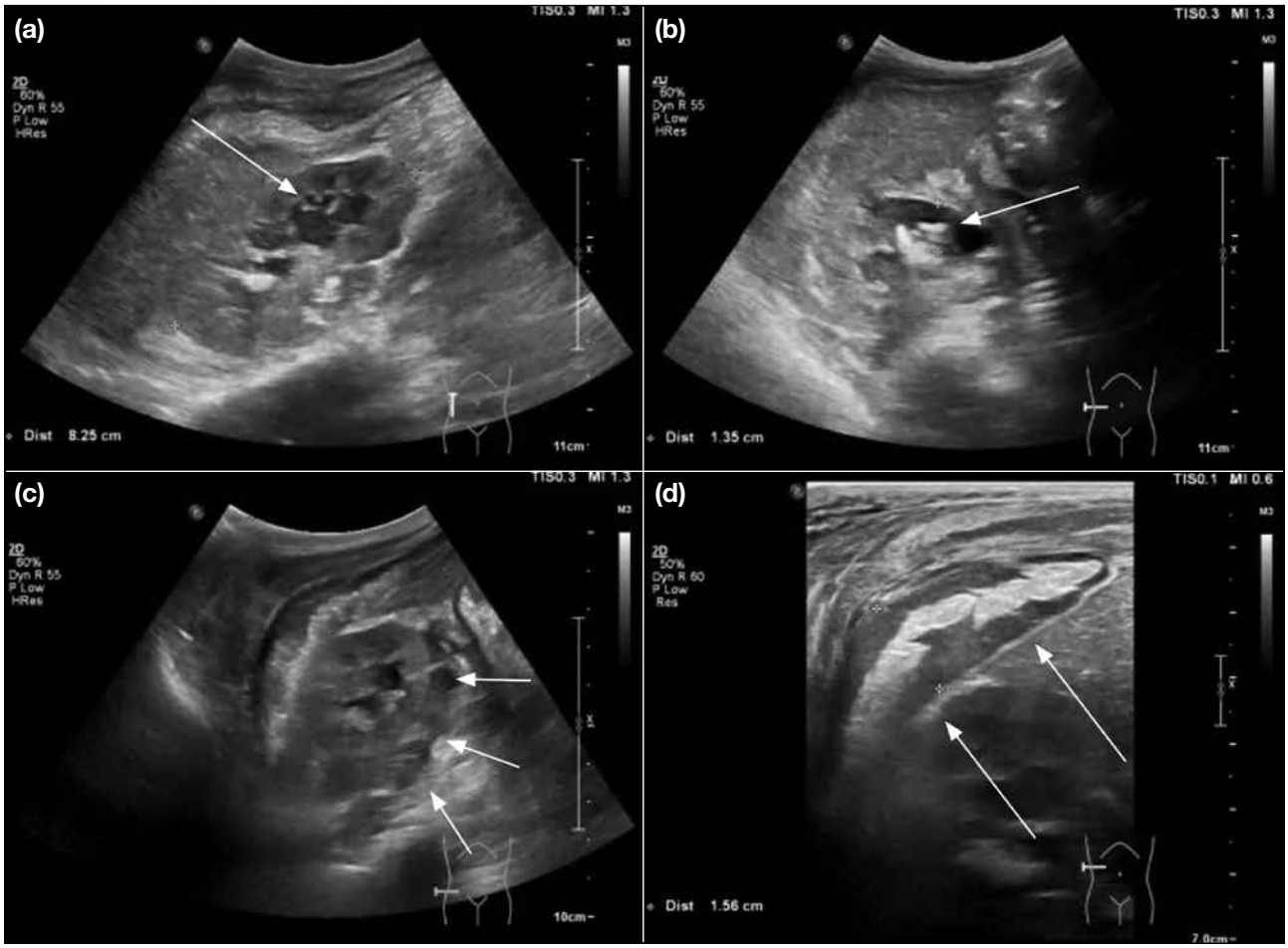

Figure 1. Ultrasound images of the patient annotated with arrows showing (a) dilated calyces at the right kidney, (b) stones within dilated right renal pelvis, (c) perinephric collection at the posterolateral aspect of the right kidney, and (d) right subphrenic collection.

Open pyeloplasty was performed around 2 months after the first presentation as underlying ureteric stricture was suspected. Surgery was unsuccessful and complicated by persistent stricture. Further balloon dilatation was attempted but this also failed. After multidisciplinary discussion, a decision was made for a long-term internal ureteric stent to remain in situ. Our patient is now well following removal of the percutaneous nephrostomy catheter. A ureteric stent remains in situ and clean intermittent catheterisation continues.

DISCUSSION

Menkes disease has an estimated incidence of 1 in 35 000 population[2] to 1 in 360 000 population[1], varying widely in different localities. The *ATP7A* gene encodes a protein that is responsible for transcellular copper transport. A defect in such protein causes impaired copper absorption in the intestines and consequent copper deficiency. This in turn results in reduced activity of various copper-dependent enzymes throughout the body, leading to neurodegeneration and defective connective tissue synthesis, manifesting in the form of connective tissue abnormalities such as frail hypopigmented hair and vascular tortuosity (Figure 3).[1]

Urological abnormalities are also frequent in Menkes disease. While the most common is urinary bladder diverticula (Figure 4), others such as vesicoureteric reflux, dilatation of the pelvicalyceal system and/or ureters, and rupture of urinary bladder diverticula have also been reported. These conditions may lead to urinary stasis and can predispose patients to recurrent urinary tract infections and urinary calculus formation.[3]

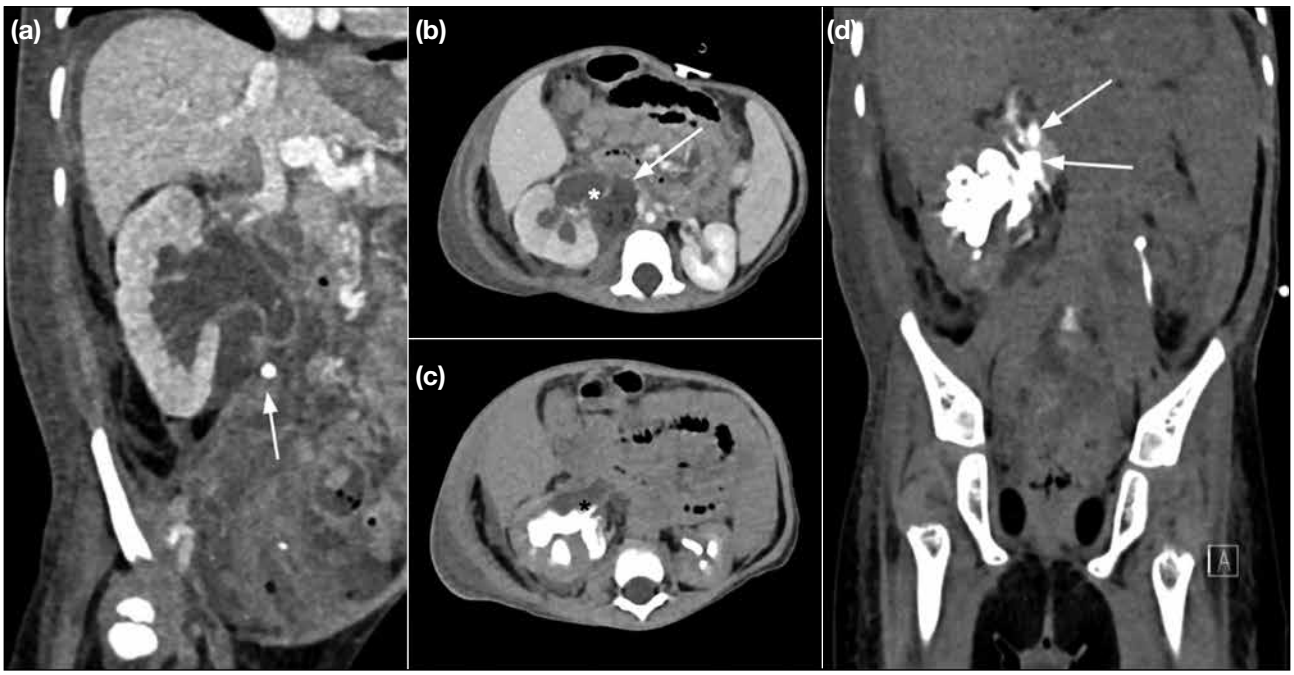

Figure 2. Contrast-enhanced computed tomography of the abdomen and pelvis of the patient. (a) Oblique coronal image showing an obstructing calculus at the right proximal ureter (arrow) with upstream hydronephrosis. (b) Axial image showing right hydronephrosis with focal mural defect (white asterisk) at the posterior aspect of the right renal pelvis and associated perinephric fluid collection (arrow) on axial images. (c) Delayed phase axial image showing contrast extravasation (black asterisk) from the renal pelvis. (d) Delayed phase coronal image showing contrast extravasation and pooling around the perinephric region (arrows).

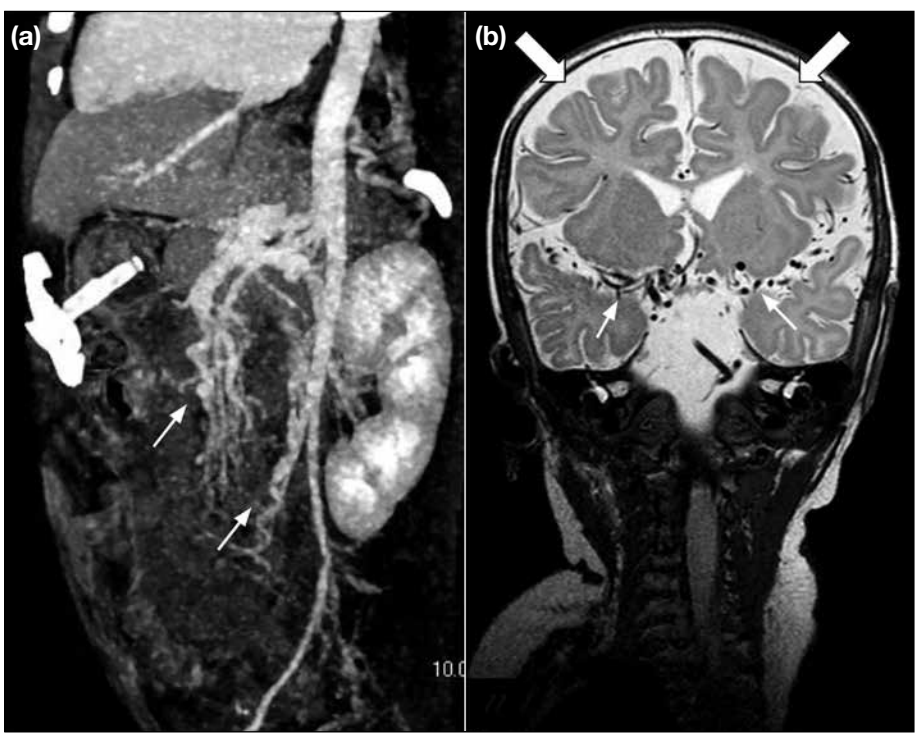

Figure 3. (a) Three-dimensional reconstructed sagittal image from contrast-enhanced computed tomography of the abdomen and pelvis of the patient on maximum intensity projection setting showing tortuous intra-abdominal vessels (arrows). (b) Selected T2-weighted coronal image from magnetic resonance imaging of the brain obtained at 5 months of age showing tortuous intracranial arteries along the bilateral Sylvian fissures (thin arrows). Also note that there are diffusely prominent subarachnoid spaces (thick arrows), most likely due to reduced brain parenchymal volume.

Figure 4. Antegrade pyelogram of the patient in prone position. Contrast injection via right percutaneous nephrostomy catheter opacifies the dilated right pelvicalyceal system and shows a stricture along the right proximal ureter. Urinary bladder shows multilobulated contour (arrows), in keeping with multiple bladder diverticula.

Rupture of the urinary collecting system is rare in the paediatric population. It has been reported in the presence of trauma[4] or due to obstruction of the collecting system, for example by stone or congenital anomaly (e.g., posterior urethral valve or ureteropelvic junction obstruction).[5,6] Conditions that cause soft tissue abnormalities such as Klinefelter syndrome and Cushing's syndrome have been reported to be associated with ureteric rupture and are thought to be predisposing factors.[7,8] We believe that Menkes disease was likely a predisposing factor for renal pelvic rupture in our patient.

Clinically, it is difficult to differentiate renal pelvic rupture from other causes of abdominal pain and tenderness; hence, the mainstay of diagnosis is imaging. In the paediatric population, ultrasound is usually the first-line imaging investigation to determine an underlying cause of acute abdominal pain due to its lack of ionising radiation. Nonetheless it is difficult to confirm the diagnosis of renal pelvic rupture by ultrasound alone. In cases with a high index of suspicion, contrast-enhanced CT urography can help confirm the diagnosis, albeit at the expense of ionising radiation.

In our patient, the most suspicious feature on ultrasound was the presence of perinephric and subphrenic fluid collection. This warranted further imaging with contrast-enhanced CT to delineate its extent and cause. As review of subsequent CT images was suspicious of renal pelvic rupture, delayed phase images were obtained. The presence of contrast extravasation from the collecting system confirmed the diagnosis.

Treatment should be individualised for each patient and take account of the degree of sepsis, extent of urinoma or abscess formation, and any suggestion of persistent urinary leakage. Small urinomas can resorb over time and may not require drainage. In cases of sizable urinoma, image-guided drainage and urinary diversion in the form of percutaneous nephrostomy or double-J stent can be considered. Surgical repair of the defect may be appropriate for ongoing urine leakage.

CONCLUSION

Rupture of the renal pelvis is an uncommon condition and difficult to diagnose clinically, particularly in children. Imaging with ultrasonography and contrast-enhanced CT urography can aid diagnosis and facilitate prompt management. Non-surgical treatment options are commonly considered for drainage of urinoma and urinary diversion, with surgical treatment reserved for cases of persistent urinary leakage.

REFERENCES

1. Tümer Z, Møller LB. Menkes disease. Eur J Hum Genet. 2010;18:511-8.
2. Kaler SG, Ferreira CR, Yam LS. Estimated birth prevalence of Menkes disease and ATP7A-related disorders based on the Genome Aggregation Database (gnomAD). Mol Genet Metab Rep. 2020;24:100602.
3. Kim MY, Kim JH, Cho MH, Choi YH, Kim SH, Im YJ, et al. Urological problems in patients with Menkes disease. J Korean Med Sci. 2018;34:e4.
4. Mariotto A, Zampieri N, Cecchetto M, Camoglio FS. Ureteral rupture after blunt abdominal trauma in a child with unknown horseshoe kidney. Pediatr Med Chir. 2015;37:pmc.2015.110.
5. Taşkınlar H, Yiğit D, Avlan D, Naycı A. Unusual complication of a urinary stone in a child: spontaneous rupture of the renal pelvis with the migration of calculus into the retroperitoneum. Turk J Urol. 2016;42:48-50.
6. Heikkilä J, Taskinen S, Rintala R. Urinomas associated with posterior urethral valves. J Urol. 2008;180:1476-8.
7. Reva S, Tolkach Y. Spontaneous pelvic rupture as a result of renal colic in a patient with Klinefelter syndrome. Case Rep Urol. 2013;2013:374973.
8. Fuse H, Hara S, Ito H, Shimazaki J. Spontaneous rupture of the ureter of a patient with Cushing's syndrome. Eur Urol. 1985;11:346-7.

Hong Kong J Radiol. 2023;26:198-201. Epub 31 Aug 2023 | https://doi.org/10.12809/hkjr2217534

CASE REPORT

Antibody-Mediated Striatal Encephalitis and Aseptic Meningitis in A Child with Neuropsychiatric Lupus: A Case Report

SM Yu[1], TY Yuen[1], KC Chan[1], KM Yam[2], WP Sze[2], ACH Ho[2]

[1]Department of Imaging and Interventional Radiology, Prince of Wales Hospital, Hong Kong SAR, China
[2]Department of Paediatrics, Prince of Wales Hospital, Hong Kong SAR, China

INTRODUCTION

Neuropsychiatric systemic lupus erythematosus (NPSLE) refers to the neurological and psychiatric symptoms that are thought to be related to systemic lupus erythematosus (SLE). NPSLE can be devastating, responsible for high rates of morbidity and mortality. It can occur any time in SLE. A recent large cohort study showed that NPSLE affects up to 25% of patients with juvenile-onset SLE.[1] The aetiology is thought to be multifactorial but vasculopathy, autoantibody production, and cytokine-induced neurotoxicity play a major role in the pathogenesis.[2]

Our clinical report highlights two infrequent subtypes of NPSLE–striatal encephalitis and aseptic meningitis, with substantial clinical and radiological response to immunosuppressants. The radiological features and treatment response of striatal encephalitis in our case are strikingly similar to those of the subset of anti–*N*-methyl-D-aspartate receptor (anti-NMDAR) autoimmune encephalitis involving the striatum.

CASE REPORT

An 11-year-old girl with known SLE presented to our hospital with a 1-week history of difficulty in passing urine, followed by acute-onset urinary retention. She was also suspected to have depersonalisation-derealisation syndrome for the last 1 year. She experienced progressive worsening with avolition, apathy, mental slowness, and insomnia 4 weeks prior to this acute presentation.

Urgent magnetic resonance imaging (MRI) brain examination demonstrated bilateral symmetrical T2 hyperintensity of the caudate nuclei, putamina, and globus pallidus without contrast enhancement or restricted diffusion. Bilateral thalami were spared (Figure 1a). Following intravenous gadolinium injection, scattered areas of leptomeningeal enhancement were present at bilateral frontal lobes and the right cerebellar hemisphere (Figure 1b and 1c). MRI of the spine demonstrated leptomeningeal enhancement along the lower thoracic cord and the conus medullaris (Figure 2).

Correspondence: *Dr SM Yu, Department of Imaging and Interventional Radiology, Prince of Wales Hospital, Hong Kong SAR, China*
Email: fayeyupwr@gmail.com

Submitted: 10 Feb 2022; Accepted: 15 Jul 2022.

Contributors: SMY designed the study. All authors acquired and analysed the data. SMY, KMY, WPS and ACHH drafted the manuscript. SMY and ACHH critically revised the manuscript for important intellectual content. All authors had full access to the data, contributed to the study, approved the final version for publication, and take responsibility for its accuracy and integrity.

Conflicts of Interest: All authors declared no conflicts of interest.

Funding/Support: This study received no specific grant from any funding agency in the public, commercial, or not-for-profit sectors.

Data Availability: All data generated or analysed during the present study are available from the corresponding author on reasonable request.

Ethics Approval: The patient was treated in accordance with the Declaration of Helsinki. Verbal consent for publication was obtained from the patient's parents.

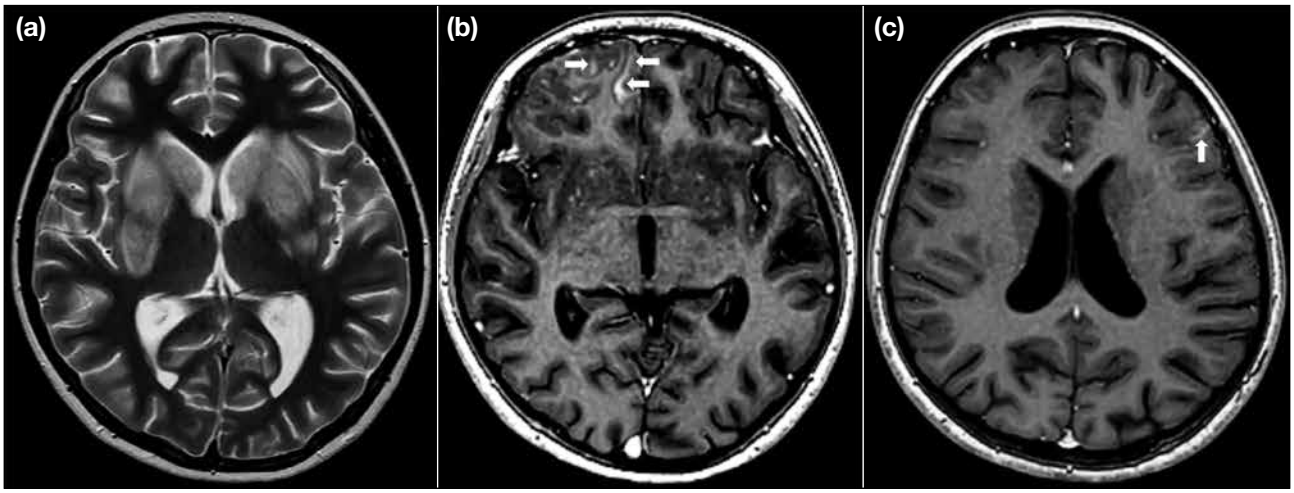

Figure 1. (a) Initial magnetic resonance imaging (MRI) of the brain. Axial T2-weighted image shows bilateral symmetric T2 hyperintensity of the caudate nuclei, putamina, and globus pallidi. Bilateral thalami are spared. (b and c) Axial T1-weighted post-gadolinium MRI of the brain show scattered areas of leptomeningeal enhancement at bilateral frontal lobes (arrows).

Figure 2. Initial magnetic resonance imaging of the spine. Sagittal T1-weighted post-gadolinium image shows leptomeningeal enhancement along the lower thoracic cord and the conus medullaris (black arrows).

The patient underwent extensive workup and was positive for antinuclear antibodies, anti–double-stranded DNA, anti-ribonucleoprotein, anti-extractable nuclear antigen antibodies including anti-Ro, anti-La and anti-Sm, as well as anti-ribosomal P antibodies; anti-NMDAR antibody was negative. Cerebrospinal fluid analysis revealed mildly elevated protein and normal leucocyte count. Cerebrospinal fluid gram stain, culture and virology were negative.

The patient was empirically treated with intravenous acyclovir, oral oseltamivir, and intravenous ciprofloxacin at the time of presentation for 2 days without any clinical improvement. Based on the clinical and characteristic MRI features, a working diagnosis was made of NPSLE with antibody-mediated striatal encephalitis and aseptic meningitis. Antiviral and antibiotic treatments were discontinued and immunosuppressive treatment was commenced. The patient received 5 days of pulse intravenous methylprednisolone and intravenous cyclophosphamide, followed by oral prednisolone and mycophenolate mofetil.

Follow-up MRI of the brain was performed 3 days later to guide clinical management. There was complete resolution of the leptomeningeal enhancement but persistent striatal T2 hyperintensity. With treatment, the clinical status of the patient gradually improved. Foley was weaned off successfully. Her mental state and sleep quality improved.

Another follow-up MRI of the brain 3 weeks from baseline demonstrated reduction in the extent of T2 signal abnormality but interval development of caudate and lentiform nuclei atrophy (Figure 3a). There was also novel T1 hyperintensity within the caudate and lentiform nuclei without associated susceptibility

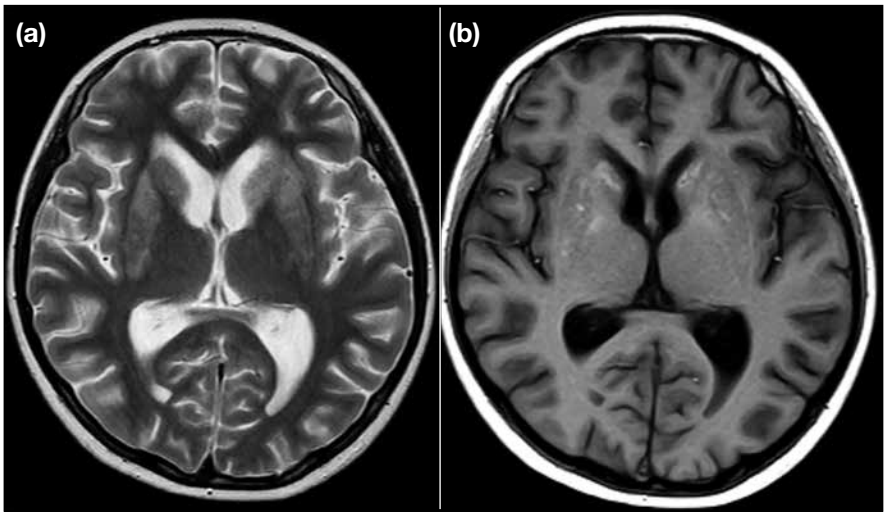

Figure 3. Follow-up magnetic resonance imaging of the brain at 3 weeks from baseline. (a) Axial T2-weighted image demonstrates markedly reduced T2 signal abnormality with atrophic change of the caudate and lentiform nuclei. Note that there is associated ex-vacuo dilatation of bilateral frontal horns relative to the baseline image. (b) Axial T1-weighted image shows new T1 hyperintense signals within caudate and lentiform nuclei without susceptibility artefacts, consistent with coagulative necrosis.

artefacts, consistent with coagulative necrosis (Figure 3b).

DISCUSSION

NPSLE describes a wide spectrum of peripheral and central nervous system manifestations. The widely quoted classification of NPSLE, made by an American College of Rheumatology expert committee in 1999, comprised 12 central and seven peripheral nervous system manifestations.[3] Case definitions including diagnostic criteria, exclusions, and methods of ascertainment were developed for each specific neuropsychiatric syndrome.[3] Among these, headache, mood disorders, cognitive dysfunction, seizures, movement disorders, and cerebrovascular disease are the most common NPSLE manifestations.[1,4,5]

Neuroimaging plays a vital role in the diagnosis of NPSLE and MRI is the preferred imaging modality for assessment of neurological manifestations although a negative scan does not exclude the presence of active NPSLE. A wide range of radiological abnormalities has been described but are often non-specific. In a single-centre retrospective study by Al-Obaidi et al,[5] the major MRI findings in juvenile-onset NPSLE were focal T2-weighted white matter hyperintensities (33%), brain atrophy (18.5%), cortical grey matter lesions (3%), and basilar artery territory infarction (3%), although a majority of patients (59%) showed no MRI abnormalities despite clinically active NPSLE. Striatal encephalitis and aseptic meningitis have rarely been described as characteristic manifestations of neuropsychiatric lupus,[6-8] although they were coexistent in our patient.

Antibody-mediated striatal encephalitis is a rare but characteristic manifestation of NPSLE.[6,7] The radiological features and clinical course of lupus-related antibody-mediated striatal encephalitis closely resemble those of anti-NMDAR striatal encephalitis. It is suggested that peripheral anti–double-stranded DNA antibodies, a specific serum autoantibody in SLE, may enter the central nervous system to cross-react with NMDAR antigens[6,7] and mediate a non-thrombotic and non-vasculitic pathology with features of neuronal excitotoxicity.[6] Other autoantibodies thought to cause NPSLE include anti-neuronal, anti-NMDAR2, anti-ribosomal P, and anti-endothelial antibodies.[9]

The radiological pattern of bilateral symmetrical T2 hyperintensity involving lentiform and caudate nuclei typically suggests systemic or metabolic causes. The characteristic sparing of bilateral thalami and lack of restricted diffusion and contrast enhancement provide important clues for excluding multiple conditions in the differential list including hypoglycaemia, hypoxic ischaemic encephalopathy, extrapontine myelinolysis, arterial occlusion, venous thrombosis, and Creutzfeldt–Jakob disease. Other differentials including organophosphate or methanol poisoning can be excluded by clinical presentation and toxicology.

In an appropriate clinical setting, such as in our patient, the presence of bilateral symmetrical T2 hyperintense signal changes within the caudate and putamen without evidence of restricted diffusion or contrast enhancement was strongly suggestive of autoimmune encephalitis of the striatum.[7] Intrinsic T1 hyperintensity within the

striatum, also evident in our patient, may indicate a poor prognosis. This has been proposed to be related to the development of coagulative necrosis secondary to prolonged antibody-mediated inflammation and excitatory glutamate neurotoxicity.[7]

Aseptic meningitis is another manifestation of NPSLE. It is possibly mediated by a combination of mechanisms such as anti-neuronal antibodies, antiphospholipid antibodies, immune complex–mediated vasculitis, and cytokines. Due to the non-specific radiological findings, more common causes of leptomeningeal enhancement, including infection and malignancy, must be excluded before establishing the diagnosis.[4] Compared with pyogenic meningitis, cerebrospinal fluid leucocytes and proteins are usually lower in cases of lupus-related aseptic meningitis.

In children with SLE, neuropsychiatric manifestation is frequently associated with high overall SLE activity. Aggressive treatment, including systemic corticosteroid and immunosuppressants, is often required to control the autoimmune process and avoid further damage.[4] Close collaboration between the radiologist, paediatric rheumatologist and neurologist is crucial to reach a prompt diagnosis and maximise clinical outcomes in these patients with NPSLE.

CONCLUSION

We present a patient with NPSLE presenting as striatal encephalitis and aseptic meningitis who demonstrated a good clinical and radiological response to immunosuppressive therapy. The clinical course and imaging features of antibody-mediated striated encephalitis in our patient closely resemble those of a striatal variant of anti-NMDAR encephalitis.

Neuroimaging plays an important role in diagnosis, monitoring treatment response and prognostication by identifying complications such as brain atrophy or intrinsic basal ganglionic T1 hyperintensity. Prompt diagnosis and early treatment facilitates optimisation of clinical outcomes.

REFERENCES

1. Giani T, Smith EM, Al-Abadi E, Armon K, Bailey K, Ciurtin C, et al. Neuropsychiatric involvement in juvenile-onset systemic lupus erythematosus: data from the UK juvenile-onset systemic lupus erythematosus cohort study. Lupus. 2021;30:1955-65.
2. Hanly JG. Neuropsychiatric lupus. Curr Rheumatol Rep. 2001;3:205-12.
3. The American College of Rheumatology nomenclature and case definitions for neuropsychiatric lupus syndromes [editorial]. Arthritis Rheum. 1999;42:599-608.
4. Kivity S, Agmon-Levin N, Zandman-Goddard G, Chapman J, Shoenfeld Y. Neuropsychiatric lupus: a mosaic of clinical presentations. BMC Med. 2015;13:43.
5. Al-Obaidi M, Saunders D, Brown S, Ramsden L, Martin N, Moraitis E, et al. Evaluation of magnetic resonance imaging abnormalities in juvenile onset neuropsychiatric systemic lupus erythematosus. Clin Rheumatol. 2016;35:2449-56.
6. DeGiorgio LA, Konstantinov KN, Lee SC, Hardin JA, Volpe BT, Diamond B. A subset of lupus anti-DNA antibodies cross-reacts with the NR2 glutamate receptor in systemic lupus erythematosus. Nat Med. 2001;7:1189-93.
7. Kelley BP, Corrigan JJ, Patel SC, Griffith BD. Neuropsychiatric lupus with antibody-mediated striatal encephalitis. AJNR Am J Neuroradiol. 2018;39:2263-69.
8. Canoso JJ, Cohen AS. Aseptic meningitis in systemic lupus erythematosus. Report of three cases. Arthritis Rheum. 1975;18:369-74.
9. Govoni M, Hanly JG. The management of neuropsychiatric lupus in the 21st century: still so many unmet needs? Rheumatology (Oxford). 2020;59(Suppl5):v52-62.

Hong Kong J Radiol. 2023;26:202-5. Epub 16 Aug 2023 | https://doi.org/10.12809/hkjr2217627

CASE REPORT

Role of Fluorine-18 Fluorodeoxyglucose Positron Emission Tomography/Computed Tomography in Monitoring Relapsing Polychondritis: A Case Report

DWK Chan, EYP Lee

Department of Diagnostic Radiology, The University of Hong Kong, Hong Kong SAR, China

INTRODUCTION

Relapsing polychondritis (RP) is a rare autoimmune inflammatory disease that affects cartilaginous tissue with consequent recurrent inflammation and deformation of the involved structures. Although the aetiology remains unknown, it is often associated with autoimmune disorders, with rheumatoid arthritis (RA) being the most common.[1,2] The sites that are first affected at disease onset include the auricular and nasal cartilages. Nonetheless other proteoglycan-rich structures including the eyes, heart valves and blood vessels can be involved. Due to its non-specific presentation and the lack of specific diagnostic methods, RP has a high risk of misdiagnosis, with a mean diagnostic delay of 2.9 years.[1]

There is no gold standard test or imaging to monitor RP. Although laboratory investigations such as erythrocyte sedimentation rate and C-reactive protein level can indicate active inflammation, they are neither sensitive nor specific.[2] Imaging modalities such as computed tomography (CT), although useful in the diagnosis of RP, are less sensitive for demonstrating the extent of active disease.[2] Histological confirmation is hindered by access difficulty and the associated complications of invasive procedures.[2] Recently, the use of fluorine-18 fluorodeoxyglucose positron emission tomography/CT (^{18}F-FDG PET/CT) has been investigated in the diagnosis, management and monitoring of RP. We present a 55-year-old man in whom ^{18}F-FDG PET/CT was used to assess RP.

CASE REPORT

A 55-year-old man with RA presented with a 3-year history of worsening shortness of breath and wheeze. The patient also experienced episodic nasal bridge pain and bilateral ear blockage. He had been treated with steroids (prednisolone) and immunosuppressants (sulphasalazine and azathioprine) for RA since 2018. In early 2021, he was admitted with increased shortness of breath, cough, and sputum. He had no chest pain or fever.

Correspondence: *Dr EYP Lee, Department of Diagnostic Radiology, The University of Hong Kong, Hong Kong SAR, China*
Email: eyplee77@hku.hk

Submitted: 11 Aug 2022; Accepted: 15 Nov 2022.

Contributors: Both authors designed the study, acquired the data, analysed the data, drafted the manuscript, and critically revised the manuscript for important intellectual content. Both authors had full access to the data, contributed to the study, approved the final version for publication, and take responsibility for its accuracy and integrity.

Conflicts of Interest: DWKC has disclosed no conflicts of interest. As an editor of the journal, EYPL was not involved in the peer review process.

Funding/Support: This study received no specific grant from any funding agency in the public, commercial, or not-for-profit sectors.

Data Availability: All data generated or analysed during the present study are available from the corresponding author on reasonable request.

Ethics Approval: This study was approved by the Institutional Review Board of The University of Hong Kong/Hospital Authority Hong Kong West Cluster, Hong Kong (Ref No.: HKWC-2022-026). The patient has provided written informed consent for all treatments, procedures, and publication.

Physical examination showed diffuse chest wheeze but was otherwise unremarkable. Chest X-ray showed no consolidation. Blood tests showed a normal white blood cell count (6.5×10^9/L) but elevated C-reactive protein level (14.4 mg/L).

CT of the thorax revealed smooth narrowing of the trachea and proximal bronchi and smooth tracheal wall thickening sparing the posterior wall. Changes were strongly suggestive of RP (Figure 1). A whole-body ^{18}F-FDG PET/CT confirmed the changes but with no corresponding increased uptake or hypermetabolic disease elsewhere (Figure 2a and 2b). A diagnosis of RP was made and the patient was treated with prednisolone, methotrexate, and mycophenolate mofetil.

The patient complained of unresolved bony pain with persistently elevated erythrocyte sedimentation rate (46 mm/h) and C-reactive protein level (71 mg/L). A follow-up ^{18}F-FDG PET/CT 12 months later to assess response to immunosuppressive therapy revealed new symmetrical uptake along the costochondral junctions (Figure 2c and 2d), suggestive of active RP. In view of the radiological findings and clinical progression, the dosage of methotrexate was increased; biologics would be considered if the disease remained refractory. The patient's symptoms subsequently improved with a decreasing trend of serum inflammatory markers.

DISCUSSION

The ^{18}F-FDG PET/CT was first reported in 2007 to provide metabolic information of an RP patient.[3] Since then, several case reports have shown ^{18}F-FDG PET/CT to be capable of determining organ involvement and evaluating disease activity and therapeutic response.[4-7]

The ^{18}F-FDG PET/CT findings in patients with RP comprise mainly airway wall thickening and calcification, airway stenosis and malacia, and air trapping.[1] The presence of symmetrically distributed high FDG-uptake lesions may also be diagnostic of RP.[2] Furthermore, ^{18}F-FDG PET/CT has a role in targeting biopsy sites, increasing remarkably the biopsy yield rate.[2] Nonetheless a retrospective study[8] found that in biopsy-proven auricular RP, or where there was tracheal involvement, the sensitivity and specificity of ^{18}F-FDG PET/CT were only 55.6% and 5.3%, respectively, raising questions about its usefulness in guiding biopsy.

A recent single-centre retrospective study compared ^{18}F-FDG PET/CT in patients before and after treatment and correlated the findings with clinical symptoms.[9] Follow-up ^{18}F-FDG PET/CT in most patients revealed a favourable treatment response, with significantly reduced visual scores and maximum standard uptake values in cartilaginous tissue. Another advantage of ^{18}F-FDG PET/CT lies in its ability to identify areas that are not clinically accessible but are of importance. In a patient with asymptomatic involvement of the aorta, ^{18}F-FDG PET/CT was able to identify increased FDG-uptake in the superior mesenteric artery and renal arteries.[9] Our case demonstrates the usefulness of ^{18}F-FDG PET/CT in assessing RP, providing objective evidence of

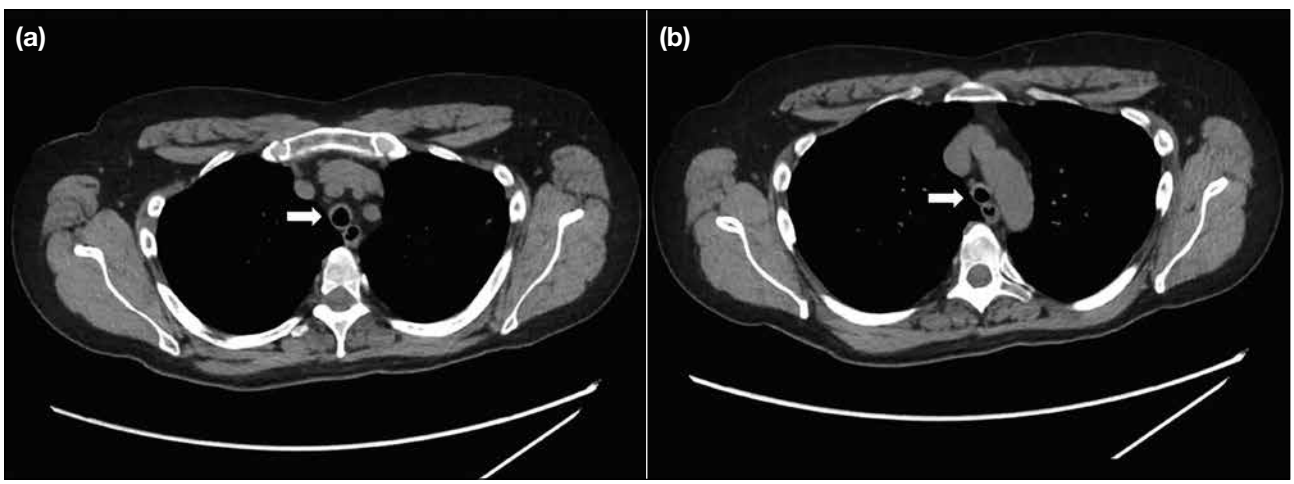

Figure 1. Axial non-contrast computed tomography images of the thorax showing (a) tracheal narrowing (arrow) and (b) smooth thickening of the tracheal wall sparing the posterior wall (arrow).

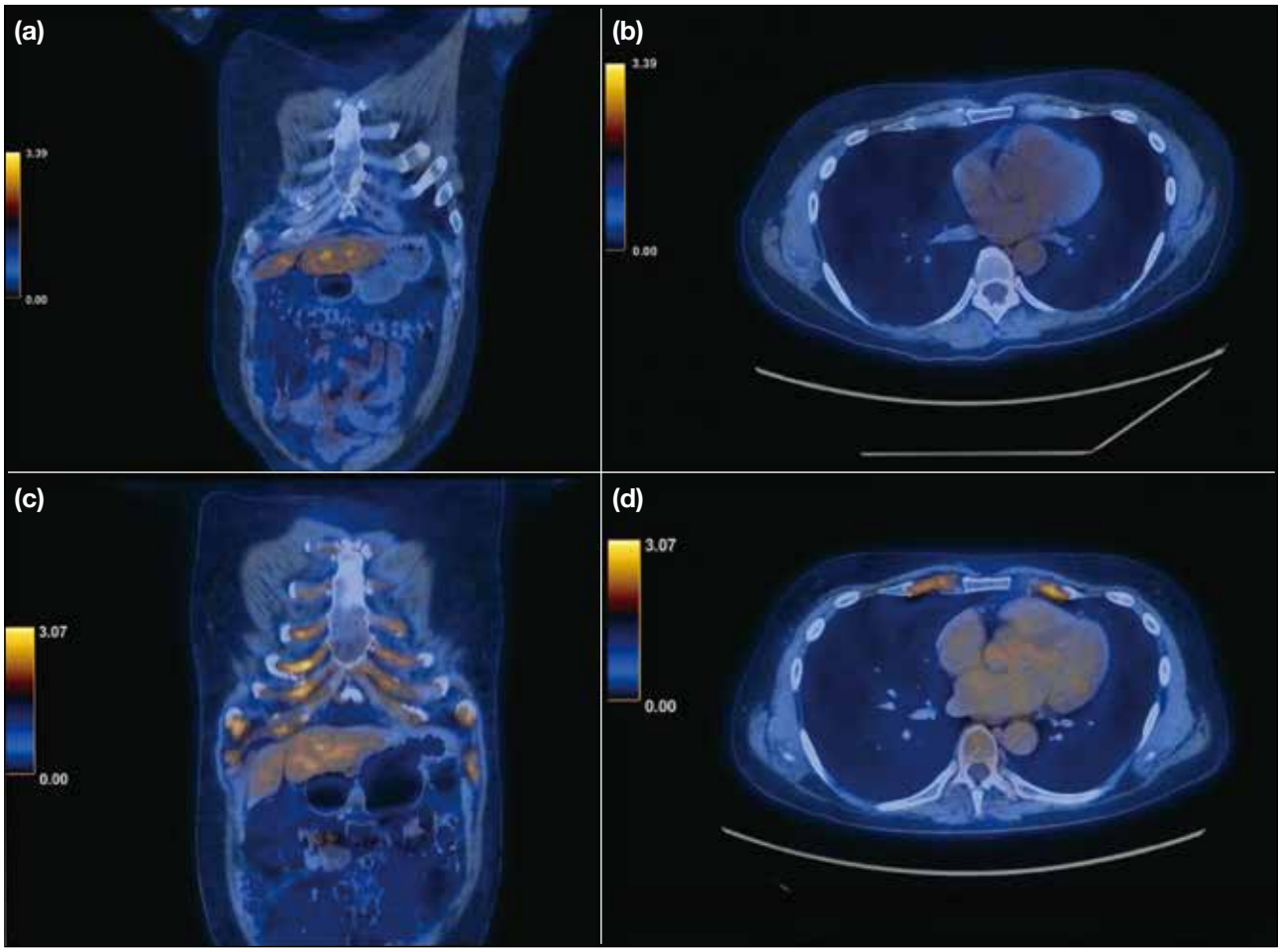

Figure 2. (a and b) Baseline fluorine-18 fluorodeoxyglucose positron emission tomography/computed tomography (^{18}F-FDG PET/CT). (a) Coronal fused ^{18}F-FDG PET/CT image shows no uptake along the costochondral junctions. (b) Axial fused ^{18}F-FDG PET/CT image shows no uptake along the costochondral junctions. (c and d) Follow-up ^{18}F-FDG PET/CT. (c) Coronal fused ^{18}F-FDG PET/CT image shows symmetrical uptake (maximum standard uptake value = 1.9-3.2) along the costochondral junctions. (d) Axial fused ^{18}F-FDG PET/CT image shows symmetrical uptake along the costochondral junctions.

active activity and prompting treatment escalation. This concurred with the clinical symptoms and serum inflammatory markers.

Apart from ^{18}F-FDG PET/CT, other imaging modalities have been investigated in the diagnosis and monitoring of RP. Although expiratory CT abnormalities are present in the majority of RP patients, only half demonstrate abnormalities on routine inspiratory CT scans.[10] Dynamic expiratory CT has been proposed as a routine diagnostic component if there is clinical suspicion of airway involvement.[10] In addition, studies have highlighted the use of bone scintigraphy using technetium-99m–methylene diphosphonate and gallium-67 citrate to evaluate disease activity and treatment response in RP patients.[11] In conclusion, ^{18}F-FDG PET/CT is useful in the follow-up of RP and in providing objective and measurable metrics to monitor disease activity.

REFERENCES

1. Borgia F, Giuffrida R, Guarneri F, Cannavò SP. Relapsing polychondritis: an updated review. Biomedicines. 2018;6:84.
2. Lei W, Zeng H, Zeng DX, Zhang B, Zhu YH, Jiang JH, et al. ^{18}F-FDG PET-CT: a powerful tool for the diagnosis and treatment of relapsing polychondritis. Br J Radiol. 2016;89:20150695.
3. Nishiyama Y, Yamamoto Y, Dobashi H, Kameda T, Satoh K, Ohkawa M. [18F]fluorodeoxyglucose positron emission tomography imaging in a case of relapsing polychondritis. J Comput Assist Tomogr. 2007;31:381-3.
4. Zhou H, Su M, Li L. ^{18}F-FDG PET/CT imaging of relapsing polychondritis: a case report. Medicine (Baltimore). 2016;95:e4496.
5. Jain TK, Sood A, Sharma A, Basher RK, Bhattacharya A, Mittal BR. Response assessment in relapsing polychondritis with

^{18}F-FDG PET/CT [in English, Spanish]. Rev Esp Med Nucl Imagen Mol. 2017;36:124-5.
6. Kamada H, Takanami K, Toyama Y, Saito M, Takase K. ^{18}F-FDG PET/CT imaging of vasculitis complicated with relapsing polychondritis. Clin Nucl Med. 2020;45:e327-8.
7. Yokoyama T, Koyama N, Kodama K, Hagiwara K, Kanazawa M. ^{18}F-fluorodeoxyglucose positron emission tomography for relapsing polychondritis as a diagnostic approach and evaluation of disease activity. BMJ Case Rep. 2009;2009:bcr02.2009.1591.
8. Zeng Y, Li M, Chen S, Lin L, Li S, He J, et al. Is ^{18}F-FDG PET/CT useful for diagnosing relapsing polychondritis with airway involvement and monitoring response to steroid-based therapy? Arthritis Res Ther. 2019;21:282.
9. Sharma A, Kumar R, Mb A, Naidu GS, Sharma V, Sood A, et al. Fluorodeoxyglucose positron emission tomography/computed tomography in the diagnosis, assessment of disease activity and therapeutic response in relapsing polychondritis. Rheumatology (Oxford). 2020;59:99-106.
10. Lee KS, Ernst A, Trentham DE, Lunn W, Feller-Kopman DJ, Boiselle PM. Relapsing polychondritis: prevalence of expiratory CT airway abnormalities. Radiology. 2006;240:565-73.
11. Güngör F, Ozdemir T, Tunçdemir F, Paksoy N, Karayalçin B, Erkiliç M. Tc-99m MDP bone scintigraphy in relapsing polychondritis. Clin Nucl Med. 1997;22:264-6.

Hong Kong J Radiol. 2023;26:206-16. Epub 11 Sep 2023 | https://doi.org/10.12809/hkjr2217558

PICTORIAL ESSAY

Molecular Classification and Respective Radiological Phenotypes of Breast Cancers: A Pictorial Essay

SM Yu[1], YH Chan[1], YS Chan[1], C Tsoi[1], GKF Tam[2], EHY Hung[1], WCW Chu[1], HHL Chau[1]

[1]Department of Imaging and Interventional Radiology, Prince of Wales Hospital, Hong Kong SAR, China
[2]Department of Radiology, North District Hospital, Hong Kong SAR, China

INTRODUCTION

According to the Centre for Health Protection, breast cancer is the most common cancer among females in Hong Kong.[1] In all, 4956 new cases of female breast cancer were diagnosed in Hong Kong and the crude incidence rate was 121.9 per 100,000 women in 2020.[1] Breast cancer is traditionally classified based on the clinicopathological analysis. In the past two decades, identification of distinct gene expression profiling in breast cancer has reshaped our understanding of breast cancer biology. Unravelling the genetic heterogeneity of breast cancer is fundamental to the development of personalised medicine, which improves clinical outcomes.

Full genomic analysis is costly and time-consuming, therefore not widely available in routine practice; the St Gallen International Expert Consensus panel has suggested the analysis of oestrogen receptor (ER), progesterone receptor (PR) and human epidermal growth factor receptor 2 (HER2) by semiquantitative immunohistochemistry (IHC) and the use of fluorescence in situ hybridisation for HER2 for equivocal IHC to define the four molecular subtypes of breast cancer (Figure 1).[2] IHC analysis may not always accurately reflect the true molecular subtypes of breast cancers. Discordance rates between IHC analysis and genetic expression profiling vary among different studies, but can be as high as 30%.[3]

The four intrinsic molecular subtypes of breast cancer include luminal A, luminal B, HER2-enriched, and basal-like (triple-negative). Each molecular subtype shows different demographics, treatment responses, preferential metastatic target organs, and prognoses. Importantly, distinctive radiological features of each molecular subtype have been identified (Table).[4-7]

This article aims to provide radiologists with a pictorial

Correspondence: *Dr HHL Chau, Department of Imaging and Interventional Radiology, Prince of Wales Hospital, Hong Kong SAR, China*
Email: helen.chau@ha.org.hk

Submitted: 30 Mar 2022; Accepted: 17 Jun 2022.

Contributors: SMY, WCWC and HHLC designed the study. SMY, YHC, YSC, CT and HHLC acquired and analysed the data. SMY and HHLC drafted the manuscript. SMY, GKFT, EHYH, WCWC and HHLC critically revised the manuscript for important intellectual content. All authors had full access to the data, contributed to the study, approved the final version for publication, and take responsibility for its accuracy and integrity.

Conflicts of Interest: As editors of the journal, YHC and WCWC were not involved in the peer review process. Other authors have disclosed no conflicts of interest.

Funding/Support: This study received no specific grant from any funding agency in the public, commercial, or not-for-profit sectors.

Data Availability: All data generated or analysed during the present study are available from the corresponding author on reasonable request.

Ethics Approval: The study was approved by the Joint Chinese University of Hong Kong–New Territories East Cluster Clinical Research Ethics Committee (Ref No.: 2022.192). A waiver of informed consent of patients was granted by the Committee due to the retrospective nature of the study and no patient identifiers were used.

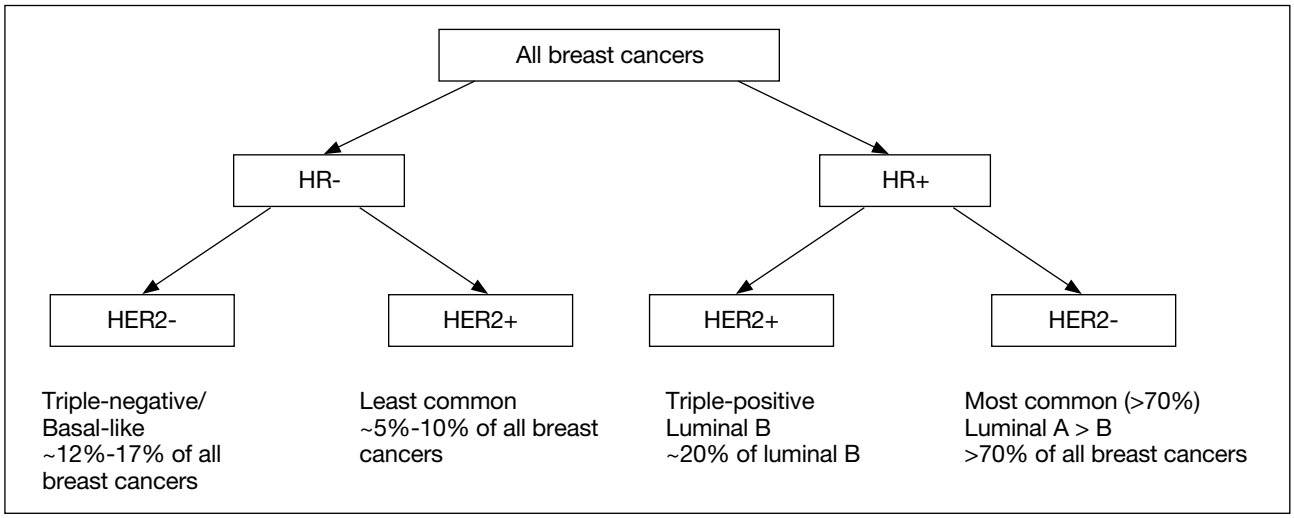

Figure 1. Simplified flowchart for molecular classification of breast cancer subtypes.
Abbreviations: HER2 = human epidermal growth factor receptor 2; HR = hormone receptor.

Table. Summary of radiological phenotypes for different breast cancer molecular subtypes.[4-7]

Subtype and cancer grade	Molecular profile	Mammography	Ultrasonography	Magnetic resonance imaging
Luminal A, usually low grade	HR+*, HER2-, low Ki-67 level	Irregular mass with spiculated margin ± microcalcifications	Irregular mass with non-circumscribed margins and posterior acoustic shadowing	Irregular mass with spiculated margins
Luminal B, usually intermediate-to-high grade	ER+, PR-/low, high Ki-67 level, ± HER2+ (20% HER2+/80% HER2-)	Irregular mass with spiculated margins ± microcalcifications	Irregular mass with non-circumscribed margins and posterior acoustic shadowing	Multicentric and/or multifocal disease
HER2-enriched, usually intermediate-to-high grade	HR-*, HER2+	Indistinct mass with microcalcifications (branching or fine linear)	Non-mass lesion with non-circumscribed/indistinct margins	A washout or fast initial kinetics Multicentric and/or multifocal disease
Basal-like (triple-negative), high grade	HR-*, HER2-	Round mass with circumscribed margins Posterior in location No microcalcifications	Mass with relatively circumscribed margins Solid-cystic mass/necrotic tumour Posterior acoustic enhancement	Mass enhancement or rim enhancement with internal high T2 signal Peritumoral oedema

Abbreviations: ER = oestrogen receptor; HER2 = human epidermal growth factor receptor 2; HR = hormone receptor; Ki-67 = antigen Ki-67; PR = progesterone receptor.
* Includes oestrogen receptor and progesterone receptor.

exhibit on imaging phenotypes of breast cancer molecular subtypes based on pathologically proven examples. It also provides an overview of molecular classification and clinical implications of each molecular subtype for the field of precision medicine.

LUMINAL SUBTYPE (LUMINAL A AND LUMINAL B)

Genetic Expression and Clinical Implications

Luminal subtype is defined by the presence of ER and PR expression.[4] Luminal subtype is divided into two distinct subgroups, namely luminal A and luminal B. Approximately 70% of breast cancers are luminal subtype breast cancers and they show a more favourable prognosis than hormone receptor–negative breast cancers.[5]

Luminal A subtypes are defined by expression of both ER and PR without amplification of the HER2/neu proto-oncogene. Patients with luminal A tumours have the best

prognosis among all molecular subtypes.[4-6] Luminal A tumours usually exhibit low histological grades with higher expression of hormone receptors (ERs and PRs) and lower proliferative activity, which can be assessed through Ki-67 expression, in which the antigen Ki-67 is a marker for cell proliferation (<14%).[4]

Luminal B subtypes also express ER and PR but they have a higher Ki-67 expression (≥14%).[4] Luminal B tumours are more often multifocal or multicentric and more likely to metastasise to regional nodes than luminal A tumours.[7] Patients with luminal B breast cancers often have a poorer prognosis compared to patients harbouring luminal A breast cancers.[5,7] Furthermore, 20% of luminal B tumours are HER2 positive by IHC analysis, referred to as the 'luminal B HER2+' subtype, which was shown to be associated with a poorer prognosis and lower 10-year breast cancer–specific survival rate among the luminal subtypes.[7]

The hormone receptor status is predictive of response to hormone therapy, the mainstay of treatment for patients with luminal breast cancers.[3,6]

Imaging Characteristics

Luminal tumours typically demonstrate suspicious mammographic features of breast cancer, namely an irregular mass with spiculated or microlobulated margins or a mass with suspicious microcalcifications (Figures 2 and 3).[6] Associated architectural distortion

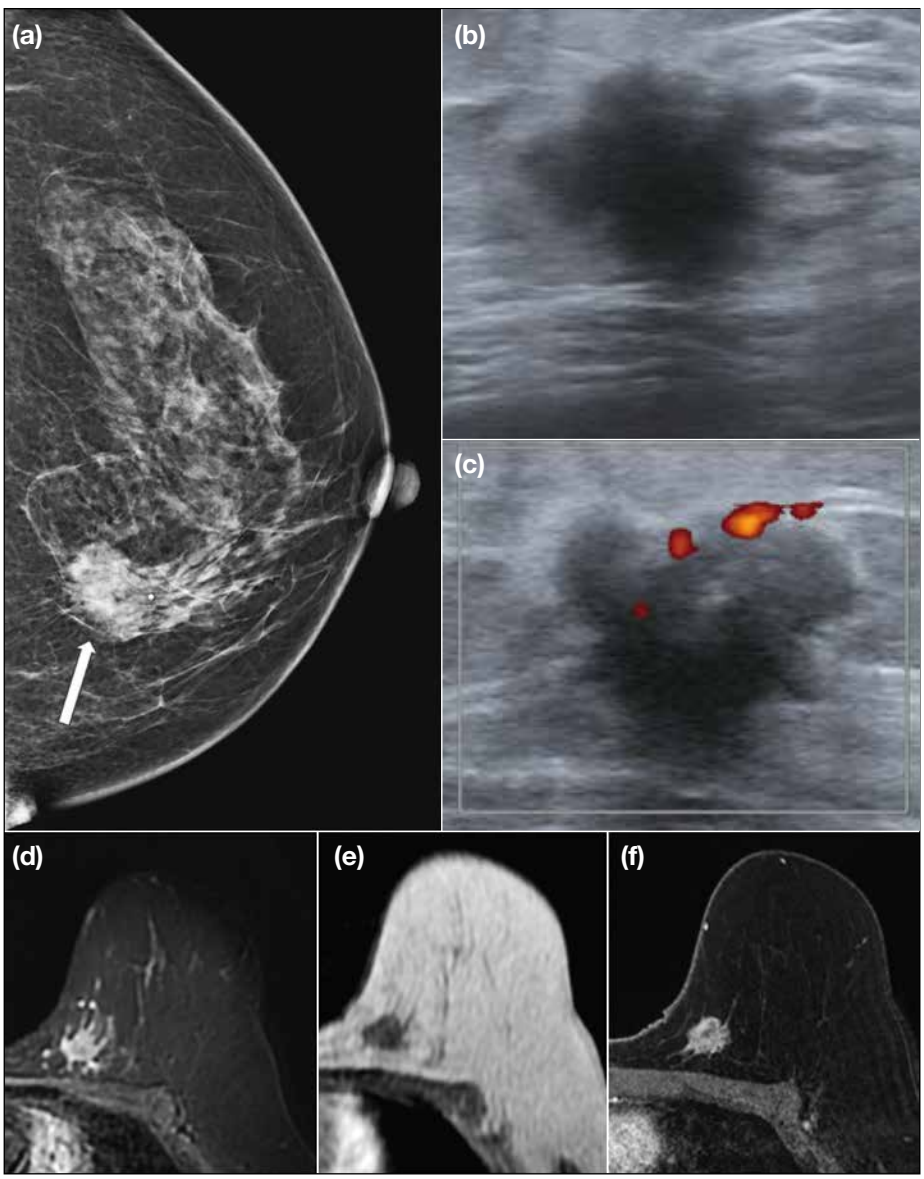

Figure 2. A 59-year-old woman with luminal A breast cancer (oestrogen receptor 95%, progesterone receptor 95%, c-*erb*B2 0+, and Ki-67 ~10%). (a) Craniocaudal mammographic view showing an irregular high-density mass (arrow) with spiculated margins in upper inner left breast. (b) Greyscale and (c) colour Doppler images showing an irregular mass with spiculated margins and intrinsic vascularity. (d) Axial fat-suppressed T2-weighted magnetic resonance (MR) image showing an irregular hyperintense mass with spiculated margins. (e) Axial non-contrast T1-weighted and (f) contrast-enhanced T1-weighted fat-saturated MR images showing heterogenous enhancement in the corresponding mass.

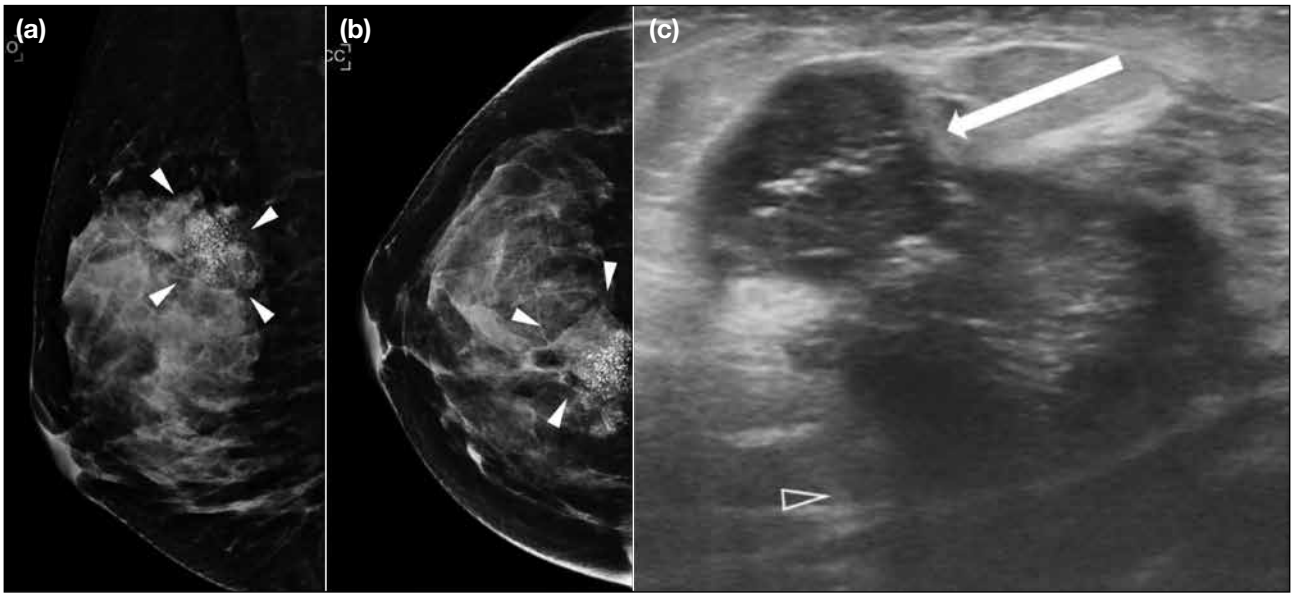

Figure 3. A 41-year-old woman with luminal B breast cancer (oestrogen receptor 70%, progesterone receptor 30%, c-*erb*B2 0+, and Ki-67 ~30%). (a) Mediolateral-oblique and (b) craniocaudal mammographic views showing an equal-density irregular mass with partially obscured margins and associated pleomorphic calcifications (arrowheads) in the upper inner right breast, which is a common presentation for luminal breast cancer. (c) Ultrasound image showing an irregular hypoechoic mass with angular margins and posterior acoustic shadowing (open arrowhead); microcalcifications (arrow) can be appreciated within the mass.

is more commonly observed in luminal A tumours than in luminal B tumours. The sonographic appearance of luminal tumours is typically an irregular mass with posterior acoustic shadowing (Figures 2 and 3).[6] On magnetic resonance imaging (MRI), luminal tumours most commonly present as an enhancing irregular mass with spiculated margins (Figure 2).[8]

Luminal B tumours are more frequently associated with axillary nodal metastases at the time of diagnosis than luminal A tumours. Luminal B tumours more often present with multifocal or multicentric disease on MRI.[3] The 'luminal B HER2+' subtype has been reported to be more likely to involve axillary lymph nodes and to present with multifocal or multicentric disease on MRI (Figure 4).[3]

Distant metastasis in luminal breast cancers shows a greater propensity to involve the skeletal system compared to other breast cancer subtypes (Figure 5).[9,10]

HUMAN EPIDERMAL GROWTH FACTOR RECEPTOR 2–ENRICHED SUBTYPE

Genetic Expression and Clinical Implications

HER2-positive cancers are defined by overexpression of the c-*erb*B2 (HER2/neu) gene, which encodes the epidermal growth factor receptor type 2.[6] Of all HER2-positive tumours, 60% are HER2-enriched, characterised by HER2 positivity and ER and PR negativity.[6] Being a proto-oncogene, amplification of c-*erb*B2 results in increased cellular aggressiveness and faster growth.

HER2-enriched breast cancers are generally intermediate-to-high-grade tumours with an aggressive course, worse survival rate, and higher recurrence rate compared to luminal breast cancers.[5]

Fortunately, HER2-directed therapy has shown success in improving clinical outcomes, and trastuzumab therapy is a widely used and effective anti-HER2 agent.

Imaging Characteristics

HER2-enriched tumours most commonly present as a mass associated with microcalcifications or as suspicious microcalcifications alone on mammography (Figure 6).[6] The margins of HER2-enriched tumours are usually spiculated. Sonographically, HER2-enriched tumours are usually iso- to hypoechoic with indistinct margins and a high degree of vascularity (Figure 6).[6] On MRI, a round mass with spiculated margins and non-mass enhancement are the most frequent patterns in HER2-enriched subtype.[6,8] HER2-enriched tumours are often multifocal and/or multicentric on MRI and are frequently associated with ductal carcinoma in situ (Figure 7).[6,8]

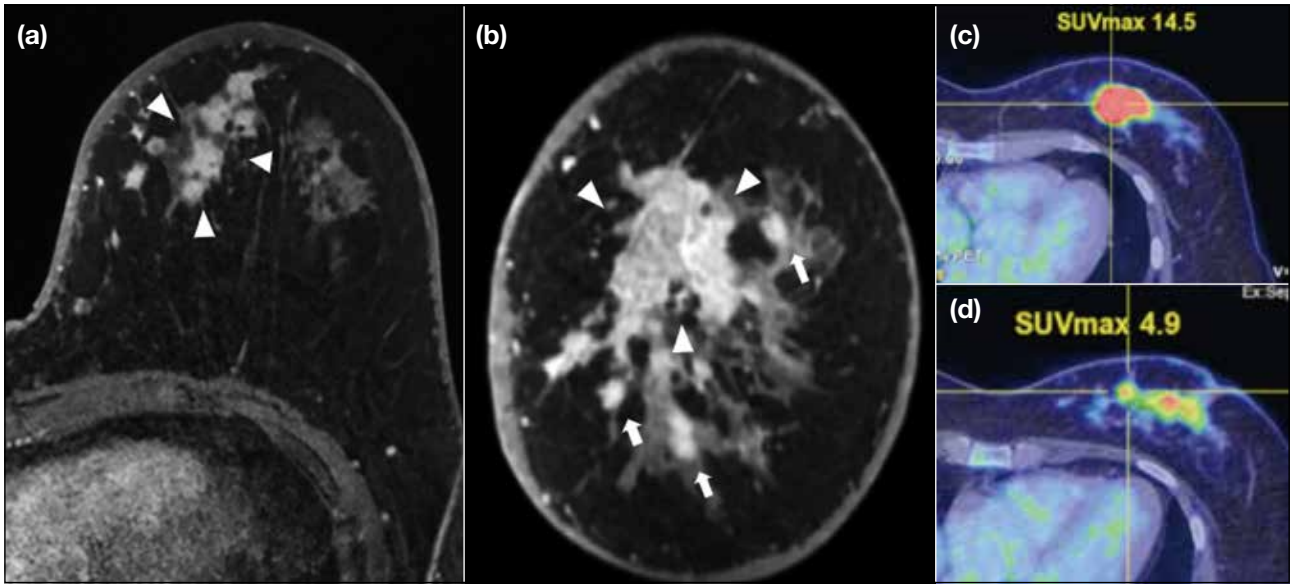

Figure 4. A 55-year-old woman with multicentric luminal B human epidermal growth factor receptor 2 + breast cancer (oestrogen receptor 90%, progesterone receptor 60%, c-*erb*B2 2+, and Ki-67 ~30%). (a) Axial and (b) coronal contrast-enhanced T1-weighted magnetic resonance images showing an irregular enhancing mass with spiculated margins in the upper inner quadrant of the left breast (arrowheads) with multiple smaller enhancing foci (arrows in [b]) in the lower inner and upper outer quadrants of the left breast, consistent with multicentric disease. (c and d) Corresponding fusion images of positron emission tomography/computed tomography depict a lobulated hypermetabolic mass in the upper inner quadrant (maximum standardised uptake value [SUV_{max}] = 14.5) and multiple small hypermetabolic foci in the lower inner quadrant (SUV_{max} = 4.9), again consistent with multicentric disease.

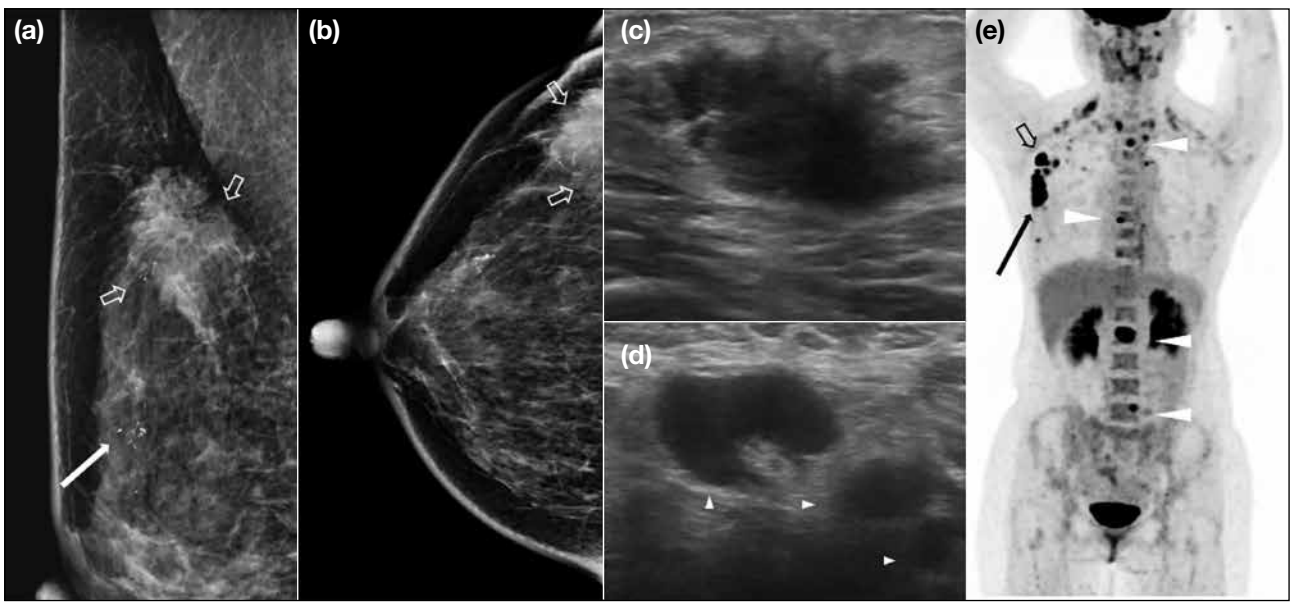

Figure 5. A 43-year-old woman with luminal B breast cancer and multiple bone metastases (oestrogen receptor 60%, progesterone receptor 30%, c-*erb*B2 0+, and Ki-67 ~20%). (a) Mediolateral-oblique and (b) craniocaudal mammographic images showing an irregular high-density mass with spiculated margins in the upper outer right breast (open arrows), with pleomorphic microcalcifications (arrow in [a]). (c) Ultrasound image of the mass shows that it is irregular and hypoechoic with spiculated margins. (d) Ultrasound of the right axilla shows multiple enlarged nodes (arrowheads) with eccentric cortical thickening and loss of fatty hilum suggestive of nodal metastases. (e) Maximal intensity projection image of whole-body positron emission tomography showing a hypermetabolic primary tumour in the upper outer quadrant of the right breast (arrow) with axillary node involvement (open arrow) and multiple sites of bone metastases in the spine (arrowheads).

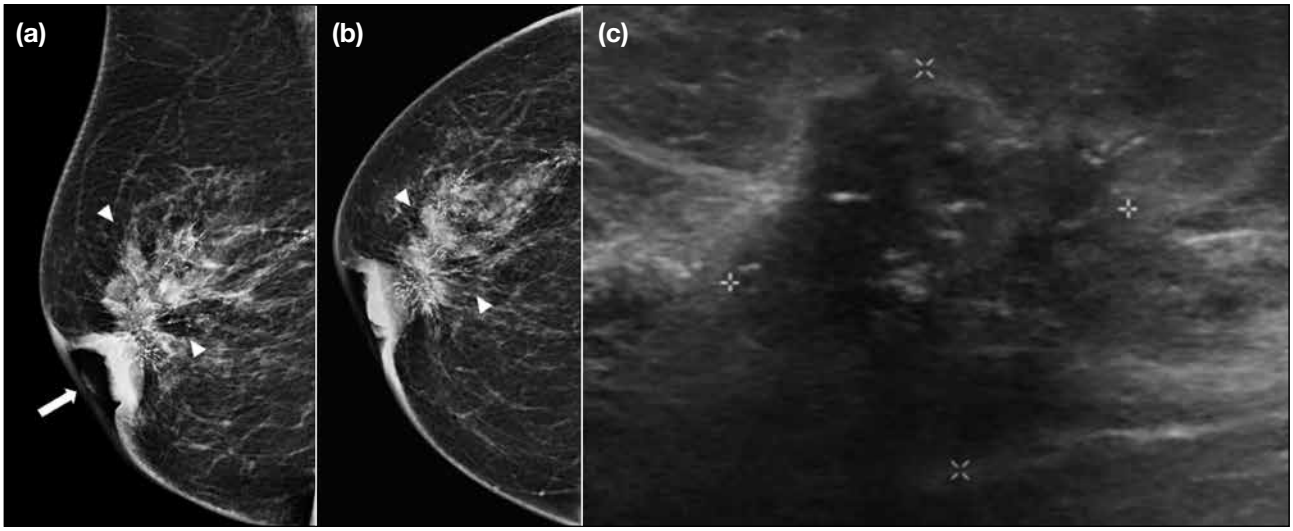

Figure 6. An 84-year-old woman with human epidermal growth factor receptor 2–enriched breast cancer (oestrogen receptor <1%, progesterone receptor <1%, c-*erb*B2 3+, and Ki-67 ~35%). (a) Mediolateral-oblique and (b) craniocaudal mammographic views of the right breast showing an irregular high-density mass in the retroareolar region, with spiculated margins and associated fine-linear branching microcalcifications in a segmental distribution (arrowheads). Marked nipple retraction (arrow in [a]) is suggestive of nipple involvement. (c) Ultrasound image showing an irregular hypoechoic mass with indistinct margins and posterior acoustic shadowing.

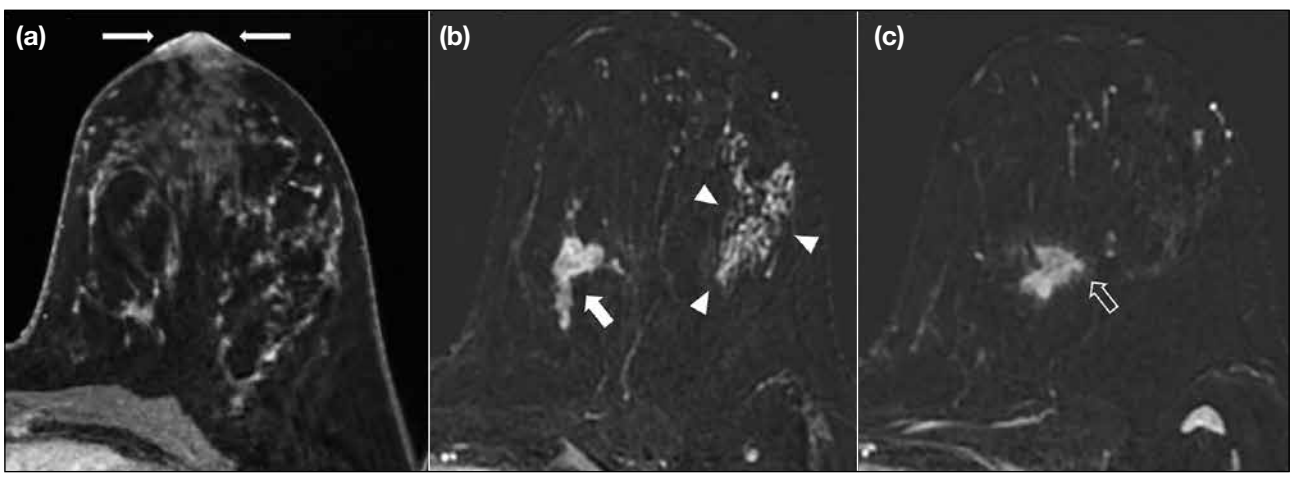

Figure 7. A 42-year-old woman presented with left mammary Paget's disease and was subsequently found to have multicentric human epidermal growth factor receptor 2 (HER2)–enriched breast cancer (oestrogen receptor <1%, progesterone receptor <1%, c-*erb*B2 3+, and Ki-67 ~20%) and ductal carcinoma in situ (DCIS). (a) Axial contrast-enhanced T1-weighted subtraction magnetic resonance (MR) image depicts abnormal enhancement involving the left nipple and periareolar region (arrows) in keeping with Paget's disease. (b and c) Axial contrast-enhanced T1-weighted subtraction MR images showing multicentric disease with two irregular and spiculated enhancing masses in the left breast (arrow in [b] and open arrow in [c]), both of which were histologically proven to be HER2-enriched breast cancer. Segmental non-mass enhancement in the outer aspect of the left breast (arrowheads in [b]) corresponds to the coexisting DCIS.

Distant metastases in HER2-enriched breast cancers show a propensity to involve the brain (Figure 8).[9]

The HER2-enriched subtype is found to be the most frequent breast cancer molecular subtype associated with mammary Paget's disease (Figure 7).[11]

BASAL-LIKE SUBTYPE (TRIPLE-NEGATIVE)

Genetic Expression and Clinical Implications

Triple-negative breast cancer (TNBC) is defined by lacking expression of ER, PR and HER2. The term 'triple-negative' is often used as a synonym for the

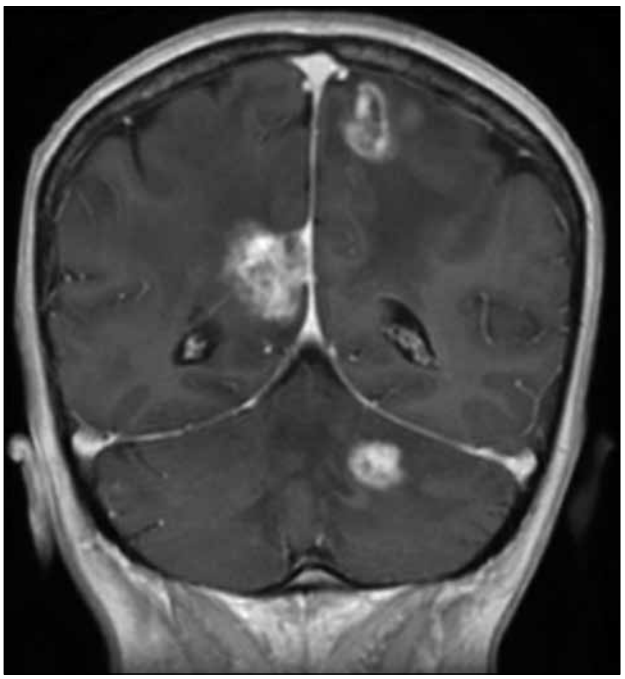

Figure 8. A 45-year-old woman with stage 4 human epidermal growth factor receptor 2–enriched breast cancer (oestrogen receptor <1%, progesterone receptor <1%, c-*erb*B2 3+, and Ki-67 ~40%). Coronal contrast-enhanced T1-weighted magnetic resonance image shows multiple enhancing brain metastases.

'basal-like' subtype because 86% of TNBC are the basal-like subtype.[6] TNBC accounts for 12% to 17% of all breast cancers,[12,13] preferentially affecting young women of African descent and carriers of germline breast cancer susceptibility gene 1 (BRCA1) and partner and localiser of BRCA2 (PALB2) mutations.[13]

TNBC has a tendency to develop early metastases to lung and brain, leading to rapid progression.[10,12] The time from distant recurrence to death is much shorter in triple-negative tumours than in other subtypes due to the relatively high mortality associated with visceral soft tissue metastases as compared to bone metastases in the luminal subtypes.[10] When compared with other breast cancer subtypes, patients with TNBC also experience a higher frequency (34% vs. 20%) and earlier onset (2.6 vs. 5.0 years after diagnosis) of distant recurrence.[10] Recurrences most commonly occur 1 to 4 years after diagnosis and are rare beyond 8 years, in contrast to the constant risk throughout the follow-up period in ER-positive tumours.[10] Due to the aggressive tumour biology and limited targeted therapy, patients harbouring TNBCs show poorer prognosis than patients with hormone receptor–positive tumours.[5,10]

TNBC has been shown to have greater sensitivity to neoadjuvant chemotherapy with a better pathological complete response than luminal and HER2 subtypes.[12] Conventional adjuvant chemotherapy using anthracycline/taxane-based regimens remains the standard of care for patients with TNBCs despite the identification of several promising agents, such as platinum.[12]

Imaging Characteristics

TNBC frequently presents as a palpable mass and often lacks the classical suspicious mammographic features, namely irregular mass, spiculated margins, and suspicious microcalcifications. Unifocal disease, circumscribed mass despite large size, necrotic mass with posterior enhancement on ultrasound, and absent calcifications on mammography are the imaging phenotype of TNBC (Figures 9 and 10).[14] TNBCs also show tendency towards a posterior or pre-pectoral location compared to other breast cancer subtypes (Figure 9).[15] Due to the apparent benign features on mammography and ultrasonography, TNBC may be mistaken as a fibroadenoma or complicated cyst (Figure 9). Besides the conventional techniques of mammography and ultrasound, dynamic contrast-enhanced MRI may serve as a useful adjunct to distinguish them by analysis of their enhancement patterns and respective kinetic curves (Figure 11). MRI breast kinetic curves, categorised into type I (progressive), type II (plateau), and type III (washout), offer distinguishing patterns in malignancy suspicion. Progressive curves, which demonstrate continuous enhancement over time, typically denote benignity. Plateau curves, characterised by initial enhancement followed by a plateau phase, raise concerns for malignancy. Washout curves, characterised by an initial uptake and subsequent washout, strongly imply malignancy.

TNBC has been shown to have a higher tumour roundness score compared with the other subtypes, reflecting a more biologically aggressive tumour type (Figures 9 and 10).[14] In contrast to luminal and HER2-enriched subtypes, there is no linear correlation between tumour size and the likelihood of lymph node involvement (Figure 12).[10,16]

Typical MRI findings in TNBC are mass enhancement and rim enhancement, which are related to tumour necrosis in these high-grade and fast-growing tumours.[8,14] The presence of peritumoral oedema was found to be the only significant variable associated with worse recurrence-free survival in patients with TNBC.[17]

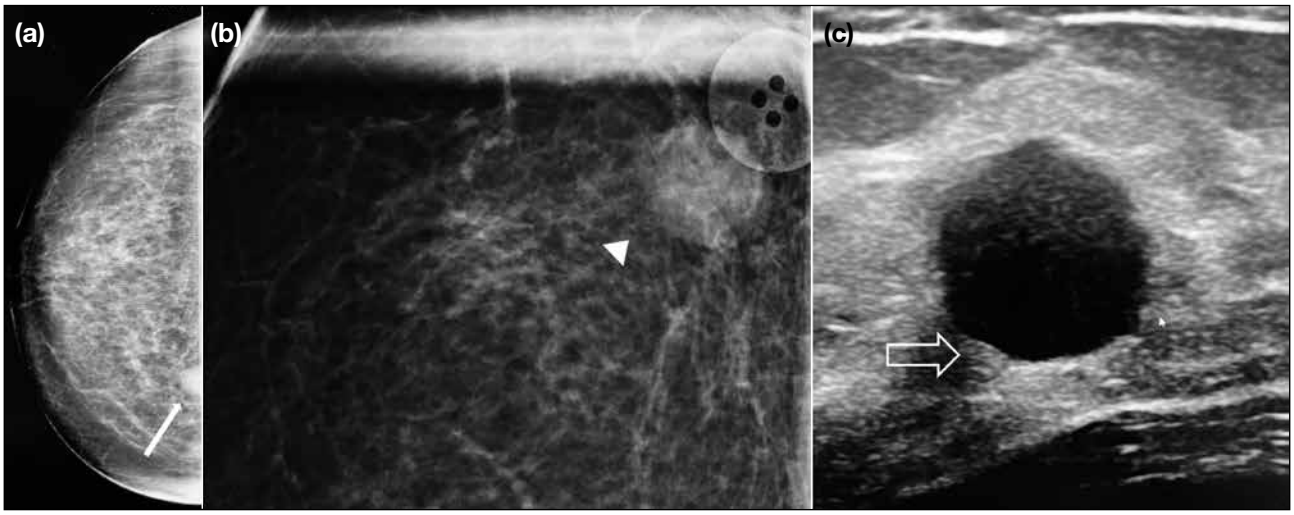

Figure 9. A 55-year-old woman with triple-negative breast cancer (TNBC) [oestrogen receptor <1%, progesterone receptor <1%, c-*erb*B2 0+, and Ki-67 ~40%]. (a) Craniocaudal mammographic view showing a partially included high-density, round mass (arrow) at posterior one-third of the inner right breast. (b) Coned magnified mediolateral mammographic view showing a high-density round mass with well-circumscribed margins (arrowhead). (c) Ultrasound showing a hypoechoic round mass with relatively circumscribed margins and posterior acoustic enhancement (open arrow). These apparently benign imaging features of TNBC could mimic a fibroadenoma or complicated cyst.

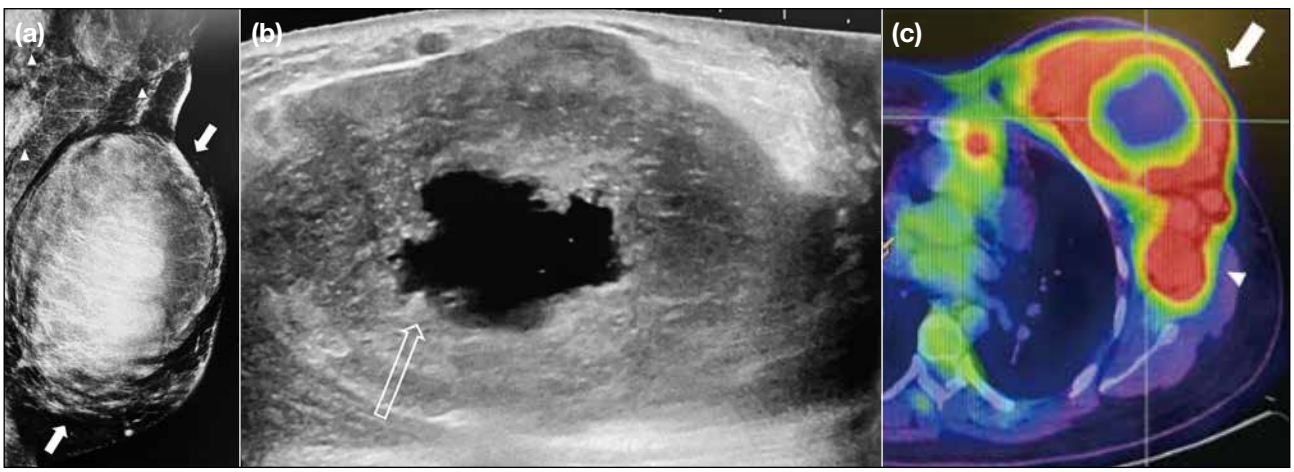

Figure 10. A 32-year-old woman with triple-negative breast cancer (oestrogen receptor <1%, progesterone receptor <1%, c-*erb*B2 0+, and Ki-67 >80%). (a) Mediolateral-oblique mammographic view showing a large, oval high-density mass (arrows) with relatively circumscribed margins occupying almost the entire left breast accompanied by bulky left axillary lymphadenopathy (arrowheads). (b) Ultrasound showing a lobulated necrotic mass with a central cystic area suggestive of tumour necrosis (open arrow). (c) Positron emission tomography/computed tomography showing hypermetabolic uptake in the left breast necrotic tumour (arrow; maximum standardised uptake value [SUV_{max}] = 19.2) and left axillary lymphadenopathy (arrowhead; SUV_{max} = 14.2).

MRI is the most sensitive imaging modality in the early prediction of neoadjuvant chemotherapy response and pathological complete response in patients harbouring TNBCs.[14] Most of the studies have shown that TNBCs are relatively chemosensitive compared to other subtypes. Placement of a marker clip within the TNBC prior to neoadjuvant chemotherapy allows precise localisation of the tumour for subsequent operation (Figures 13 and 14).

CONCLUSION

Knowledge of molecular classification of breast cancers allows better understanding of the clinical behaviour and prognosis of the different breast cancer subtypes, thus facilitating implementation of individualised therapies.

Precision medicine is the emerging approach for individualising patient treatment, which is the standard

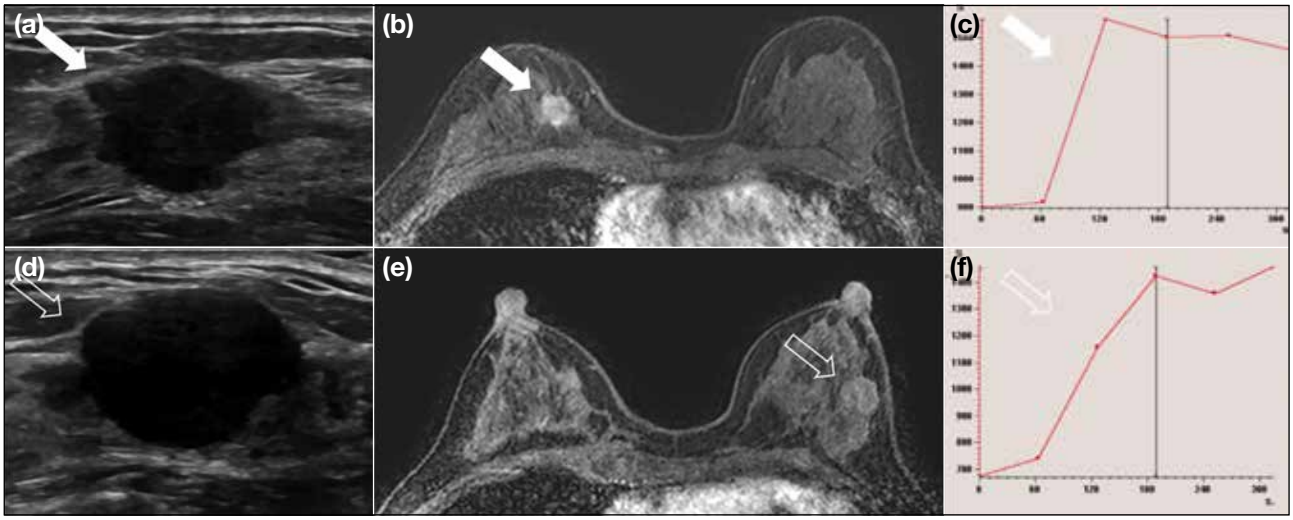

Figure 11. A 56-year-old woman with triple-negative right breast cancer (TNBC) [oestrogen receptor <1%, progesterone receptor <1%, c-*erb*B2 1+/confirmed negative by fluorescence in situ hybridisation, and Ki-67 <10%] in the background of multiple fibroadenomas. (a-c) Biopsy-proven TNBC is found in the right breast (arrows). Ultrasound images show an irregular mass with angular margin in the right breast, with corresponding enhancement and a type III kinetic curve in dynamic contrast enhancement magnetic resonance imaging (MRI), which suggests malignancy. (d-f) Biopsy-proven fibroadenoma in the left breast (open arrows). Ultrasound images show a circumscribed mass in the left breast with corresponding enhancement and a type I kinetic curve in dynamic contrast enhancement MRI, which suggests benignity.

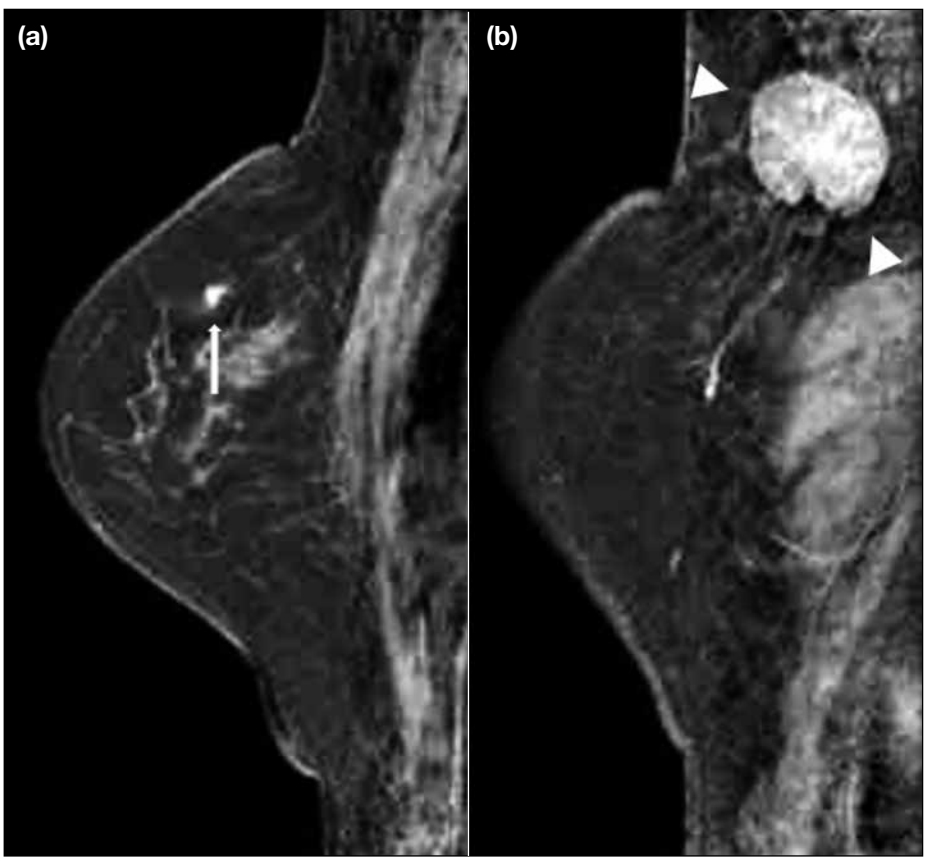

Figure 12. A 57-year-old woman with triple-negative breast cancer (TNBC) and a large axillary nodal metastasis (oestrogen receptor <1%, progesterone receptor <1%, and c-*erb*B2 0+). Sagittal contrast-enhanced T1-weighted magnetic resonance images showing (a) a small (0.5 cm) enhancing focus (arrow) in the upper right breast and (b) a large round, enhancing node (arrowheads) in the ipsilateral axilla, demonstrating non-linear correlation between the primary tumour size and the likelihood of lymph node involvement, a typical feature for TNBC.

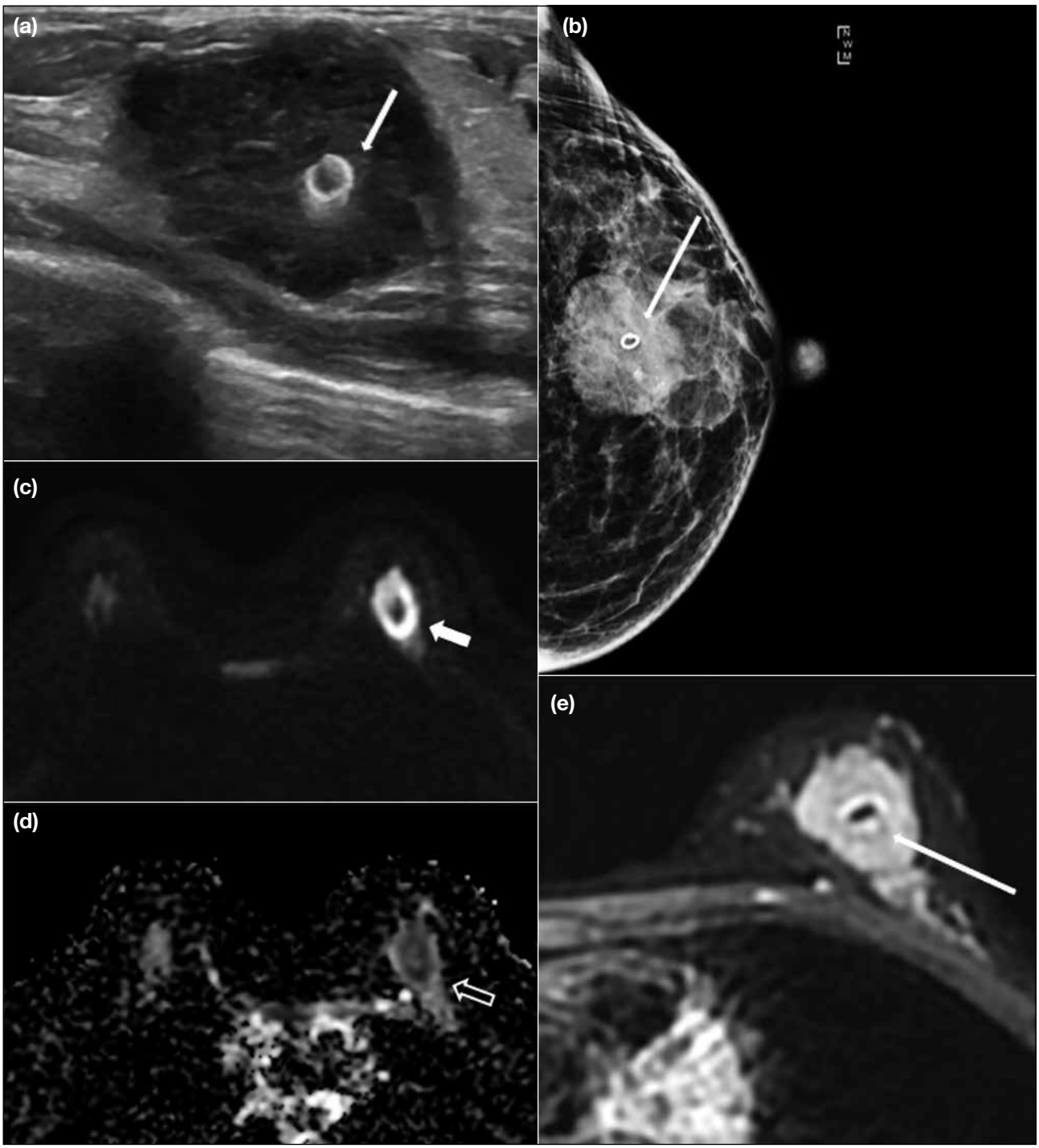

Figure 13. A 51-year-old woman with triple-negative breast cancer (TNBC) in the left breast [oestrogen receptor <1%, progesterone receptor <1%, c-*erb*B2 0+, and Ki-67 ~95%] underwent ultrasound-guided marker insertion before neoadjuvant chemotherapy. (a) Ultrasound-guided insertion of marker (arrow) was performed via a 17-G needle. (b) Craniocaudal mammographic image demonstrates the correct placement of marker (arrow) within the biopsy-proven TNBC. (c) Axial diffusion-weighted image shows significant restriction of diffusion (arrow) in the tumour. (d) Corresponding apparent diffusion coefficient (ADC) image showing decreased ADC, as evidenced by the dark signal (open arrow) in the region of restricted diffusion. (e) Axial contrast-enhanced T1-weighted magnetic resonance image shows a signal void (arrow) within the enhancing breast mass, corresponding to the marker.

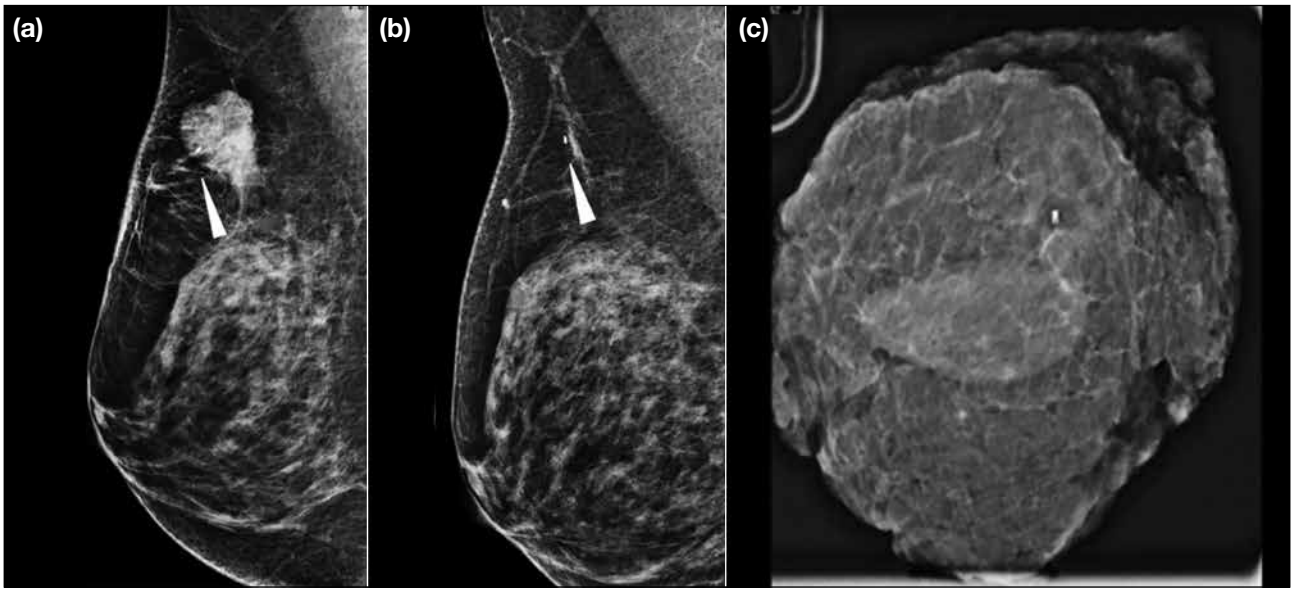

Figure 14. A 58-year-old woman with triple-negative breast cancer (TNBC) [oestrogen receptor <1%, progesterone receptor <1%, c-*erb*B2 0+, and Ki-67 ~65%] with complete radiological response to neoadjuvant chemotherapy. (a) Mediolateral-oblique mammographic image showing the placement of biopsy marker (arrowhead) within the biopsy-proven TNBC in the right breast. (b) Mediolateral-oblique mammographic image following neoadjuvant chemotherapy showing the marker (arrowhead) with complete resolution of the mass. (c) Radiograph of the lumpectomy specimen confirms the marker in situ with sufficient surgical margins.

of care for breast cancer management in the current era. The role of radiologists is no longer limited to establishing the diagnosis, staging, and surveillance of breast cancers. They play a vital role in guiding the investigation options based on the specific biology of breast cancer, assessment of neoadjuvant treatment response, and facilitating clinicians in optimising individualised patient care. Thorough understanding of breast cancer molecular subtypes is one of the biggest steppingstones amongst breast radiologists to participate in precision medicine practice.

REFERENCES

1. Centre for Health Protection, Department of Health, Hong Kong SAR Government. Breast cancer. Available from: https://www.chp.gov.hk/en/healthtopics/content/25/53.html. Accessed 4 Sep 2023.
2. Goldhirsch A, Wood WC, Coates AS, Gelber RD, Thürlimann B, Senn HJ, et al. Strategies for subtypes—dealing with the diversity of breast cancer: highlights of the St. Gallen International Expert Consensus on the Primary Therapy of Early Breast Cancer 2011. Ann Oncol. 2011;22:1736-47.
3. Johnson KS, Conant EF, Soo MS. Molecular subtypes of breast cancer: a review for breast radiologists. J Breast Imaging. 2021;3:12-24.
4. Ades F, Zardavas D, Bozovic-Spasojevic I, Pugliano L, Fumagalli D, de Azambuja E, et al. Luminal B breast cancer: molecular characterization, clinical management, and future perspectives. J Clin Oncol. 2014;32:2794-803.
5. Fallahpour S, Navaneelan T, De P, Borgo A. Breast cancer survival by molecular subtype: a population-based analysis of cancer registry data. CMAJ Open. 2017;5:E734-9.
6. Trop I, LeBlanc SM, David J, Lalonde L, Tran-Thanh D, Labelle M, et al. Molecular classification of infiltrating breast cancer: toward personalized therapy. Radiographics. 2014;34:1178-95.
7. Cheang MC, Chia SK, Voduc D, Gao D, Leung S, Snider J, et al. Ki67 Index, HER2 status, and prognosis of patients with luminal B breast cancer. J Natl Cancer Inst. 2009;101:736-50.
8. Navarro Vilar L, Alandete Germán SP, Medina García R, Blanc García E, Camarasa Lillo N, Vilar Samper J. MR imaging findings in molecular subtypes of breast cancer according to BI-RADS system. Breast J. 2017;23:421-8.
9. Bertos NR, Park M. Breast cancer—one term, many entities? J Clin Invest. 2011;121:3789-96.
10. Dent R, Trudeau M, Pritchard KI, Hanna WM, Kahn HK, Sawka CA, et al. Triple-negative breast cancer: clinical features and patterns of recurrence. Clin Cancer Res. 2007;13(15 Pt 1):4429-34.
11. Arafah M, Arain SA, Raddaoui EM, Tulba A, Alkhawaja FH, Al Shedoukhy A. Molecular subtyping of mammary Paget's disease using immunohistochemistry. Saudi Med J. 2019;40:440-6.
12. Newman LA, Reis-Filho JS, Morrow M, Carey LA, King TA. The 2014 Society of Surgical Oncology Susan G. Komen for the Cure Symposium: triple-negative breast cancer. Ann Surg Oncol. 2015;22:874-82.
13. Howard FM, Olopade OI. Epidemiology of triple-negative breast cancer: a review. Cancer J. 2021;27:8-16.
14. Dogan BE, Turnbull LW. Imaging of triple-negative breast cancer. Ann Oncol. 2012;23 Suppl 6:vi23-9.
15. Kim WH, Han W, Chang JM, Cho N, Park IA, Moon WK. Location of triple-negative breast cancers: comparison with estrogen receptor-positive breast cancers on MR imaging. PLoS One. 2015;10:e0116344.
16. Foulkes WD, Metcalfe K, Hanna W, Lynch HT, Ghadirian P, Tung N, et al. Disruption of the expected positive correlation between breast tumor size and lymph node status in BRCA1-related breast carcinoma. Cancer. 2003;98:1569-77.
17. Bae MS, Shin SU, Ryu HS, Han W, Im SA, Park IA, et al. Pretreatment MR imaging features of triple-negative breast cancer: association with response to neoadjuvant chemotherapy and recurrence-free survival. Radiology. 2016;281:392-400.

Hong Kong J Radiol. 2023;26:217-32. Epub 15 Sep 2023 | https://doi.org/10.12809/hkjr2217525

PICTORIAL ESSAY

Conventional and Advanced Post-treatment Magnetic Resonance Imaging of Primary and Metastatic Brain Tumours: A Pictorial Essay

JCY Lau[1], AYT Lai[1], KYK Tang[1], CY Chu[1], PY Wu[2], WK Kan[1]

[1]Department of Radiology, Pamela Youde Nethersole Eastern Hospital, Hong Kong SAR, China
[2]Department of Clinical Oncology, Pamela Youde Nethersole Eastern Hospital, Hong Kong SAR, China

INTRODUCTION

Both primary and secondary brain neoplasms are commonly encountered in neuroimaging. Glioblastoma is the most common primary malignant brain tumour in adults.[1] Mortality remains high despite development of different treatment options with combinations of surgery, radiotherapy, and chemotherapy. The 2-year and 5-year survival rates after diagnosis of glioblastoma are reported to be approximately 26.5%[2] and 5% to 10%,[3] respectively. Evaluation of treatment response and detection of treatment-related complications are crucial in patient management and rely heavily on neuroimaging.

Brain tumour treatment response criteria have been established to evaluate treatment progression or regression of gliomas. Currently, the most widely used set of criteria is the Response Assessment in Neuro-Oncology (RANO) criteria.[1] First proposed in 2010, the RANO criteria assess measurable disease, non-measurable disease, use of corticosteroids, and clinical status[2] for assessment of treatment response, which are discussed in this article.

There are significant overlapping features with conventional magnetic resonance imaging (MRI) techniques among treatment response and disease progression and/or treatment-related complications. Advanced MRI techniques, including MR spectroscopy (MRS) and perfusion, are useful adjuncts to facilitate interpretation of post-treatment brain tumour images, especially in identifying pseudoprogression or pseudoresponse.[4,5]

This pictorial essay illustrates the broad spectrum of treatment-related complications, the different treatment responses of brain tumours as classified by the RANO criteria, and utilisation of advanced MRI techniques in identifying treatment-related changes, e.g., pseudoprogression or pseudoresponse.

Correspondence: *Dr JCY Lau, Department of Radiology, Pamela Youde Nethersole Eastern Hospital, Hong Kong SAR, China*
Email: lcy486@ha.org.hk

Submitted: 5 Jan 2022; Accepted: 17 May 2022.

Contributors: JCYL and AYTL designed the study. JCYL, AYTL and PYW acquired the data. JCYL and AYTL analysed the data. JCYL drafted the manuscript. All authors critically revised the manuscript for important intellectual content. All authors had full access to the data, contributed to the study, approved the final version for publication, and take responsibility for its accuracy and integrity.

Conflicts of Interest: All authors have disclosed no conflicts of interest.

Funding/Support: This study received no specific grant from any funding agency in the public, commercial, or not-for-profit sectors.

Data Availability: All data generated or analysed during the present study are available from the corresponding author on reasonable request.

Ethics Approval: The study was approved by the Hong Kong East Cluster Research Ethics Committee of Hospital Authority, Hong Kong (Ref No.: HKECREC-2022-001). A waiver for written informed consent of patients was granted by the Committee as this manuscript is for pictorial review only and does not involve patient treatment/procedures.

TREATMENT RESPONSE ASSESSMENT USING THE RESPONSE ASSESSMENT IN NEURO-ONCOLOGY CRITERIA

Definitions

Measurable disease is defined as bi-dimensionally (two perpendicular diameters) contrast-enhancing lesions of at least 10 mm, while non-measurable disease is defined as either unidimensionally measurable lesions, masses with unclear margins, or lesions with maximal perpendicular diameters of <10 mm.[4] Cysts or the surgical cavity should be considered non-measurable unless there is a nodular component measuring at least 10 mm in diameter.[4] Lesions with T2/fluid-attenuation inversion recovery (FLAIR) hyperintense signals are considered non-measurable.[1]

Multiple Lesions

A minimum of two and a maximum of five target lesions may be counted to reflect tumour burden. The sum of the products of the perpendicular diameters are used for determining treatment response. Although the largest lesions are commonly selected, emphasis should be made on lesions with reproducible measurements.[4]

Categories of treatment response, which are from Leao et al[1] and Wen et al,[4] are summarised as follows.

Complete response

It requires all of the following: complete disappearance of all enhancing measurable and non-measurable diseases sustained for at least 4 weeks; no new lesions; and stable or improved non-enhancing (T2/FLAIR hyperintensity) lesions. Patients must be off corticosteroids (or on physiological replacement doses only) and should be in a stable or clinically improved status (Figure 1).[4]

Partial response

It requires all of the following: ≥50% decrease in the sum of products of perpendicular diameters of all measurable enhancing lesions compared with baseline scan sustained for at least 4 weeks; no progression of non-measurable disease; no new lesions; stable or improved non-enhancing (T2/FLAIR hyperintensity) lesions on the same or a lower dose of corticosteroids compared with baseline scan; and the patient being on a corticosteroid that is not greater than the dose at time of the baseline scan and should be in stable or clinically improved status (Figure 2).[4]

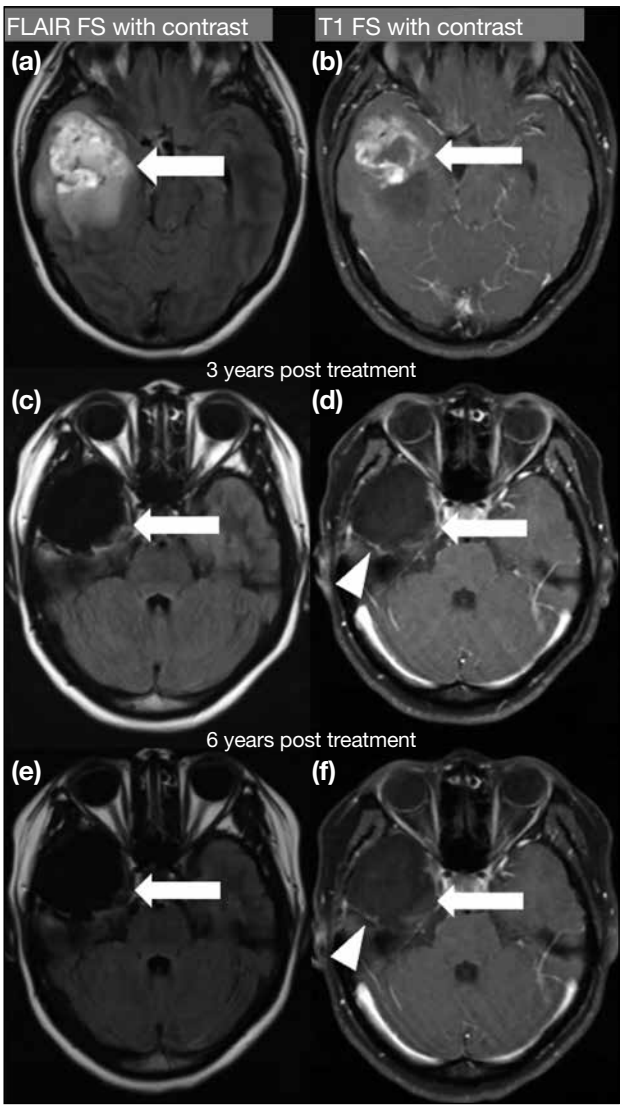

Figure 1. Complete response shown in post-contrast fluid-attenuation inversion recovery (FLAIR) fat suppression (FS) sequences (a, c, and e) and post-contrast T1-weighted FS sequences (b, d, and f). An ill-defined contrast-enhancing mass with vasogenic oedema was demonstrated in the right temporal lobe in a 20-year-old patient (arrows in [a] and [b]). Gross total excision was performed, confirming oligodendroglioma. No adjuvant therapy was prescribed. Follow-up magnetic resonance imaging performed 3 years (c and d) and 6 years (e and f) later revealed encephalomalacia (arrows in [c] to [f]) and stable enhancement (arrowheads in [d] and [f]) of the dura, suggesting postoperative changes. Features are compatible with complete response.

Stable disease

It requires all of the following: not qualified for complete response, partial response or progression; stable non-enhancing (T2/FLAIR hyperintensity) lesion; the patient being on the same or lower dose of corticosteroids compared with baseline scan and should be in clinically stable status (Figures 2 and 3).[1,4]

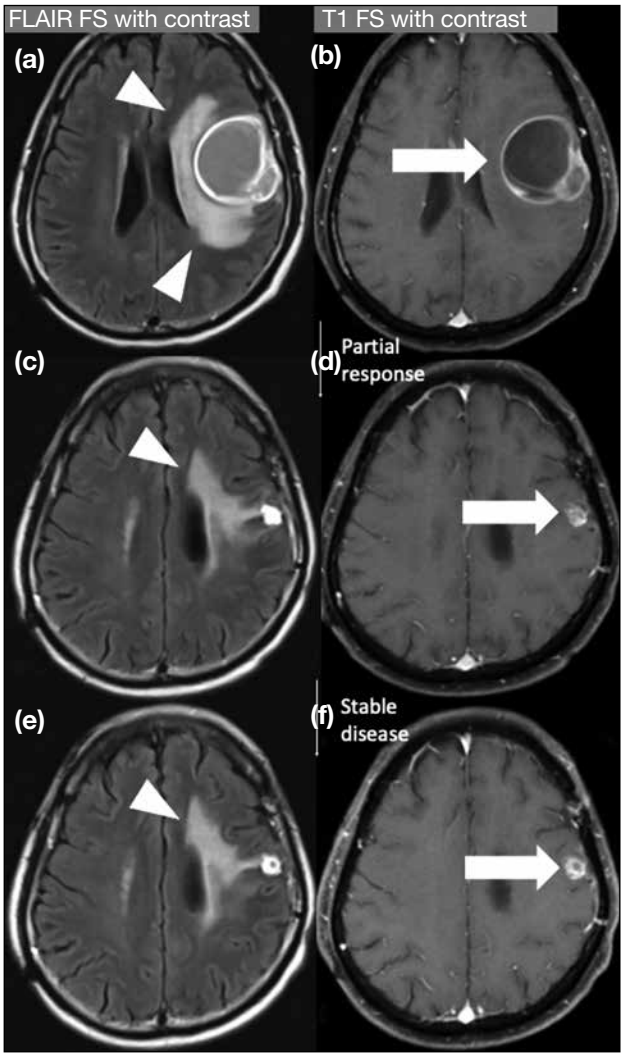

Figure 2. Partial response and stable disease shown in post-contrast fluid-attenuation inversion recovery (FLAIR) fat suppression (FS) sequences (a, c, and e) and post-contrast T1-weighted FS sequences (b, d, and f). (a and b) A rim-enhancing complex cystic lesion with eccentric enhancing-solid component (arrow in [b]) and perifocal FLAIR hyperintensity (arrowheads in [a]) are illustrated in the left frontal lobe of a 73-year-old patient. Histology of World Health Organization grade 4 glioblastoma was confirmed with gross total excision. The patient was then managed with adjuvant chemoirradiation. Follow-up magnetic resonance imaging (MRI) at 1 year (c and d) revealed significant reduction in the left frontal contrast-enhancing lesion (arrow in [d]) and perilesional FLAIR hyperintensity (arrowhead in [c]), compatible with partial response. MRI performed 2 years after the excision (e and f) demonstrated no significant change (arrow in [f] and arrowhead in [e]), suggestive of stable disease.

Disease progression

It is defined by any of the following: ≥25% increase in sum of the products of perpendicular diameters of enhancing lesions compared with the smallest tumour measurement obtained either at baseline scan (if no decrease) or best response; on stable or increasing doses of corticosteroids; significant increase in non-enhancing T2/FLAIR hyperintensity lesion on stable or increasing doses of corticosteroids compared with baseline scan or best response after initiation of therapy, not caused by comorbid events; any new lesion; clear clinical deterioration not attributable to other causes apart from the tumour or changes in corticosteroid dose; failure to return for evaluation as a result of death or deteriorating condition; or clear progression of non-measurable disease (Figures 4 to 6).[1,4]

PSEUDOPROGRESSION

The Stupp protocol, consisting of maximal safe excision and adjuvant radiotherapy with concurrent and adjuvant temozolomide, is considered the standard of care for glioblastoma.[2]

New or progressive contrast enhancement can develop as a result of irradiation or treatment, in addition to true tumour progression. The RANO criteria define phenomenon that eventually subsides without alteration of management as pseudoprogression (Figures 7 and 8),[1,4] with reported incidence of up to 21% to 36%.[1,6] It is more commonly encountered in glioblastoma with positive methylated O^6-methylguanine–DNA methyltransferase gene promoter, which carries a better prognosis.

Pseudoprogression is likely the consequence of transient increase in tumour vasculature and permeability due to irradiation and is exacerbated by temozolomide. During the early post-radiotherapy period (usually around 3-6 months), most new lesions on MRI represent a mixture of residual tumour and pseudoprogression. The predominant component will dictate the clinical and radiological picture over time. Imaging features during this period might be difficult to interpret even with the help of advanced MRI techniques. The RANO criteria suggest that progression can only be determined <12 weeks after completion of adjuvant chemoradiation if the new enhancing focus is outside of the high-dose radiation field or by unequivocal histological findings.[4] Classically, pseudoprogression presents with a mass of 'Swiss cheese' appearance[1] (Figure 7) on conventional imaging. At 3 to 6 months after the commencement of chemoradiation, when there are new or progressive lesions, advanced MRI might potentially aid radiologists in interpreting these lesions.

Magnetic Resonance Perfusion

Dynamic susceptibility contrast (DSC) and dynamic contrast enhancement (DCE) are the most commonly

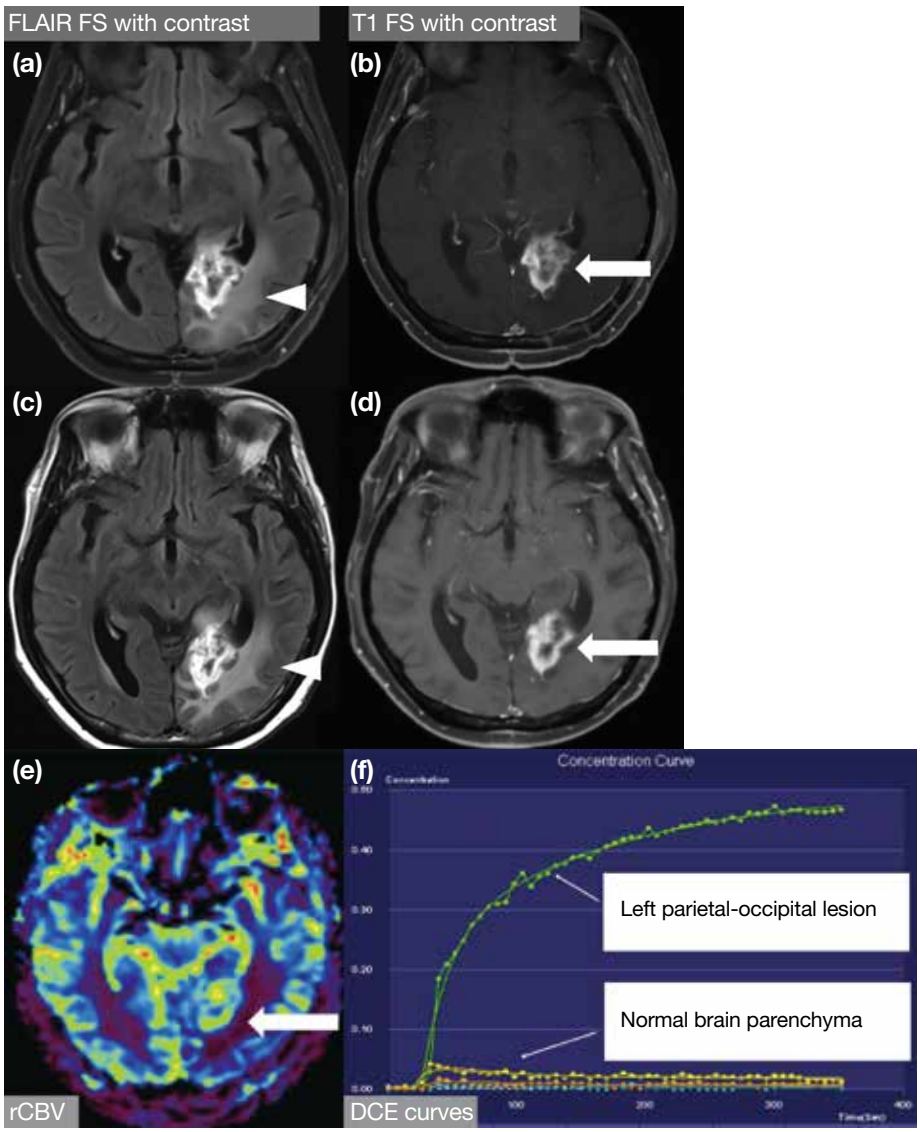

Figure 3. Stable disease shown in post-contrast fluid-attenuation inversion recovery (FLAIR) fat suppression (FS) sequences (a and c) and post-contrast T1-weighted FS sequences (b and d). (e) shows the relative cerebral blood volume (rCBV) colour map while (f) shows the dynamic contrast enhancement (DCE) concentration-time curve. A 53-year-old patient underwent subtotal excision of a left parietooccipital tumour, confirming a glioblastoma with negative O^6-methylguanine–DNA methyltransferase methylation and isocitrate dehydrogenase wild-type. The patient was then managed with combined radiotherapy and temozolomide. Follow-up magnetic resonance imaging (MRI) performed 5 months (a and b) and 9 months (c and d) after chemoradiotherapy demonstrated no significant interval change in the left parietal-occipital contrast-enhancing lesion (arrows in [b] and [d]) and the perilesional FLAIR hyperintense signals (arrowheads in [a] and [c]). MR perfusion (e and f) performed 9 months after chemoradiotherapy illustrated increase in rCBV (arrow in [e]), rapid initial uprise of the concentration-time curve and larger initial area under the curve at the left parietal-occipital lesion, suggestive of residual tumour. Features are in keeping with stable disease.

used perfusion techniques for assessment of tumour perfusion. DSC perfusion imaging utilises the susceptibility gradient from loss of T2* signal secondary to the passage of contrast through brain tissue and hence derives the relative cerebral blood volume (rCBV).[1,6] High rCBV would suggest the presence of tumour (Figures 5 and 6) due to their hypervascularity, whereas low rCBV may represent post-treatment changes (Figure 8).[5]

DCE perfusion involves plotting a contrast signal–time curve, also known as a concentration-time curve, enhancement-time curve or permeability curve, by estimating the extravasation of contrast from the intravascular space into the extravascular extracellular space (EES).[7] Measurements derived from this permeability curve have been found to provide valuable clinical information concerning tumour behaviour. Quantification of enhancement characteristics can be performed using a range of techniques, from simple measures of the rate of enhancement to complex algorithmic analyses that apply pharmacokinetic models to the imaging data, one of which bears the intention of measuring the transfer constant of contrast between the plasma and the EES, i.e., the time-dependent leakage constant K^{trans}.[7] K^{trans} is dependent on plasma blood flow, vascular permeability, and capillary surface area. The slope of the concentration-time curve is therefore one of the factors in determining the level of this constant.[8] K^{trans} is described to be elevated, compared to that of normal brain tissue, in tumour progression (Figures 5 and 6) and reduced in pseudoprogression (Figure 8).[1,4,6] However,

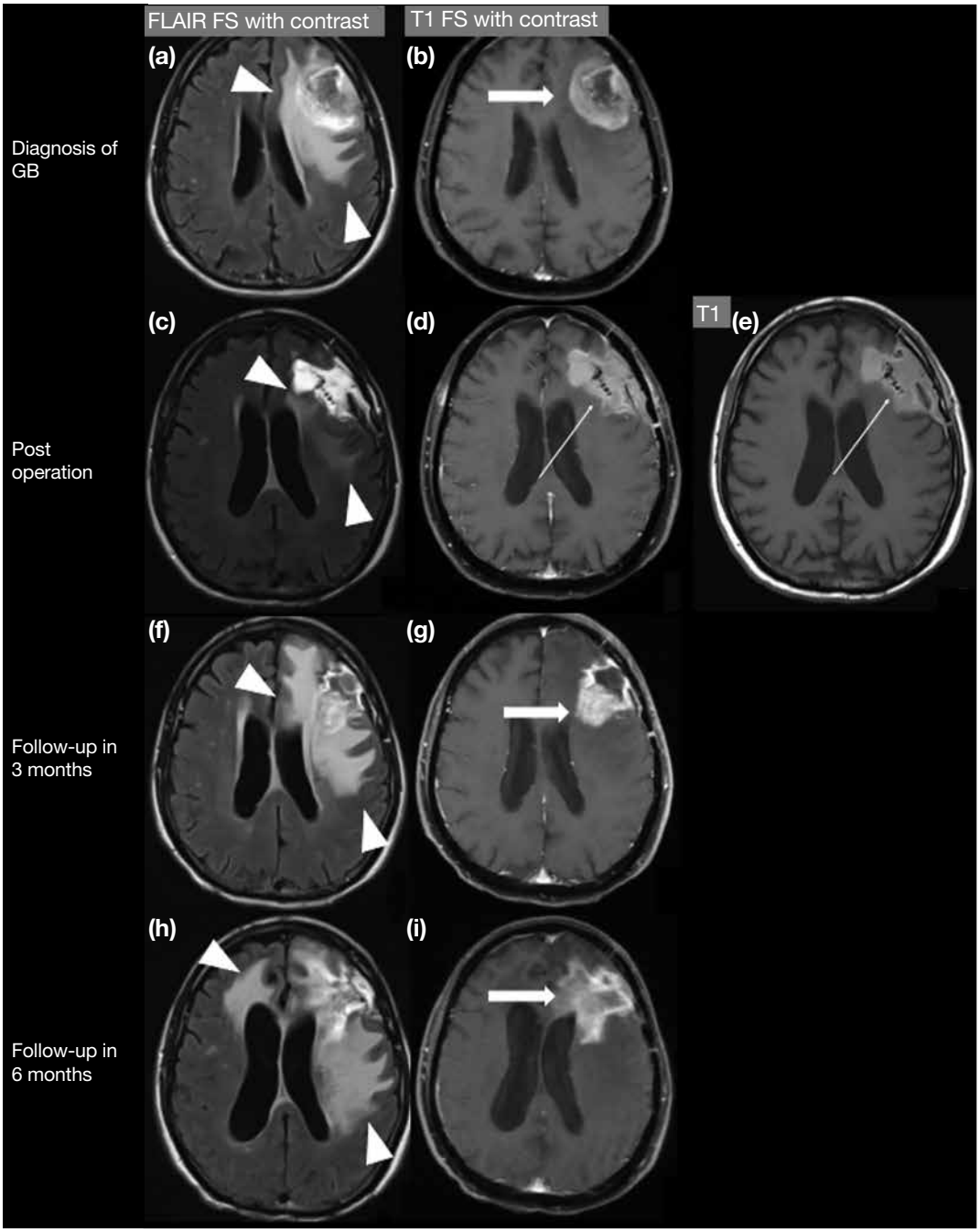

Figure 4. Disease progression shown in post-contrast fluid-attenuation inversion recovery (FLAIR) fat suppression (FS) sequences (a, c, f, and h), post-contrast T1-weighted FS sequences (b, d, g, and i), and T1-weighted sequence (e). A 72-year-old patient presented with a heterogeneously enhancing left frontal mass (arrow in [b]) with perilesional FLAIR hyperintense signals (arrowheads in [a]). The patient underwent gross total excision of the tumour with pathology suggesting glioblastoma (GB). Early postoperative magnetic resonance imaging (MRI) [c, d, and e] showed significant reduction in size of the left frontal tumour and FLAIR signals (arrowheads in [c]) with presence of T1-weighted hyperintensity (thin arrows in [d] and [e]), suggesting subacute blood products. Radiotherapy was prescribed and follow-up MRI performed 3 months later (f and g) revealed increased contrast enhancement (arrow in [g]) and FLAIR hyperintensity (arrowheads in [f]) in the left frontal-parietal region. Combined with the findings in Figure 5, features are most compatible with disease progression, which was confirmed in subsequent follow-up MRI (h and i), showing increase in size of the enhancing mass (arrow in [i]) and perilesional FLAIR hyperintensity (arrowheads in [h]).

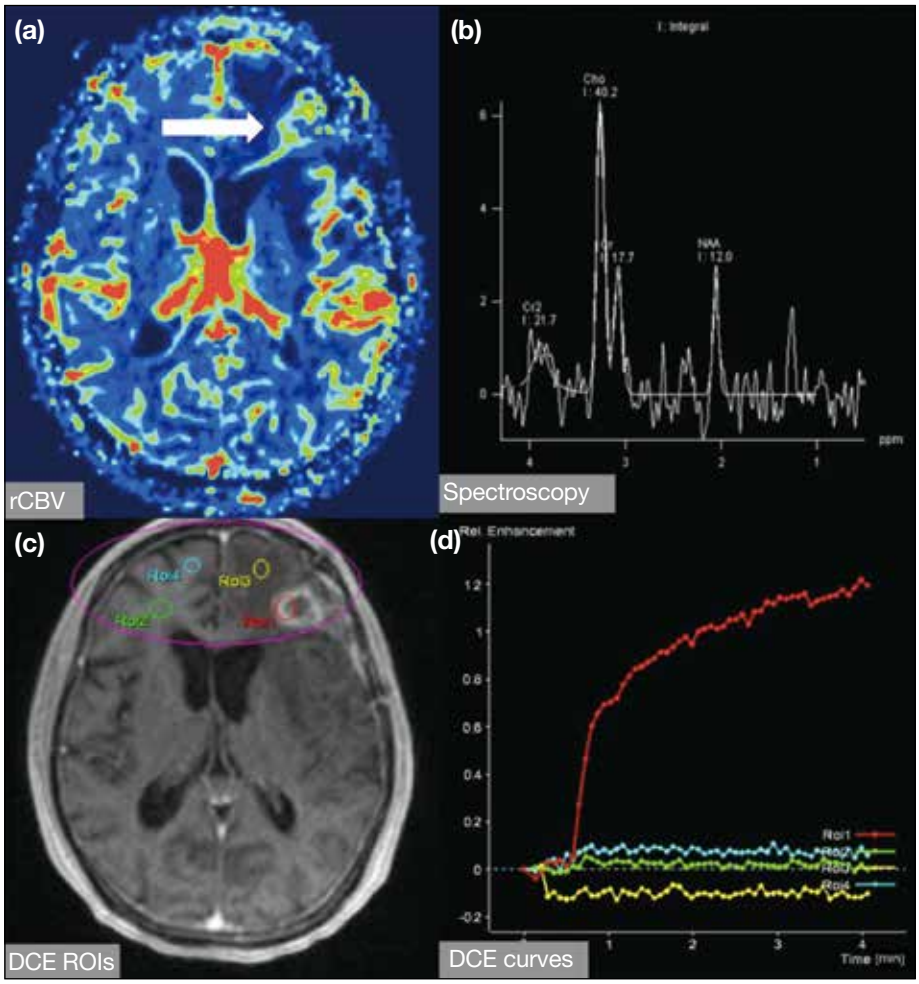

Figure 5. Disease progression in the same patient as in Figure 4 with magnetic resonance (MR) perfusion and MR spectroscopy (MRS) performed 3 months after excision of the left frontal glioblastoma. (a) shows relative cerebral blood volume (rCBV) map, (b) shows MRS, (c) shows dynamic contrast enhancement (DCE) regions of interest [ROIs], and (d) shows DCE concentration-time curves. The left frontal lesion demonstrated elevated rCBV (arrow in [a]), an elevated choline (Cho) peak with reversed Cho-to–*N*-acetylaspartate (NAA) ratio (b), a rapid rise in initial DCE enhancement, and a larger initial area under the curve as compared to the normal brain parenchyma (d). Together with the findings in Figure 4, features are in keeping with disease progression.

detailed discussion on the compartmental models is beyond the scope of this article.

The concentration-time curve derived from the DCE perfusion consists of two phases, namely the initial vascular phase and the subsequent delayed equilibrium phase.[9] The initial upslope reflects early enhancement, mostly from the contrast agent in the blood vessels and early leakage into the EES due to disrupted blood-brain barrier, which is again dependent on blood flow and vascular surface area. On the other hand, the delayed equilibrium phase includes mostly delayed permeability and slow accumulation of contrast agent into the EES, depending on the backflow of contrast agent into the intravascular compartment. These factors are affected by the volume of EES, interstitial pressure, and total vascular area.

Compared to treatment-induced necrosis, recurrent or progressive brain tumour shows an elevated maximum slope in the initial vascular phase due to increased blood flow from neo-angiogenesis.[9] The slope of the delayed equilibrium phase is higher in treatment-induced necrosis as a result of low cellularity and more tissue damage, allowing more retention of contrast in the EES and less backflow to the intravascular compartment, resulting in reduced washout.[9]

The area under the curve (AUC) of the concentration-time curve can also help differentiate between recurrent tumour and radiation necrosis. The initial AUC (iAUC) is found to be higher in recurrent tumour than in radiation necrosis, as a result of neovascularity in the tumour.[9] The ratio of iAUC to final AUC (defined as between 320 and 350 seconds after contrast agent arrival in the same enhancing voxel of interest as iAUC) is found to be elevated in recurrent tumours compared to radiation necrosis, explained by the fact that high vascularity in recurrent tumour results in elevated iAUC while more retention of contrast in the EES due to low cellularity and more tissue damage in radiation necrosis contributes to higher final AUC.[10]

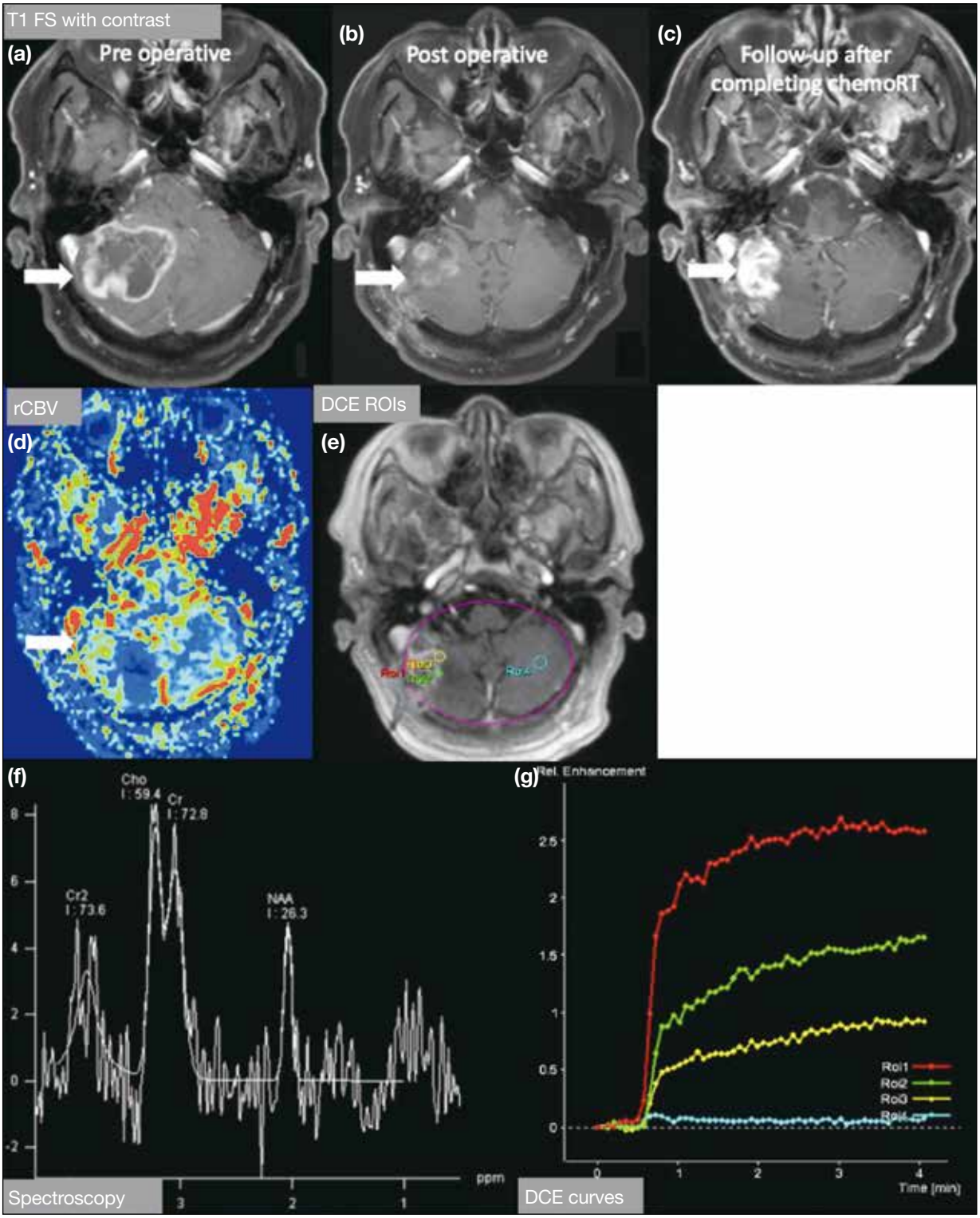

Figure 6. Disease progression. A 79-year-old patient with right cerebellar glioblastoma underwent gross total excision and managed with adjuvant radical radiotherapy (a to c). The images show a contrast enhancing lesion at right cerebellum on post-contrast T1-weighted fat saturation (FS) sequences at preoperation (arrow in [a]), 1 month postoperation (arrow in [b]), and after completing chemoradiotherapy (arrow in [c]); (d) shows relative cerebral blood volume (rCBV) colour map while (f) shows magnetic resonance spectroscopy. After completing chemoradiotherapy, the enlarging right cerebellar mass (arrow in [c]) showed elevated cerebral perfusion (arrow in [d]) and an elevated choline (Cho) peak with a reversed Cho-to–*N*-acetylaspartate (NAA) ratio of >2 (f). Dynamic contrast enhancement (DCE) regions of interest (ROIs) were demonstrated in (e) [purple circle]. Steep upslope of the concentration-time curves and larger initial areas under the curve were illustrated as compared to the normal left cerebellar hemisphere (g). This was histologically proven to be tumour recurrence and disease progression.

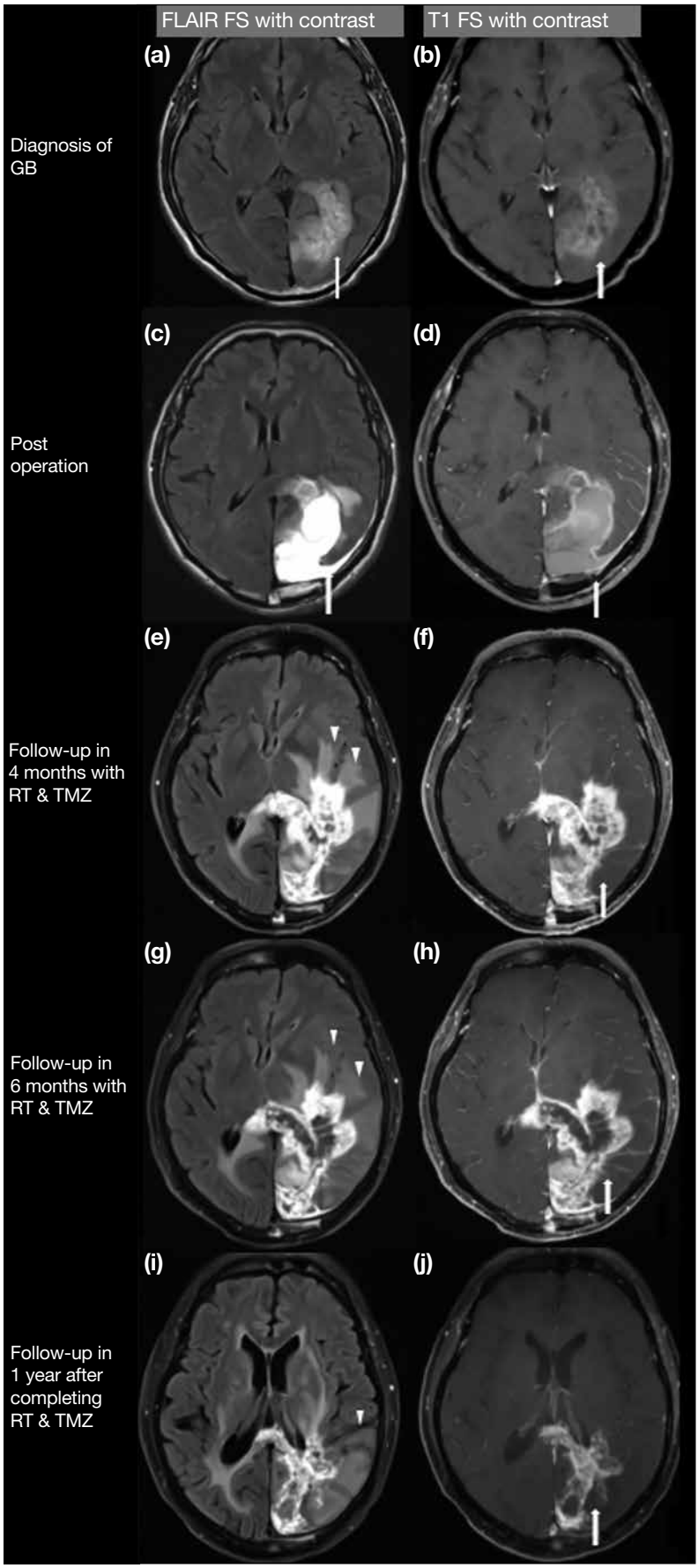

Figure 7. Pseudoprogression shown in post-contrast fluid-attenuation inversion recovery (FLAIR) fat suppression (FS) sequences (a, c, e, g, and i) and post-contrast T1-weighted images with FS sequences (b, d, f, h, and j). A 63-year-old patient with an ill-defined enhancing left parietooccipital tumour that was compatible with glioblastoma [GB] (arrows in [a] and [b]) was subsequently removed by near-total excision. Histology showed glioblastoma with positive O^6-methylguanine–DNA methyltransferase methylation. Postoperative magnetic resonance imaging (MRI) illustrated no gross parenchymal enhancement (arrows in [c] and [d]). The patient was managed with combined radiotherapy (RT) and temozolomide (TMZ). Follow-up MRI performed 4 months (e and f) and 6 months (g and h) after surgery showed progression of the contrast enhancement with a 'Swiss cheese' appearance (arrows in [f] and [h]) and perilesional FLAIR hyperintense signals (arrowheads in [e] and [g]). Advanced MRI was then performed in view of suspicion of pseudoprogression (see Figure 8). The patient was continued on the same chemotherapy. Follow-up MRI performed 1 year after completion of the adjuvant therapy (i and j) demonstrated decreased enhancement and FLAIR hyperintensities (arrowhead in [i] and arrow in [j]). The constellation of the findings was compatible with pseudoprogression.

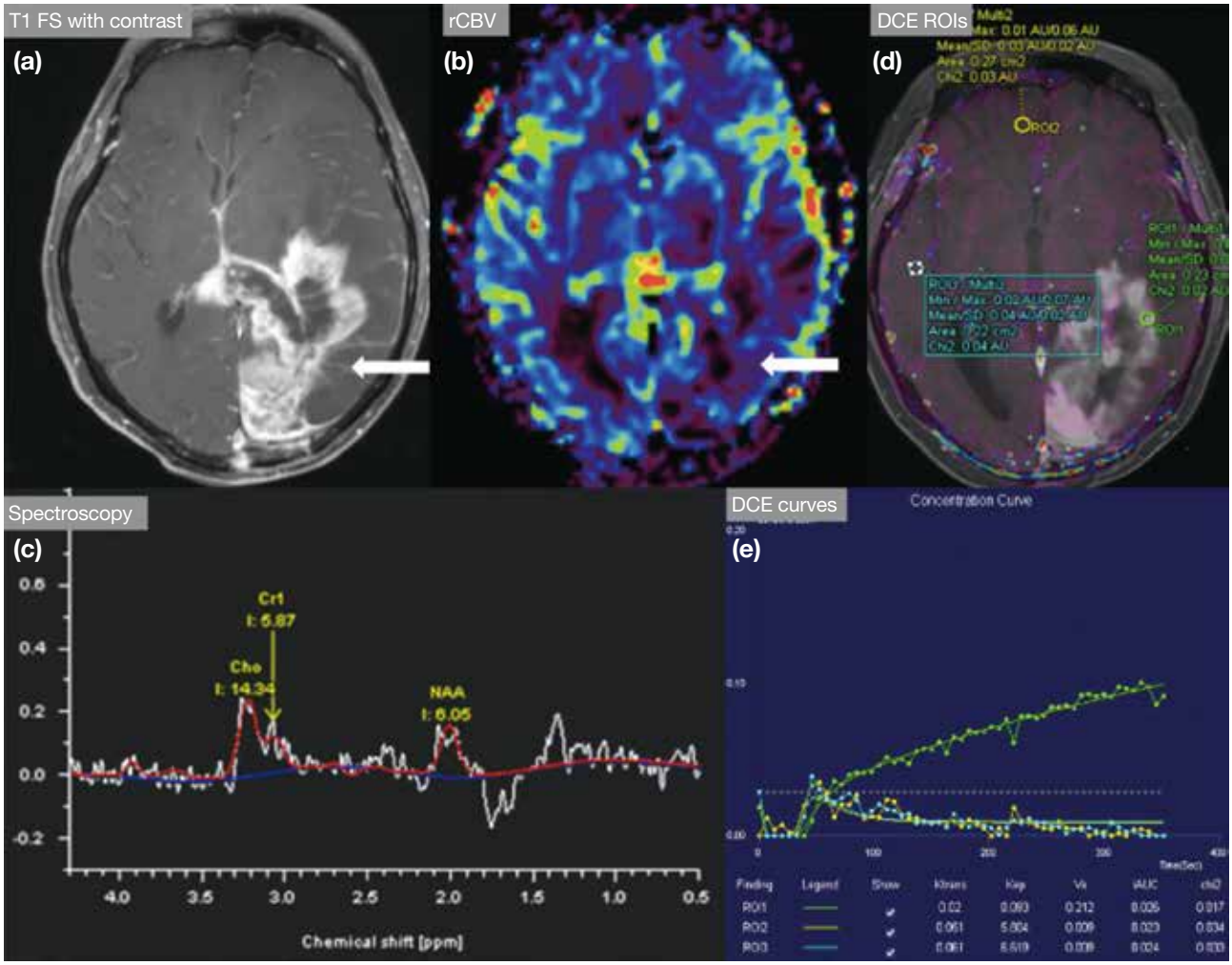

Figure 8. Pseudoprogression in the same patient as in Figure 7 at 6 months after commencement of radiotherapy and temozolomide. Post-contrast T1-weighted fat saturation (FS) sequence (a), relative cerebral blood volume (rCBV) colour map (b), magnetic resonance spectroscopy [MRS] (c), dynamic contrast enhancement (DCE) regions of interest (ROIs) [d], and ROI curves (e) reveal a left parietal-occipital contrast enhancing mass (arrow in [a]). Decreased cerebral perfusion was shown (arrow in [b]). The low concentration of metabolites was demonstrated on MRS, suggesting background noise and representing 'empty space'. No significant elevation of the time-dependent leakage constant K^{trans} or initial area under the curve and no rapid uprise of the slope of the concentration-time curve were demonstrated. Features are consistent with pseudoprogression.

Non-contrast MR perfusion techniques, including arterial spin-labelling, can serve as an alternative to DCE and DSC.[1,6] They measure cerebral blood flow by labelling arterial water as the tracer and might be performed in patients in whom gadolinium-based contrast is contraindicated.

These techniques appear promising, but currently there is no established cut-off value that can reliably differentiate between tumour progression and treatment response.

Magnetic Resonance Spectroscopy

MRS reflects the concentration of brain metabolites based on their precession frequency; representative metabolites include *N*-acetylaspartate (NAA, marker of neuronal viability) and choline (Cho, marker of cell proliferation). Viable tumours typically demonstrate an elevated Cho peak and reduced NAA level[1] (Figures 5 and 6), while treatment-related injury classically reveals decreased Cho and NAA peaks, respectively, and an elevated lipid/lactate peak (Figure 8).[6] Lack of external validation and technical difficulty in evaluating peripheral brain lesions may limit its potential benefits on post-treatment brain tumour imaging interpretation.

PSEUDORESPONSE

Antiangiogenic agents, such as bevacizumab, antagonise the vascular endothelial growth factor

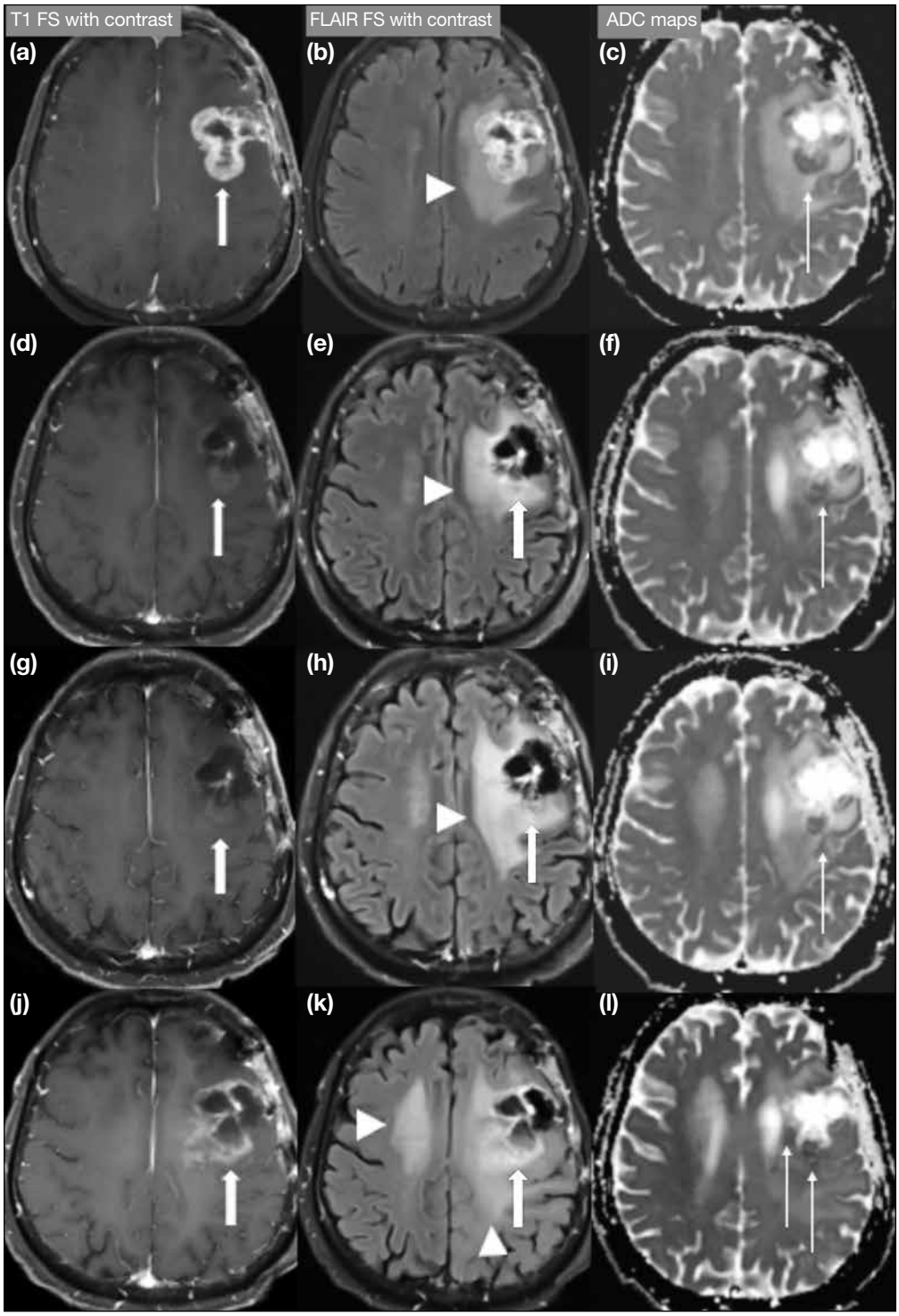

Figure 9. Pseudoresponse shown in post-contrast T1-weighted fat suppression (FS) sequence images (a, d, g, and j), post-contrast fluid-attenuation inversion recovery (FLAIR) FS sequence images (b, e, h, and k), and apparent diffusion coefficient (ADC) map images (c, f, i, and l). Disease progression was identified in a 66-year-old patient with a histology-proven left frontal glioblastoma managed with chemotherapy, presenting with a left frontal contrast-enhancing lesion (arrow in [a]) with perilesional FLAIR hyperintensity (arrowhead in [b]) and low ADC value (thin arrow in [c]). Second-line treatment with bevacizumab was started and follow-up magnetic resonance imaging (MRI) performed 4 months later (d to f) showed reduction in contrast enhancement (arrows in [d] and [e]). There was no significant interval change in the perilesional FLAIR hyperintensities (arrowhead in [e]) and low ADC value (thin arrow in [f]) at the left frontal lesion was observed. MRI performed 9 months from commencement of bevacizumab (g to i) demonstrated further reduction in contrast enhancement (arrows in [g] and [h]). Further increase in FLAIR hyperintensities (arrowhead in [h]) and persistent low ADC value (thin arrow in [i]) were illustrated. The treatment regime was continued and disease progression was found in subsequent follow-up MRI (j to l) with increase in contrast enhancement (arrows in [j] and [k]), FLAIR hyperintense signals (arrowheads in [k]), and a new focus of low ADC signal (thin arrows in [l]). The findings are suggestive of pseudoresponse.

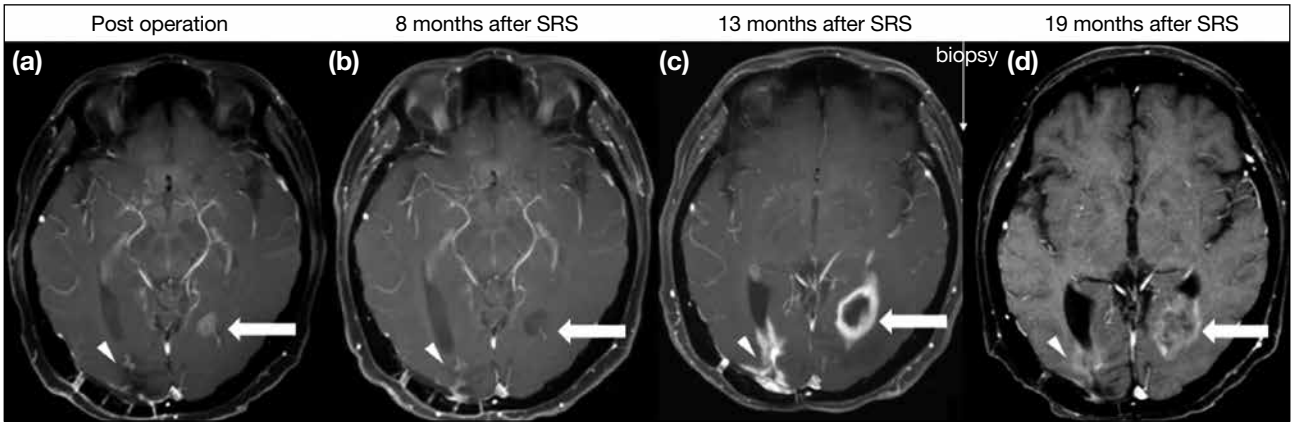

Figure 10. Radiation necrosis shown in post-contrast T1-weighted fat saturation sequences. Histologically proven radionecrosis of a left periventricular contrast-enhancing lesion (arrows) is found in a 57-year-old patient with known metastatic breast cancer. Surgical excision of the right periventricular lesion (arrowheads) was performed, with histology confirming metastasis, followed by chemotherapy and stereotactic radiosurgery (SRS) to the surgical bed and the left posterior parietal lesion (a). T1-weighted magnetic resonance imaging (MRI) 8 months after SRS demonstrated reduction in contrast enhancement in the left periventricular lesion and slight increase in contrast enhancement at the right-sided lesion (b). Follow-up MRI performed 5 months later revealed progression in enhancement of both lesions with a cut-pepper–like appearance on the left side. Biopsy of the left-sided lesion suggested radionecrosis (c). Contrast enhancement in both occipital lobes decreased on MRI performed at 6 months' follow-up after the biopsy (d). Histological findings were consistent with radiation necrosis.

receptors to produce an antitumour effect. It is considered a second-line treatment if patients fail the Stupp protocol. It can result in rapid and promising reduction in contrast enhancement but has less effect on non-enhancing infiltrative disease on neuroimaging.[1,4] This discrepancy is characteristic of pseudoresponse (Figure 9). Clinical symptoms and signs may improve after the antiangiogenic agents, but survival benefit remains controversial.[4]

RADIATION NECROSIS

Radiation necrosis, as the name implies, refers to a delayed necrotic injury of either tumour or normal brain parenchyma, secondary to high radiation exposure as in radiosurgery or high-dose radiotherapy. Most radiation necrosis occurs within a few years after the irradiation.[11] A combination of fibrinoid changes in blood vessels, coagulative necrosis, demyelination, and gliosis can be found on histology. Concomitant use of chemotherapy, targeted therapy for brain metastasis, or immunotherapy may increase the risk of treatment-related necrosis.[11] The typical imaging appearance includes new enhancement at the resection margin that was irradiated at a higher dosage (Figure 10), new periventricular enhancement that lies within the high-dose radiation field, and new distant enhancement within the radiation field but not at the expected sites of tumour spread.[8] On conventional imaging, these can present as a soap-bubble or cut-pepper–like lesion (Figure 10).

On advanced MRI, radiation necrosis can demonstrate reduced rCBV and low permeability on perfusion imaging. Low NAA and Cho peaks and an elevated lipid/lactate peak are classical features observed on MRS (Figure 11).[12]

STROKE-LIKE MIGRAINE ATTACKS AFTER RADIATION THERAPY SYNDROME

Stroke-like migraine attacks after radiation therapy (SMART) syndrome is a rare, recurrent, and late complication of irradiation with partial to complete recovery.[13] It is more commonly seen in men and clinical presentation includes migraine-like headache, stroke-like focal neurological deficit, and seizures. The pathophysiology is not well understood but proposed mechanisms include cerebral hyperexcitability with impaired autoregulation and endothelial damage as well as reversible radiation-induced vasculopathy. No pathological correlation has been identified on brain biopsy so far and no consensus on effective treatment has been established although antiepileptics and steroids have been used in some of the reported cases of SMART syndrome.[13]

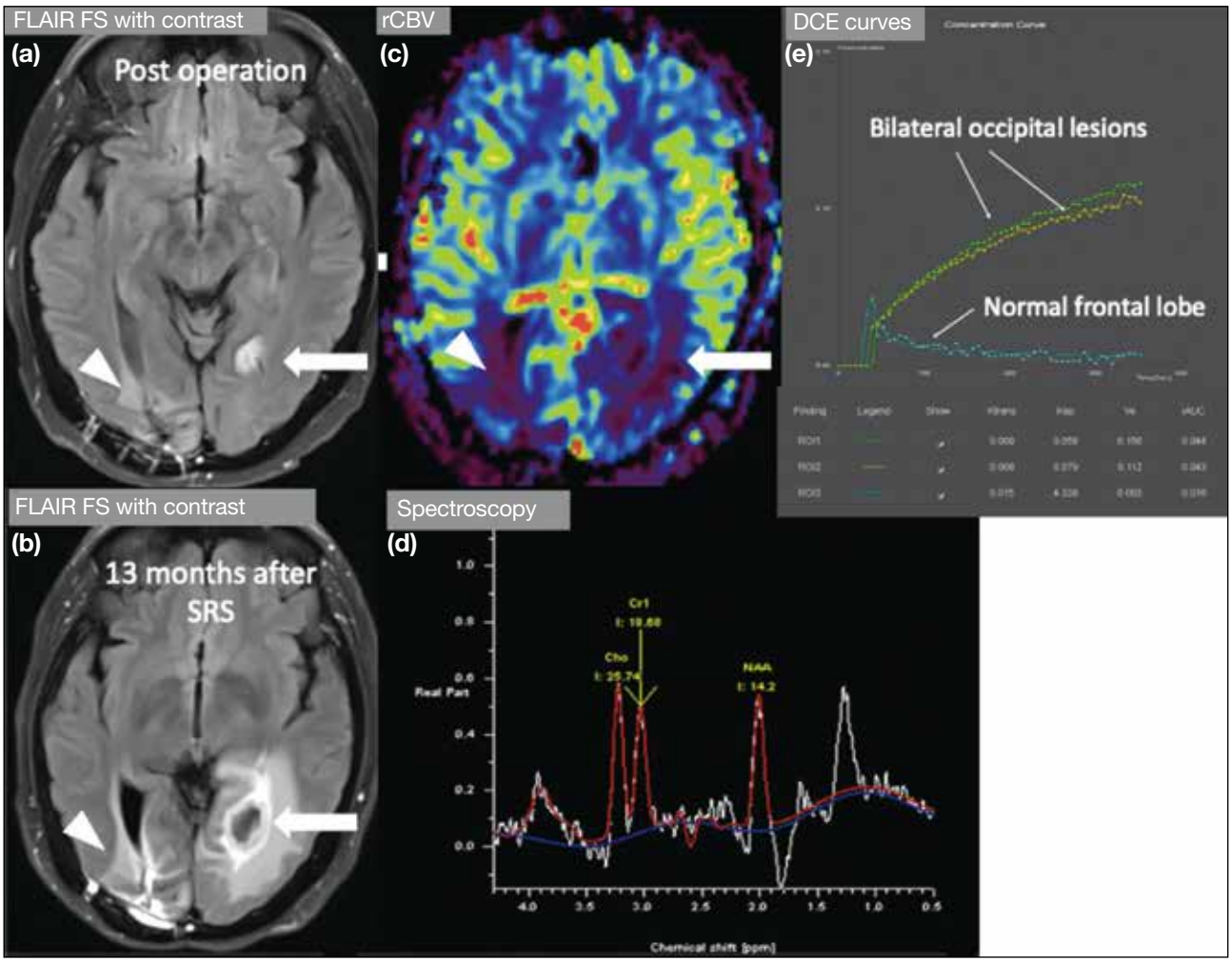

Figure 11. Radiation necrosis in the same patient as in Figure 10 with known metastatic breast cancer and bilateral periventricular cerebral lesions. The left periventricular cerebral lesion was histologically proven to be radionecrosis after chemotherapy and stereotactic radiosurgery (SRS). (a) and (b) show post-contrast fluid-attenuation inversion recovery (FLAIR) fat saturation (FS) sequences postoperation and 13 months after SRS, respectively, while (c) shows relative cerebral blood volume (rCBV) colour map, (d) shows magnetic resonance spectroscopy [MRS], and (e) shows dynamic contrast enhancement (DCE) curves in the set of magnetic resonance images performed 13 months after SRS. Increase in perilesional vasogenic oedema was found around both lesions 13 months after SRS (arrow and arrowhead in [b]), as compared to that before SRS (arrow and arrowhead in [a]). Absence of elevated cerebral perfusion was demonstrated (arrow and arrowhead in [c]). On MRS, the concentration of metabolites was found to be reduced, suggesting background noise in the vicinity of 'empty space'. In (e), DCE regions of interest (ROIs) 1 and 2 drawn on bilateral occipital lesions and ROI 3 drawn on normal frontal lobe brain parenchyma revealed no significant increase in the time-dependent leakage constant K^{trans} and mildly increased the initial area under the curve as compared to the normal frontal lobe. In combination with Figure 10, the overall features were compatible with the biopsy-proven radiation necrosis.

Classical imaging findings of SMART syndrome include unilateral cortical gyriform swelling as well as cortical and dural enhancement with or without diffusion restriction, typically found in the parietal-temporal-occipital lobes[13] (Figures 12 and 13). The differential diagnosis of the combined clinical and radiological features includes tumour recurrence/leptomeningeal carcinomatosis, meningoencephalitis, and posterior reversible encephalopathy syndrome (PRES).

Similar to SMART syndrome, PRES commonly manifests as a reversible entity without designated treatment.[14] The pathophysiology of PRES is postulated to be cerebral hyperperfusion from insufficient autoregulation secondary to rapidly developing hypertension and activation of cytokines and inflammatory responses due to systemic disorders such as autoimmune disorders, cytotoxic drugs or sepsis.[5] The typical imaging features of PRES include vasogenic oedema in the bilateral parietal-occipital subcortical white matter, while contrast enhancement and restricted diffusion may be present in up to 20% to 30% of patients,[15]

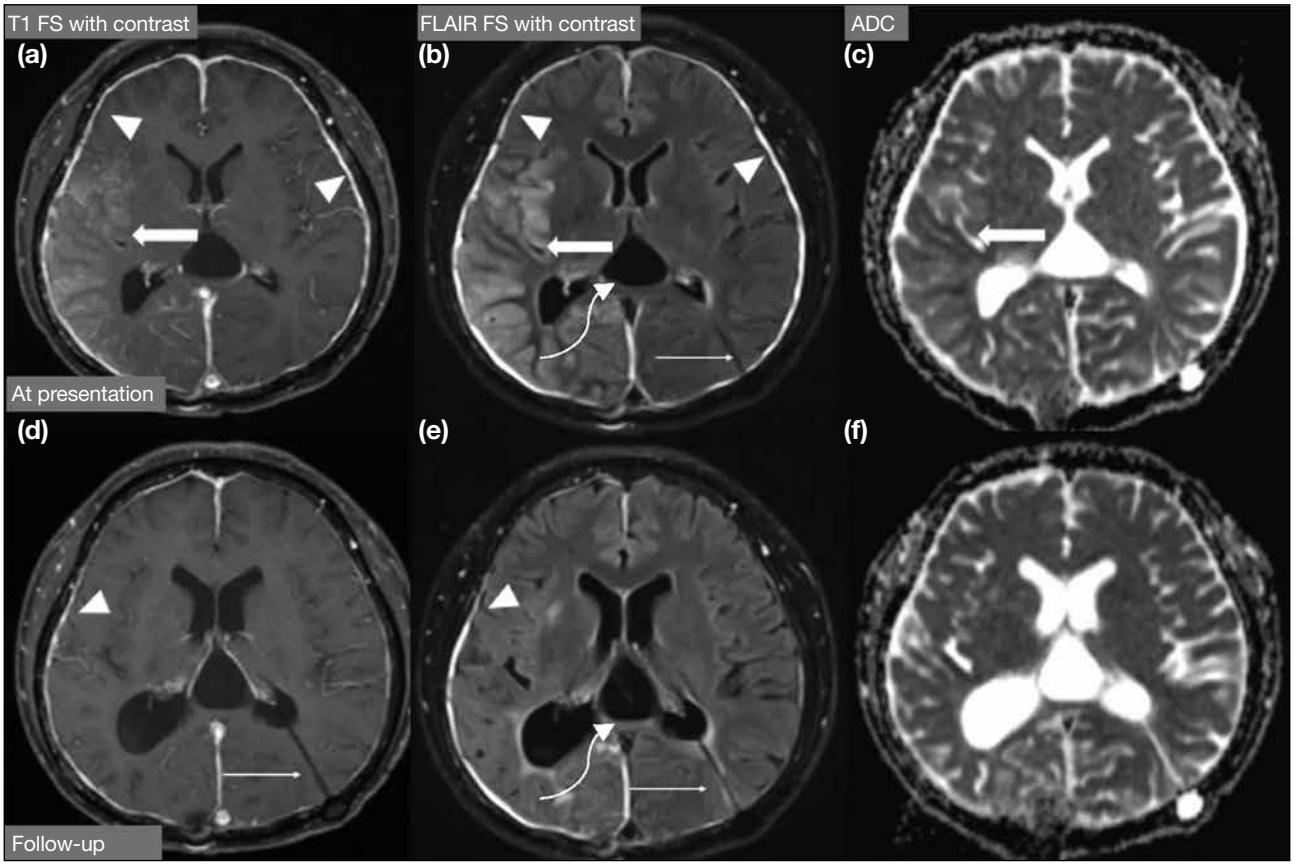

Figure 12. Stroke-like migraine attacks after radiation therapy (SMART) syndrome. A 40-year-old patient with history of treated right parietal glioblastoma and stable disease for >5 years presented with headache, seizure, and left hemiplegia. MRI with a post-contrast T1-weighted fat suppression (FS) sequence (a), post-contrast fluid-attenuation inversion recovery (FLAIR) FS sequence (b), and apparent diffusion coefficient (ADC) imaging (c) demonstrated gyriform contrast enhancement and gyral oedema in the right frontal-parietal-occipital cortex with low ADC values (arrows). Incidental note was made of shunt-related diffuse bilateral pachymeningeal enhancement (arrowheads in [a] and [b]) with a left ventriculoperitoneal shunt in situ (thin arrows in [b], [d], and [e]). Follow-up post-contrast T1-weighted FS sequence (d), post-contrast FLAIR FS sequence (e), and ADC imaging (f) when the symptoms subsided revealed improvement in the dural enhancement (arrowheads in [d] and [e]) and gyral swelling with normal ADC signal. Features are in keeping with SMART syndrome. Interval reduction in pachymeningeal enhancement and dilatation of the ventricles suggested improvement of overshunting. Incidental finding of an extra axial cystic lesion at the pineal region was suggestive of an arachnoid cyst (curved arrows in [b] and [e]) which remained stable in size for >5 years.

as opposed to the unilaterality and predominant cortical involvement of SMART syndrome, which usually aids in radiological differentiation from PRES.

RADIATION-INDUCED NEOPLASM

Radiation-induced tumour is generally defined as a secondary neoplasm of different histology, developing in the radiation field after an asymptomatic latency period. Meningioma is the most common radiation-induced central nervous system tumour and World Health Organization grade I meningioma is the most common subtype (Figure 14).[16] The overall survival is comparable to that of de novo meningiomas with similar grades.[17]

Acute to Subacute Radiation-Induced Injury

Acute radiation encephalopathy can occur in days to weeks after irradiation, due to alterations in capillary permeability, disruption of the blood-brain barrier, and development of vasogenic oedema. Clinical manifestations may include acute neurological symptoms such as nausea, vomiting, drowsiness, headache, or acute worsening of pre-existing neurological symptoms.[11] Diffuse brain swelling, T2-weighted hyperintensity in the white matter, or new or enlarged contrast-enhancing lesions in the vicinity of irradiation can be demonstrated on MRI. Corticosteroids may be helpful to control patients' signs and symptoms.[11]

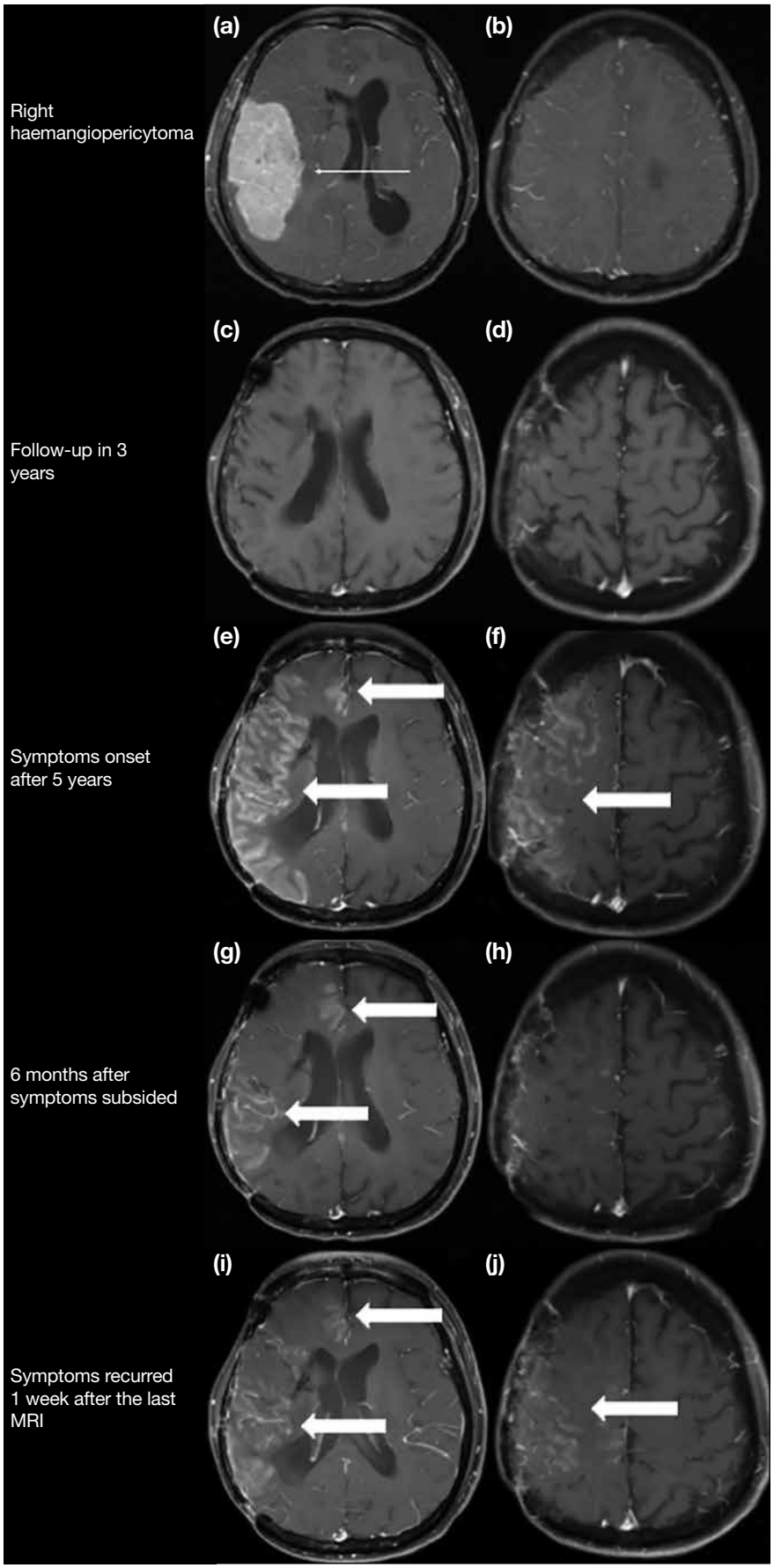

Figure 13. Stroke-like migraine attacks after radiation therapy (SMART) syndrome. (a, c, e, g, and i) show post-contrast T1-weighted fat suppression (FS) sequence at the level of lateral ventricles over time and (b, d, f, h, and j) show post-contrast T1-weighted FS sequence acquired above the ventricles. A 40-year-old patient presented with an extra-axial right supratentorial contrast-enhancing mass (thin arrow in [a]), which was proven to be a haemangiopericytoma, was treated with total excision (a and b) followed by adjuvant radiotherapy. No disease recurrence was identified in follow-up magnetic resonance imaging (MRI) performed 3 years after the excision (c and d). The patient presented again with intermittent and reversible left-hand weakness and numbness and seizures 5 years after the operation. MRI (e and f) demonstrated gyriform and leptomeningeal enhancement involving the right cerebral hemisphere (arrows). Follow-up MRI performed 6 months later when symptoms subsided (g and h) illustrated radiological improvement of the contrast enhancement (arrows in [g]). However, symptoms recurred shortly after the MRI and rescan in 1 week showed new leptomeningeal enhancement at the high right frontoparietal lobe (arrows in [i] and [j]). Overall features are most compatible with recurrent SMART syndrome.

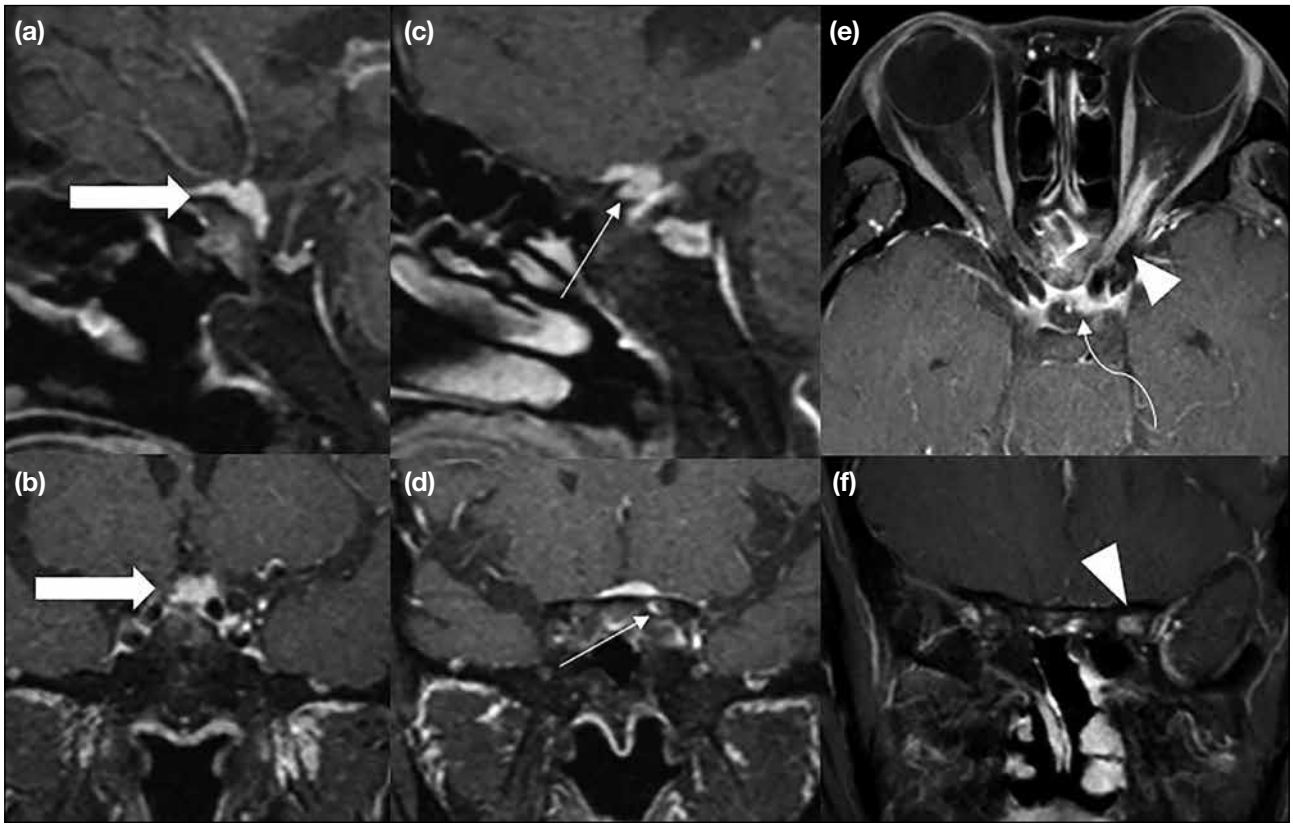

Figure 14. Radiation-induced meningioma in a 62-year-old patient. (a and c) and (b and d) show sagittal and coronal post-contrast T1-weighted fat saturation sequences performed 10 years after excision and radiotherapy of left pituitary microadenoma, respectively. (e) and (f) show axial and coronal post-contrast T1-weighted fat saturation sequences of magnetic resonance imaging (MRI) performed 15 years after radiotherapy, respectively. MRI performed 10 years after treatment revealed the dural tail and suprasellar location of an extra-axial enhancing lesion at the planum sphenoidale (arrows in [a] and [b]) with early extension to the intracanalicular segment of the left optic nerve sheath (thin arrows in [c] and [d]). Partial excision was performed, revealing World Health Organization grade I meningioma. Follow-up MRI performed 15 years after the initial treatment demonstrated 'tram-track' enhancement of the left optic nerve sheath (arrowheads in [e] and [f]) with a sharp anterior margin at the intraorbital segment. Residual tumour in the left suprasellar region encased the left internal carotid artery (curved arrow in [e]). Overall features are compatible with radiation-induced meningioma with progressive left optic nerve sheath involvement.

RADIATION-INDUCED LEUCOENCEPHALOPATHY

Radiation-induced leucoencephalopathy generally refers to delayed radiation-induced white matter injury with a reported incidence of up to 34% in patients receiving lower radiation dosages, e.g., in whole-brain radiotherapy. The mechanisms of this leucoencephalopathy include damage to the oligodendrocytes, resulting in axonal demyelination, disruption of vascular endothelium, and focal mineralisation.[11] Patients may be asymptomatic or present with varying degrees of neurocognitive decline. Imaging features typically include progressive symmetric and confluent T2/FLAIR hyperintense signals mainly in the periventricular white matter and brain atrophy (Figure 15).[6]

CONCLUSION

The combination of conventional and advanced MRI techniques in post-treatment brain tumour imaging aids radiologists in distinguishing between treatment response and treatment-related changes and recognising post-treatment complications. Familiarity with these techniques might help to avoid unnecessary alteration of the patients' management or invasive procedures.

REFERENCES

1. Leao DJ, Craig PG, Godoy LF, Leite CC, Policeni B. Response assessment in neuro-oncology criteria for gliomas: practical approach using conventional and advanced techniques. AJNR Am J Neuroradiol. 2020;41:10-20.
2. Stupp R, Mason WP, van den Bent MJ, Weller M, Fisher B, Taphoorn MJ, et al. Radiotherapy plus concomitant and adjuvant temozolomide for glioblastoma. N Engl J Med. 2005;352:987-96.

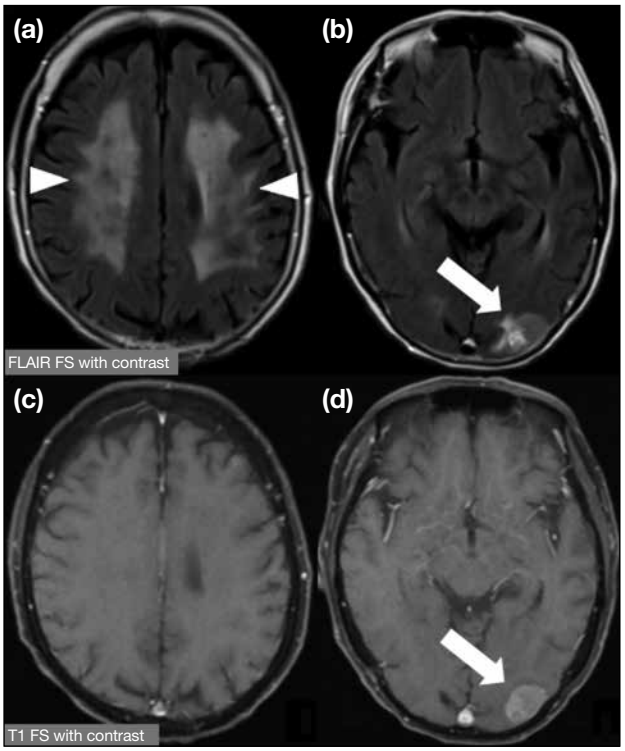

Figure 15. Radiation-induced leucoencephalopathy. A 70-year-old patient with metastatic pulmonary malignancy was diagnosed with brain metastases and managed with whole-brain radiotherapy (WBRT). Follow-up magnetic resonance post-contrast fluid-attenuation inversion recovery (FLAIR) fat suppression (FS) sequences (a and b) and post-contrast T1-weighted FS sequences (c and d) performed 4 years after WBRT demonstrated bilateral non-enhancing FLAIR hyperintensity involving the supratentorial white matter (arrowheads in [a]). Features could represent radiotherapy-induced leucoencephalopathy. A contrast-enhancing lesion is illustrated in the left occipital lobe (arrows in [b] and [d]), suggestive of brain metastasis.

3. Stupp R, Taillibert S, Kanner A, Read W, Steinberg D, Lhermitte B, et al. Effect of tumor-treating fields plus maintenance temozolomide vs maintenance temozolomide alone on survival in patients with glioblastoma: a randomized clinical trial. JAMA. 2017;318:2306-16.
4. Wen PY, Macdonald DR, Reardon DA, Cloughesy TF, Sorensen AG, Galanis E, et al. Updated response assessment criteria for high-grade gliomas: response assessment in Neuro-Oncology Working Group. J Clin Oncol. 2010;28:1963-72.
5. Prager AJ, Maritnez N, Beal K, Omuro A, Zhang Z, Young RJ. Diffusion and perfusion MRI to differentiate treatment-related changes including pseudoprogression from recurrent tumors in high-grade gliomas with histopathologic evidence. AJNR Am J Neuroradiol. 2015;36:877-85.
6. Kessler AT, Bhatt AA. Brain tumour post-treatment imaging and treatment-related complications. Insights Imaging. 2018;9:1057-75.
7. Jackson A, Jayson GC, Li KL, Zhu XP, Checkley DR, Tessier JJ, et al. Reproducibility of quantitative dynamic contrast-enhanced MRI in newly presenting glioma. Br J Radiol. 2003;76:153-62.
8. Heye AK, Culling RD, Valdés Hernández MdC, Thrippleton MJ, Wardlaw JM. Assessment of blood-brain barrier disruption using dynamic contrast-enhanced MRI. A systematic review. Neuroimage Clin. 2014;6:262-74.
9. Narang J, Jain R, Arbab AS, Mikkelsen T, Scarpace L, Rosenblum ML, et al. Differentiating treatment-induced necrosis from recurrent/progressive brain tumor using non-model–based semiquantitative indices derived from dynamic contrast-enhanced T1-weighted MR perfusion. Neuro Oncol. 2011;13:1037-46.
10. Chung WJ, Kim HS, Kim N, Choi CG, Kim SJ. Recurrent glioblastoma: optimum area under the curve method derived from dynamic contrast-enhanced T1-weighted perfusion MR imaging. Radiology. 2013;269:561-8.
11. Katsura M, Sato J, Akahane M, Furuta T, Mori H, Abe O. Recognizing radiation-induced changes in the central nervous system: where to look and what to look for. Radiographics. 2021;41:224-48.
12. Kumar AJ, Leeds NE, Fuller GN, Van Tassel P, Maor MH, Sawaya RE, et al. Malignant gliomas: MR imaging spectrum of radiation therapy- and chemotherapy-induced necrosis of the brain after treatment. Radiology. 2000;217:377-84.
13. Black DF, Morris JM, Lindell EP, Krecke KN, Worrell GA, Barleson JD, et al. Stroke-like migraine attacks after radiation therapy (SMART) syndrome is not always completely reversible: a case series. AJNR Am J Neuroradiol. 2013;34:2298-303.
14. Patel UK, Patel K, Malik P, Elkady A, Patel Nidhi, Lunagariya A. Stroke-like migraine attacks after radiation therapy (SMART) syndrome—a case series and review. Neurol Sci. 2020;41:3123-34.
15. Fugate JE, Rabinstein AA. Posterior reversible encephalopathy syndrome: clinical and radiological manifestations, pathophysiology, and outstanding questions. Lancet Neurol. 2015;14:914-25.
16. Yamanaka R, Hayano A, Kanayama T. Radiation-induced meningiomas: an exhaustive review of the literature. World Neurosurg. 2017;97:635-44.e8.
17. Lee JW, Wernicke AG. Risk and survival outcomes of radiation-induced CNS tumors. J Neurooncol. 2016;129:15-22.

CATEGORIES OF PAPERS

Hong Kong Journal of Radiology publishes various categories of articles. Each category serves a distinct purpose and is judged by different criteria.

EDITORIAL

Commissioned article presenting the author's opinion on a topical subject or an article published in the current issue. Unsolicited Editorials are not accepted.

Format: An abstract is not required. The text is limited to 1000 words, with a maximum of 1 table or figure, and up to 10 references.

REVIEW ARTICLE

Systematic reviews or meta-analyses of recent developments in a specific topic. Scoping reviews of the literature that identify area(s) for future research will also be considered. No new information is described, and no subjective opinion or personal experiences are expressed.

Format: A structured abstract of ≤ 250 words; headings should include: Objective(s), Methods, Results, Conclusion. The text is limited to 5000 words, with a maximum of 20 tables and figures (total), and up to 60 references.

ORIGINAL ARTICLE

Provides new information based on original research. Includes prospective studies with in-depth statistical analysis, unique retrospective observations of a disease or disorder, and studies of novel applications of an interventional procedure or treatment method.

Format: A structured abstract of ≤ 250 words; headings should include: Objective(s), Methods, Results, Conclusion. The text is limited to 3500 words, with a maximum of 20 tables and figures (total), and up to 50 references.

PERSPECTIVE

Narrative review articles discussing recent developments in a specific topic. No new information is described; may include subjective opinion or personal experiences.

Format: An unstructured abstract of ≤ 250 words. The text is limited to 2500 words, with a maximum of 20 tables and figures (total), and up to 60 references.

PICTORIAL ESSAY

Teaching exercise with message in the figures and legends. Emphasis is on quality of the illustrations and clinical relevance of the message.

Format: An abstract is not required. The text is limited to 2500 words, with a maximum of 20 tables and figures (total), and up to 15 references.

CASE REPORT

Brief discussion of a case with unique features not previously described. Additional cases (case series) may be added to augment the discussion. The discussion should be succinct and focus on a specific message.

Format: An abstract is not required. The text is limited to 1500 words, with a maximum of 8 tables and figures (total), and up to 15 references.

BRIEF COMMUNICATION

This includes post-meeting commentary, update on new imaging or therapeutic advances, brief description of a specific technique or procedure or new equipment. Teaching exercise aimed at describing a certain radiological or radiotherapeutic technique for trainees and practising radiologists is also welcome.

Format: An abstract is not required. The text is limited to 1500 words, with a maximum of 8 tables and figures (total), and up to 15 references.

LETTER TO THE EDITOR

Short letter on any matter of interest to journal readers, including comments on an article that has previously appeared in the journal. The authors of the article commented on would be invited to reply.

Format: An abstract is not required. The text is limited to 500 words, with up to 5 references. Figures and tables are permitted only exceptionally.

INFORMATION FOR AUTHORS

Aims and Scope

Hong Kong Journal of Radiology is the official peer-reviewed academic journal of the Hong Kong College of Radiologists. It is a multidisciplinary journal covering research work pertaining to the science and practice of the component specialties of the College. The journal publishes various categories of papers, including Reviews, Original Articles, Perspectives, Pictorial Essays, Case Reports, Brief Communications, and Letters to the Editor. Manuscripts will be subject to rigorous peer review. *HKJR* adheres to the Recommendations for the Conduct, Reporting, Editing, and Publication of Scholarly Work in Medical Journals of the International Committee of Medical Journal Editors (ICMJE; www.icmje.org), and the Core Practices of the Committee on Publication Ethics (COPE; publicationethics.org/).

Journal Policies

Reporting Guidelines: *HKJR* recommends the use of reporting guidelines in the preparation of manuscripts, such as those advocated by the EQUATOR Network (eg, CONSORT for randomised trials).

Funding: Any sponsor(s) of the research involved, along with grant number(s) should be provided.

Conflicts of interest: All authors must provide a statement reporting any conflicts of interest. Where none exist, please state 'The authors have no conflicts of interest to declare.'

Ethics: All studies must be conducted in accordance with the Declaration of Helsinki. For studies involving humans, a statement must be included in the manuscript that provides the name of the review board and approval number (or waiver). A statement on patient/guardian consent must also be included. For studies involving animals, appropriate ethics approval is required, and this should be stated in the manuscript.

Submission: Manuscripts should be submitted online via HKAMedTrack (www.hkamedtrack.org/hkjr). Manuscripts must be unpublished works that are not under consideration by another publication.

Copyright: On acceptance of an article by the journal, the corresponding author will be asked to transfer copyright of the article to the College.

Editing: Accepted manuscripts will be copyedited according to journal style. Authors are responsible for all statements made in their work, including changes made by the copy editor.

Proofs and Reprints: The corresponding author will receive page proofs, which should be proofread and returned promptly. Corrections are limited to printer's errors — no substantial author's changes will be made without charge. Quotes for extra copies of reprints are available at the Editorial Office.

Manuscript Preparation

In general, manuscripts should be prepared following the 'IMRaD' structure as recommended by the ICMJE. Please provide a **blinded** manuscript and separate title page in Word format (.doc or .docx). Manuscripts must be written in English. For accepted manuscripts, an abstract in Traditional Chinese will also be required.

Authors: Provide the full name, qualifications (maximum of two), and affiliation (where the study was conducted) for all authors. The authors' names in Chinese characters, if available, should also be provided. **The corresponding author**, on behalf of the authors, is responsible for all contact with the journal. Provide the full name, postal address, telephone and fax numbers, and email address of the corresponding author.

Title: Concisely convey the main topic of the study. Avoid obvious terms such as "a study of" or "novel". If appropriate, please include the study design in the title (eg, 'randomised controlled trial', 'systematic review', 'case report'). An abbreviated title of <45 characters is also required.

Abstract: For article types requiring an abstract, this should provide a complete summary of the article, including the aims/purpose, main methods, key results, and conclusions. Abbreviations and clinical or technical jargon should be avoided. Please refer to the Categories of Papers for details.

Key Words: Five relevant index terms should be provided, selected from the Medical Subject Headings (MeSH; www.ncbi.nlm.nih.gov/mesh).

Tables: Submit tables on separate pages in as simple a format as possible. They should be numbered and concisely titled. Abbreviations should be defined in footnotes.

Figures: Restricted to the minimum necessary to support the textual material. Illustrations should be submitted as separate files (.jpg format, ≥350-dpi resolution). All figures should be numbered with a legend to indicate the anatomical area and pathological condition shown. All symbols and abbreviations should be defined in the legend. Please ensure that legends and illustrations correspond.

References: Should be numbered in the order in which they are first cited in the text. Each reference citation should be in superscript Arabic numerals after full-stops and commas. In the reference list, include the complete title, and names and initials of all authors.

Acknowledgement(s): Any individuals who contributed substantially to the study but does not qualify for inclusion as an author should be acknowledged. Written permission from acknowledged individuals is required.

Please refer to the *HKJR* website for further guidance:
http://www.hkjr.org/page/information-authors

TAXOTERE®
(docetaxel)

GENERAL DRUG STATUS

Taxotere has been approved as "General Drug Status" as of April 2023 in the Hospital Authority of Hong Kong

Indicated for the following:

- Prostate Cancer
- Breast Cancer
- Non-small Cell Lung Cancer (NSCLC)
- Head and Neck Cancer
- Gastric Adenocarcinoma

Presentation: Docetaxel concentrate and solvent for solution for infusion. Indications and dosage: Breast Cancer: In combination with doxorubicin and cyclophosphamide for adjuvant treatment of operable node-positive and node-negative breast cancer (docetaxel 75 mg/m² 1-hour after doxorubicin 50 mg/m² and cyclophosphamide 500 mg/m² every 3 weeks for 6 cycles); in combination with doxorubicin for treatment of locally advanced or metastatic breast cancer with no previous cytotoxic therapy (docetaxel 75 mg/m² and doxorubicin 50 mg/m2 every three weeks); monotherapy for the treatment of locally advanced or metastatic breast cancer after failure of cytotoxic therapy containing an anthracycline or an alkylating agent (docetaxel 100 mg/m² every three weeks); in combination with trastuzumab for treatment of metastatic breast cancer whose tumors overexpress HER2 and with no previous chemotherapy for metastatic disease (docetaxel 100 mg/m² every three weeks with trastuzumab administered weekly); in combination with capecitabine for treatment of locally advanced or metastatic breast cancer after failure of cytotoxic chemotherapy containing an anthracycline (docetaxel 75 mg/m² every three weeks combined with capecitabine at 1250 mg/m² twice daily [within 30 minutes after a meal] for 2 weeks followed by 1-week rest period). Non-small cell lung cancer (NSCLC): Treatment of locally advanced or metastatic NSCLC after failure of prior platinum-based chemotherapy (docetaxel 75 mg/m² every three weeks); in combination with cisplatin for treatment of unresectable, locally advanced or metastatic NSCLC with no previous chemotherapy for this condition (docetaxel 75 mg/m² immediately followed by cisplatin 75 mg/m² over 30-60 minutes every three weeks). Prostate cancer: In combination with prednisone or prednisolone for treatment of metastatic castration-resistant prostate cancer (docetaxel 75mg/m² every three weeks and prednisone or prednisolone 5mg orally twice daily administered continuously); in combination with androgen-deprivation therapy (ADT), with or without prednisone or prednisolone for treatment of metastatic hormone-sensitive prostate cancer (docetaxel 75 mg/m² every three weeks for 6 cycles and prednisone or prednisolone 5 mg orally twice daily may be administered continuously). Head and Neck cancer: In combination with cisplatin and 5-fluorouracil for induction treatment of locally advanced squamous cell carcinoma of the head and neck (followed by radiotherapy: docetaxel 75mg/m² as a 1 hour infusion, followed by cisplatin 75mg/m² over 1 hour, on day one, followed by 5-fluorouracil 750mg/m² per day as a continuous infusion for 5 days, repeated every 3 weeks for 4 cycles) (followed by chemoradiotherapy: docetaxel 75mg/m² as a 1 hour infusion on day 1, followed by cisplatin 100mg/m² as a 30-minute to 3-hour infusion, followed by 5-fluorouracil 1000mg/m²/day as a continuous infusion from day 1 to day 4, repeated every 3 weeks for 3 cycles). Gastric Adenocarcinoma: In combination with cisplatin and 5-fluorouracil for treatment of metastatic gastric adenocarcinoma, including adenocarcinoma of the gastroesophageal junction, with no prior chemotherapy for metastatic disease (docetaxel 75mg/m² as a 1-hour infusion, followed by cisplatin 75mg/m², as a 1- to 3-hour infusion (both on day 1 only), followed by 5-fluorouracil 750mg/m² per day given as a 24-hour continuous infusion for 5 days, starting at the end of the cisplatin infusion, repeated every 3 weeks). Further Dosage Information: Docetaxel is administered as a 1-hour infusion every three weeks. (Breast, NSCLC, gastric & head and neck cancers) Premedication consisting of an oral corticosteroid, such as dexamethasone 16 mg per day (e.g. 8 mg BID) for 3 days starting 1 day prior to docetaxel administration, unless contraindicated, can be used. Prophylactic G-CSF may be used to mitigate the risk of hematological toxicities. (Metastatic castration-resistant prostate cancer) Given the concurrent use of prednisone or prednisolone the recommended premedication regimen is oral dexamethasone 8 mg, 12 hours, 3 hours and 1 hour before the docetaxel infusion. (Metastatic hormone-sensitive prostate cancer) Irrespective of the concurrent use of prednisone or prednisolone, the recommended premedication regimen is oral dexamethasone 8 mg 12 hours, 3 hours, and 1 hour before docetaxel infusion. For dosage adjustments during treatment, please refer to detailed prescribing information. Contraindications: Hypersensitivity to docetaxel or any excipients, patients with baseline neutrophil count of <1,500 cells/mm³, pregnancy and lactation, severe liver impairment. Precautions: Premedication consisting of an oral corticosteroid is needed. Frequent monitoring of complete blood counts (retreat with docetaxel if ANC ≥1,500 cells/mm³ before next cycle, and dose reduction recommended if severe neutropenia, i.e. <500 cells/mm³ for seven days or more). Patients treated with docetaxel in combination with cisplatin and 5-fluorouracil should receive prophylactic G-CSF to mitigate the risk of complicated neutropenia (febrile neutropenia, prolonged neutropenia or neutropenic infection) and should be closely monitored. Closely monitor patients for early manifestations of serious gastrointestinal toxicity. Enterocolitis could develop at any time and could lead to death as early as on the first day of onset. Observe closely for hypersensitivity reactions especially during the first and second infusions. Hypersensitivity reactions may occur within a few minutes following the initiation of the infusion of docetaxel, thus facilities for the treatment of hypotension and bronchospasm should be available. Severe reactions, such as severe hypotension, bronchospasm or generalised rash/erythema require immediate discontinuation of docetaxel and appropriate therapy and should not be re-challenged. Monitor closely patients who have previously experienced a hypersensitivity reaction to paclitaxel, they may be at risk to develop more severe hypersensitivity reaction. Inform patients about signs and symptoms of serious skin manifestations and closely monitor these patients. If signs and symptoms suggestive of these reactions appear, consider discontinuation of docetaxel. Monitor closely for severe fluid retention. If new or worsening pulmonary symptoms develop, patients should be closely monitored, promptly investigated, and appropriately treated. Interruption of docetaxel therapy is recommended until diagnosis is available. For patients with elevated liver function test (LFTs), recommend dose is 75 mg/m² and LFTs should be measured at baseline and before each cycle. For patients with serum bilirubin levels >ULN and/or ALT and AST >1.5 times the ULN concurrent with serum alkaline phosphatase levels >6 times the ULN, docetaxel should not be used unless strictly indicated. The development of severe peripheral neurotoxicity requires a reduction of dose. When patients are candidates for treatment with docetaxel in combination with trastuzumab, they should undergo baseline cardiac assessment and further monitored during treatment (e.g. every three months). Patients with impaired vision should undergo a prompt and complete ophthalmologic examination. In case cystoid macular oedema is diagnosed, docetaxel treatment should be discontinued and appropriate treatment initiated. Patients should be monitored for second primary malignancies. Closely monitor patients at risk of tumour lysis syndrome. Contraceptive measures must be taken during and for at least three months after cessation of therapy. Concomitant use of docetaxel with strong CYP3A4 inhibitors should be avoided. Amount of alcohol in this product and the side effects may impair ability to drive or use machines. Patients should be warned of this potential impact and be advised not to drive or use machines if they experience these side effects. Additional precautions in adjuvant treatment of breast cancer: G-CSF and dose reduction should be considered in complicated neutropenia. Evaluate and treat promptly on symptoms such as abdominal pain and tenderness, fever, diarrhea, with or without neutropenia. Monitor for symptoms of congestive heart failure during therapy and during the follow up period. Interactions: Metabolism of docetaxel may be modified by the concomitant administration of compounds which induce, inhibit or are metabolised by cytochrome P450-3A. Docetaxel may increase the clearance of carboplatin. CYP3A4 inhibitors. Undesirable effects: Neutropenia, anaemia, alopecia, nausea, vomiting, stomatitis, diarrhoea, asthenia, hypersensitivity reactions (flushing, rash with or without pruritis, chest tightness, back pain, dyspnoea, fever or chills etc.). Parasesthesia, dysesthesia, pain, infusion site reactions, infections, thrombocytopenia, anorexia, peripheral sensory neuropathy, peripheral motor neuropathy, arrhythmia, hypertension, haemorrhage, nail disorders, myalgia, arthralgia, fluid retention, increase in blood bilirubin, alkaline phosphatase, AST, ALT. For uncommon, rare and very rare undesirable effects, please refer to the full prescribing information. Preparations: 20mg x 1 vial, 80mg x 1 vial. Legal Classification: Part 1, First & Third Schedules Poison Full prescribing information is available upon request. API-HK-DOC-20-11

MAT-HK-2300364 (1/2023) 4IC_2779

sanofi

Sanofi Hong Kong Limited
1/F & SECTION 212 on 2/F, AXA SOUTHSIDE, 38 WONG CHUK HANG ROAD,
WONG CHUK HANG, HONG KONG
Tel: (852) 2506 8333 Fax: (852) 2506 2537

The Hong Kong Society of Diagnostic Radiologists Trust Fund

Hong Kong Society of Diagnostic Radiologists Research Grant

The Hong Kong Society of Diagnostic Radiologists (HKSDR) was founded in 1977 to promote interflow of professional knowledge in diagnostic radiology and to foster close contact among doctors working in the field of diagnostic radiology. The HKSDR Trust Fund was established in 1985.

Taking into account the rapid progress in imaging technology and thus the need to promote research to advance our knowledge and to serve our patients better, the Trust Fund offers three awards of up to HK$17,000 each and is open to application.

The application should be made by the principal investigator of the research project related to the scientific or clinical aspects of diagnostic radiology to be conducted in Hong Kong. The principal investigator should be a trainee/specialist in the field of diagnostic radiology. He/she has to be a registered medical practitioner in Hong Kong.

Application and enquiry can be directed to:

Dr. Lam Chiu Ying Flora, Hon Secretary of Trust Fund Working Group
c/o Ms. HY Ng, Department of Diagnostic & Interventional Radiology
Kwong Wah Hospital
25 Waterloo Road, Yaumatei, Kowloon, Hong Kong.
Tel: (852) 3517 5189

Hong Kong College of Radiologists
The Fourth Lilian Leong Oration
香港放射科醫學院第四屆梁馮令儀講座

MRI services for underserved populations in South East Asia

Professor Pek-Lan Khong 孔碧蘭教授

MBBS, MD, FRCR, FHKCR, FHKAM (Radiology), FAMS

Head and Senior Consultant, Department of Diagnostic Imaging, National University Hospital
Professor & Head, Department of Diagnostic Radiology and Director,
Clinical Imaging Research Centre, Yong Loo Lin School of Medicine, National University of Singapore
Singapore

7:00pm, 18th November 2023 (Saturday)

Run Run Shaw Hall, 1/F
Hong Kong Academy of Medicine Jockey Club Building

All are welcome

For further information
Hong Kong College of Radiologists
Tel: (852) 2871 8788
Fax: (852) 2554 0739
E-mail: enquiries@hkcr.org
Website: https://www.hkcr.org

A harmonious amalgamation between South East Asian countries flowers and MR images of fruit harvest

Poster design by Drs. CC Yau, Kevin Fung & Lilian Leong